Nucleosynthesis in accretion disks around black holes

Neige Frankel

Lund Observatory
Lund University

2017-EXA114

Degree project of 60 higher education credits (for a degree of Master)
May 2017

Supervisor: Melvyn B. Davies

Lund Observatory
Box 43
SE-221 00 Lund
Sweden

Abstract

Nucleosynthesis is the mechanism which produces new elements in nuclear reactions. Nuclear reaction rates are highly temperature dependant, and nuclear reactions take place in very hot environments. Current theories predict that the light elements such as hydrogen and helium were produced during the Big Bang. On the other hand, the core of stars produce heavier elements through nuclear fusion. These new elements are then released to the interstellar medium through stellar winds, enriching the gas which will form later generations of stars. Black hole accretion disks also can contain material of high temperatures generated by high accretion rates, allowing nuclear fusion to take place. Nucleosynthesis products can be expelled in winds driven by a super-Eddington accretion, and enrich the interstellar medium.

I wrote a computer program [1] integrating a nuclear burning network in a black hole accretion disk for various ranges of black hole mass and accretion rates. I found that the accretion rate needed for nucleosynthesis to take place increases with the black hole mass. The highest temperatures are located in the inner disk, and the black hole event horizon increases linearly with its mass, preventing the disk from attaining high temperatures. For a stellar mass black hole, highly super-Eddington accretion rates allow nuclear burning and powerful winds. Such accretion rates can be supplied by unstable mass transfer during the disruption of a white dwarf. The alpha chain reactions, involving captures of helium nuclei, structure the disk composition radially, with isotope abundances dominating at specific radii. Assuming a given fraction of the disk material is expelled in winds due to Super-Eddington accretion, and knowing the rate at which such events happen in the Galaxy allowed me to compute upper limits of the contribution of accretion disks to the interstellar medium enrichment. Comparing this production to combined stellar yields from stars, I find that black hole–white dwarf accretion disks produce at most 10^{-4} times the amount of the same elements that stars produce. This result shows that such a small contribution can be neglected to the overall content of the Galaxy. But the nucleosynthesis involved in general may perhaps play a role in observing these systems, for example a light curve emitted by radioactive elements produced in these short-lived black hole accretion disks.

[1] available online from Monday 15 May 2017: `https://github.com/NeigeF/MSc_Project`

Acknowledgements

" *Give a man a fish, and you feed him for a day. Teach a man to fish, and you feed him for a lifetime.*" This proverb of contested origin[2] describes well the interactions I had with my supervisor, Melvyn Davies, along this project. And I would like to express my gratitude to him for his guidance. I would like to thank Anders Johansen for useful comments and advices on writing the present thesis. I also acknowledge Anders' flexibility when I integrated the Master's programme first as an exchange student, and for inviting me to some Planet Formation group meetings just because "I know you are a chondrule fan". Many thanks to Sofia Feltzing for managing Master's students and the Master's Programme which was, for me, an incredible adventure. This work would have been very different without the scientific discussions I had with Alexey Bobrick and Ross Church, and the technical conversations with Chao-Chin Yang and Guido Moyano. I thank Dainis Dravins and Staffan Sölve for commenting on my Swedish. Thanks to Lennart Lindegren for useful comments. I also wish to thank all the people in the department, who contributed to building such an interactive and quality working environment every day. My office-mates, thank you for bearing me and my moods. And thanks to Eric Andersson for our daily "early morning discussions" which were scientifically very rich. I thank Colin Carlile, for a very very long list of things I was helped with. Acknowledgements to Solange and PO for support and good advices, Susanne and Floor for useful comments. Finally, I wish to thank Julie and Lisa for moral assistance, and my parents for encouragements and support. In particular, thank you for providing French food supplies without which half of this thesis would not have existed. Merci à mes grand parents pour le soutien, et à Papi de la mer, pour l'intérêt porté à mon travail, et pour avoir participé généreusement à son financement. J'aurais aimé t'en montrer l'aboutissement.

[2] quote investigator website `http://quoteinvestigator.com/2015/08/28/fish/`

Populärvetenskaplig sammanfattning: Nukleosyntes i ackretionsskivor kring svarta hål

Hur bildas atomerna som bygger upp oss människor - till exempel atomer av kol, syre eller kalcium? Den idag gällande teorin är att lättare atomer såsom väte, helium och litium skapades vid ”Big Bang”, medan en supernova från en döende stjärna producerade och frigjorde bland annat kol, syre, kalcium och järn. Det som stjärnor och Big Bang har gemensamt i sin förmåga att fungera som kärnreaktorer är att de utmärks av väldigt hög värme och en hög densitet. Ett svart hål som mycket snabbt fångar gaser från en omgivande ansamlingsskiva, som vi kallar ackretionsskiva, skapar också mycket hög värme och hög densitet. Detta tillstånd har också alla förutsättningar att fungera som en kärnreaktor och att skapa nya tyngre grundämnen.

I mitt examensarbete har jag undersökt kärnreaktioner i sådana ackretionsskivor kring svarta hål. Temperaturen och densiteten blir tillräckligt hög endast om infångningen av gaser sker mycket hastigt. Detta kan inträffa om ansamlingsskivan kommer från en vit dvärg, vilken ökar i storlek när den kastat ut massa. Jag har skrivit ett program som beräknar hur mycket av nya tyngre atomer som skapas och frigörs. Jämfört med stjärnor är produktionen av nya grundämnen betydligt mindre förekommande. Eftersom en vit dvärg utgör slutprodukten från en död stjärna, kan vi alltid säga att vi människor har erhållit våra byggstenar från stjärnstoft.

Résumé: La nucléosynthèse dans les disques d'accrétion autour de trous noirs

"*Nous sommes faits de poussières d'étoiles*", comme le décrit Huber Reeves, reprenant, dans son magninifique ouvrage sur la synthèse des éléments dans l'Univers, l'idée de Carl Sagan. Cela signifie que les éléments qui nous composent aujourd'hui, carbone, oxygène, calcium, etc., ont été fabriqués à partir de l'hydrogène et de l'hélium hérités du Big Bang, dans les denses coeurs brûlants des étoiles. Mais est-ce là la fin de l'histoire ? La synthèse des éléments nécessite des conditions extrêmes de températures et densités. Ces conditions sont atteignables dans les disques formés par le gas qui se fait avaler par les trous noirs, objets si denses que même la lumière ne peut s'en échapper. Du gas orbitant un trou noir chauffe par friction, permettant à des réactions nucléaires d'avoir lieu. Si une partie des éléments produits peut s'échapper, à l'aide de vents par exemple, alors peut-être que les disques d'accrétions autour des trous noirs jouent un rôle dans la synthèse des éléments nous composant. Seulement, les températures ne sont suffisantes que dans de rares conditions qui mettent en jeu la destruction d'objets compacts, tels que les naines blanches et les étoiles à neutrons, qui sont respectivement les restes de vies d'étoiles légères, et massives. Le travail décrit dans ce mémoire se concentre sur les réactions nucléaires dans les disques d'accrétion provenant de la destruction d'une naine blanche par un trou noir. Comme ces événements sont très rares, leur contribution à la synthèse des éléments qui nous composent aujourd'hui est négligeable comparée à tout ce que les nombreuses étoiles de notre galaxie produisent. En revanche, le cas des étoiles à neutrons n'a pas dit son dernier mot et est toujours un sujet de recherche actuel. Quoi qu'il en soit, les cas les plus prometteurs de synthèse des éléments dans les disques d'accrétions autour de trous noirs mettent en jeu des étoiles, donc il est bien vrai, nous sommes des poussières d'étoiles.

Contents

Acronyms

AIC accretion induced collapse. 3, 54

BH black hole. 3, 32–34, 36, 38, 40, 42, 45, 46, 49–55, 57, 60–64

IMBH intermediate mass black hole. 3, 33, 44

ISCO innermost stable circular orbit. 3, 27, 31, 32, 40

ISM interstellar medium. 3, 5–7, 16, 41, 44, 57, 58, 63, 65, 68

LMXB low mass X-ray binary. 3, 51

NS neutron star. 3, 51, 52, 54

RG red giant. 3, 51, 52

SMBH super-massive black hole. 3, 29, 30, 33

UCXB ultra compact X-ray binary. 3, 5, 51, 53–55, 62–64

WD white dwarf. 3, 34–36, 38, 40, 42, 45, 46, 50–54, 60–64

Concepts

Accretion is the growth of an object due to accumulation of material. In the context of this thesis, the material falls into the gravitational potential of a black hole, and gives up gravitational energy. As gas often has angular momentum, the material does not fall straight into the black hole but forms an accretion disk around it. 3

Accretion rate is the rate at which an object of mass M grows by accretion, $\dot{M} = \frac{\mathrm{d}M}{dt}$. 3

Circularisation radius is, during mass transfer between two bodies, the radius where most of the material from the doner tends to concentrate due to angular momentum conservation. The circularisation radius determines the size of the accretion disk around the accreting object.. 3

Eddington accretion rate is the limiting accretion rate at which the released gravitational energy in the form of radiation reaches the Eddington limit. 3

Eddington luminosity is the luminosity at which the radiation pressure forces, coming from heated gas due to accretion, exerted onto a proton-electron pair balances gravitational forces acting on them. 3

Roche lobe is the volume within which a point mass is uniquely bound to one of the two members of a binary system where two gravitationally bound bodies move on a circular orbit around their common centre of mass. 3

Chapter 1

Introduction

The isotopic content of different structures in the Universe (gas clouds, stars, galaxies) plays a major role in our understanding of their evolution. Nuclear isotopes are produced by nuclear reactions of which the rates change exponentially with temperature. Due to this dependency, nucleosythesis occurs in a limited number of events described below. The general content of the Universe is dominated by hydrogen (about 75%) and helium (about 25%) which were synthesized during the Big Bang (Schneider, 2015). Nuclear reactions in stellar cores produce heavier elements, for example carbon, oxygen, neon and iron. A fraction of the products is expelled in the interstellar medium through stellar winds. Explosive events such as supernovae are very good nucleosynthesis nests and their feedback has a significant effect on star formation in galaxies. But nucleosynthesis may also happen in other highly energetic events.

Observations of X-ray sources suggest the existence of accretion disks around compact objects. Accretion disks are disks of material orbiting around a central object, and being accreted because of angular momentum loss through viscous dissipation. The temperature in such disks can be very high, possibly high enough to make nuclear burning effective. These high temperatures can be provided in disks around compact objects either by low viscosity, radiatively inefficient accretion disks, or by geometrically thin viscous disks with very high accretion rates. The former scenario has been investigated intensively by Arai & Hashimoto (1992), Mukhopadhyay & Chakrabarti (2000) and Chakrabarti et al. (1987) for example with a viscosity parameter $\alpha \approx 10^{-4}$. Hu & Peng (2008) investigated nucleosynthesis with sub-Eddington accretion around a $10M_{\odot}$ black hole and find a very low contamination of new elements, with for instance a production of aluminium 26 of $0.05M_{\odot}$ per Myr from all the black holes in the Milky-Way. For thin disks, numerical constraints on the nature of the viscosity suggest magneto-rotational instablility to set the viscosity parameter $\alpha \approx 0.01$ (Balbus & Hawley, 1998). Metzger (2012) and Margalit & Metzger (2016) studied nucleosynthesis in these accretion disks around neutron stars, with a stage of unstable mass transfer during a tidal disruption of a white dwarf by a neutron star.

In this work, I argue on the possibility of nucleosynthesis in black hole accretion disks and investigate the limits of their effects on the interstellar medium enrichment. In particular, I discuss how they compete with stars and stellar winds. The present master thesis is organised as follows:

Chapter 2: I use existing literature (Clayton, 1968; Arnett, 1996) on nucleosynthesis to understand the conditions in which nucleosynthesis happens, and recall the production of

isotopes during the Big Bang and in stellar cores for further comparison. I identify the thermodynamical variables determining which nuclear reactions dominate and how fast they occur. In particular, the rate r of a nuclear reaction goes as

$$r \propto \rho^{\alpha} T^{\beta} \tag{1.1}$$

where ρ is the material density (mass per unit volume) and T the temperature. Different nuclear reactions have a different dependency on these quantities, and the rates change extremely fast with the temperature, indicating $\beta \gg 1$ and α of the order of unity in most cases.

Chapter 3: The background theory of accretion disks and the major disk models used in the community are presented. I focus on the properties of the accretion disks which have the greater effects on nucleosynthesis, namely the mass density ρ and the temperature T. The density and temperature at a certain radius r in the disk are functions of the accretion rate $\dot{M}$ and the central black hole mass $M_{\rm BH}$. I provide details for a simple disk, the thin accretion disk model (Shakura & Sunyaev, 1973), for which the temperature and the density at a given radius scale as

$$\begin{aligned} T &\propto \dot{M}^{3/10} \left(\frac{M_{\rm BH}}{M_{\odot}}\right)^{1/4}, \\ \rho &\propto \dot{M}^{11/20} \left(\frac{M_{\rm BH}}{M_{\odot}}\right)^{5/8}. \end{aligned} \tag{1.2}$$

Both temperature and density increase with accretion rate. But accretion rates cannot be indefinitely large. The important concept of Eddington accretion rate, $\dot{M}_{\rm Edd}$ is introduced: it is the limit above which accretion does not occur without outflows. If gas flows towards a black hole at a faster rate than $\dot{M}_{\rm Edd}$, we should expect disk winds. These outflows may transport the nucleosynthesis products to the interstellar medium (ISM).

Chapter 4: I model nucleosynthesis in a thin accretion disk, and investigate its effectiveness for various ranges of black hole masses and accretion rates. In particular, I focus on the systems with temperatures allowing the production of elements heavier than helium, because production of light elements is not expected to be competitive against stellar feedback (elements released through stellar winds). I find restrictive thermodynamical conditions which can be reached in particular systems only. Super-Eddington accretion rates, of the order of $> 10^6 \dot{M}_{\rm Edd}$ for stellar black holes, are needed to provide the temperatures favourable to nucleosynthesis. The accretion rate is roughly determined by the density of the material from which the black hole accretes. In the case of an accretion disk provided by a companion star in a binary system, such high rates are reached in unstable mass transfers. They can be provided by a close binary system with a short period ($P < 1$h), composed of a stellar mass black hole and a white dwarf, defining an ultra compact X-ray binary (UCXB). This chapter focuses on the physical processes involved in nucleosynthesis in accretion disks. Technical details about the program I wrote are available in appendices.

Chapter 5: The system black hole–white dwarf is studied in detail. I simulate an alpha chain reaction network, which consists of successive captures of helium nuclei, in a simple code I wrote. I compute the composition of the disk and the mass of new elements produced and expelled in winds. I investigate the effect of the black hole mass, the accretion rate, and the initial composition of the accretion disk on the production of heavier elements.

Chapter 6: I use literature to understand how black hole–white dwarf systems which transfer material form, and at which rate they form. A black hole colliding with a red giant star can become bound to the core of the red giant, and the newly formed binary system can lose energy to the envelope. This scenario might result in a tight black hole–white dwarf binary system, and such collisions are more likely to happen in globular clusters than in the Galactic field. In the field, the most likely formation channel is the evolution of a system which was already born as a binary.

Chapter 7: Other systems of interests are discussed in this chapter, such as Bondi accretion onto primordial black holes, and neutron capture reactions in systems created by the merger of two neutron stars, leading to a black hole surrounded by a neutron-rich disk. The first scenario is interesting because if, in the early universe, accretion disks around primordial black holes do host nucleosynthesis and do enrich the ISM, this could induce the first stars, or the stars of the next generation to contain more metals, influencing their evolution. The later scenario is under current research (Wu et al., 2016) and is a proposed scenario for short gamma ray bursts and the enrichment of metal poor stars in r-process elements.

Chapter 8: I find in the literature stellar production of elements. Carbon comes mainly from the third dredge up, after the asymptotic giant branch phase of stellar evolution of low mass stars. In this phase, convection brings to the surface helium, carbon and elements from slow neutron capture processes. Heavier elements are released by massive stars as they die in a supernova explosion. Assuming an initial mass function and a star formation rate, I worked out the relative production rate of black hole – white dwarf systems and stars releasing the same elements as these systems. Finally, I inferred the relative contribution of black hole – white dwarf systems and stars to the enrichment of the ISM.

Chapter 2

Nucleosynthesis physics

Nucleosynthesis is the production of chemical elements through nuclear reactions. These reactions are very dependant on the temperature and on the density, because they consist in getting positively charged nuclei, undergoing Couloumb repulsion, close enough to react. In this chapter, I describe the conditions to meet for nucleosynthesis to happen and the physical principles involved. I explain why it occurs during the Big Bang and in stars and describe their role in producing the isotopic content of the Universe today. If high densities and high temperatures can be met in others systems, such as accretion disks, viscously heated, then they must have an additional effect of the content of the ISM.

2.1 Nuclear reactions

Nuclear reactions involve interactions between the nucleons which compose the nucleus: protons and neutrons. Protons are positively charged. The charge of a nucleus X is written Z in units of elementary charge. The number of nucleons is written A. Writing ${}^{A}_{Z}X$ gives all the information of the isotope X. Isotopes of the same element can exist with different numbers of neutrons, but not all combinations are stable: the number of protons and neutrons generally tend to be the same in stable nuclei. The question of stability of nuclei brings the concept of binding energy from the strong interaction. This is the amount of energy one has to provide to completely unbind the system (i.e. separate completely all protons and neutrons in a nucleus). The binding energy corresponds to a mass difference between the sum of masses of all components of the nucleus and the mass of the bound nucleus. In nuclear reactions, if the measured mass of the products is different from the measured mass of the reactants, the system must have exchanged energy with its environment as:

$$\Delta E = \Delta m c^2, \tag{2.1}$$

which is the formula established by Einstein in his theory of special relativity in 1905. If the products of a nuclear reaction are less bound than the reactants, the reaction is qualified of exothermic: the equivalent amount of energy to ΔE is emitted in radiation. If the difference of energy is positive, the reactions takes ΔE from its environment.

Unstable nuclei decay in different processes: β^+ with emission of a positron when the number of protons dominates neutrons, β^- with emission of an electron when the number of neutron dominates protons, α with emission of a helium nucleus, typical for heavy nuclei. These reactions are described respectively as follows:

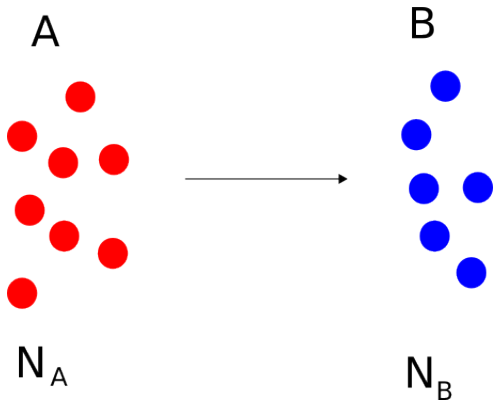

Figure 2.1: Schematic view of the reaction described by Equation 2.5. A flux of projectiles A towards targets of a different species B where N_{A} and N_{B} are the number density of each species A and B. The total number of pairs is $N_{\mathrm{A}}N_{\mathrm{B}}$.

$$ {}^{A}_{Z}X \longrightarrow {}^{A}_{Z-1}Y + e^{+} + \nu \tag{2.2} $$

$$ {}^{A}_{Z}X \longrightarrow {}^{A}_{Z+1}Y + e^{-} + \bar{\nu} \tag{2.3} $$

$$ {}^{A}_{Z}X \longrightarrow {}^{A-4}_{Z-2}Y + {}^{4}_{2}\mathrm{He} \tag{2.4} $$

These reactions are spontaneous when there exists a state of lower energy available to the nucleus.

Nuclear fission is a nuclear reaction in which the produced elements are lighter than the reactant. It can be a spontaneous decay of a heavy element or a reaction between several nuclei. Spallation is the breaking of a nucleus when hit by an energetic particle, for example a proton or a neutron.

Nuclear fusion consists in the merging of several nuclei to form a heavier nucleus and possibly other smaller products. The nucleons forming a nucleus are bound through the short range, attractive, strong nuclear interaction. To involve this type of interaction to build a new heavy nucleus, the nuclei need to become very close due to the short range interactions. But they are repelled from each other because of the repulsive Coulomb interaction decreasing as the inverse square of the distance r between the two particles. A fusion of two reactants A and B producing C and D (as in Figure 2.1),

$$ \mathrm{A} + \mathrm{B} \longrightarrow \mathrm{C} + \mathrm{D}, \tag{2.5} $$

has a given probability to happen at each instant (or happens at a certain rate).

The probability of reaction of a pair of different nuclei A and B is directly linked to the collision probability at relative velocity v between the the particles A and B: $N_{\mathrm{A}}N_{\mathrm{B}}\sigma v$, where N_i is the number density of particles i, σ is the cross section and has the dimensions of a surface. The product $N_{\mathrm{A}}N_{\mathrm{B}}$ is the number of pairs A–B. The relative velocity has a Maxwellian distribution, and the total reaction rate is the sum over all possible relative velocities. It is equal to

$$r_{\mathrm{AB}} = [\text{number of particle pairs}] \times [\text{reaction rate per pair}], \tag{2.6}$$

$$r_{\mathrm{AB}} = N_{\mathrm{A}} N_{\mathrm{B}} \langle \sigma v \rangle_{\mathrm{AB}}, \tag{2.7}$$

where the notation $\langle x \rangle$ stands for the mean value of x, here $\langle \sigma v \rangle_{\mathrm{AB}}$ is the reaction rate per particle pair. The cross section σ characterises the interaction between the two nuclei. This is a combination of the electrostatic repulsion, tunnelling effect, and intrinsic properties of the nuclei. We can give arguments for different terms involved in the cross section. Approximating the two nuclei as non interacting solid spheres, the probability of collision is proportional to the cross section $\sigma = \pi(R_{\mathrm{A}} + R_{\mathrm{B}})^2$, where R_i is the geometrical radius of a particle i. But at the scale of a nucleus size, the cross section is calculated in a quantum mechanic formalism with the de Broglie wavelength: $\propto \pi\lambda^2 \propto 1/E$. The electrostatic repulsion is characterised by the potential

$$V = \frac{1}{4\pi\epsilon_0} \frac{Z_{\mathrm{A}} Z_{\mathrm{B}} e^2}{r}. \tag{2.8}$$

Gamow (1928) showed that two particles with a relative velocity v have a probability P to penetrate each other's Coulomb repulsion which goes as

$$P \propto \exp(-2\pi \frac{Z_{\mathrm{A}} Z_{\mathrm{B}} e^2}{\hbar v}) \propto \exp(-b/\sqrt{E}) \tag{2.9}$$

due to tunnelling effect, with $b = \sqrt{2m_{\mathrm{p}}}\pi e^2 Z_{\mathrm{A}} Z_{\mathrm{B}}/\hbar$. Nuclei need to get close and penetrate this electrostatic repulsion in order to react. The probability of reaction may therefore be proportional to this penetration factor P. Finally, intrinsic properties of the nuclei (such as possible resonances) are determined by the astrphysical S factor $S(E)$, which varies slowly in function of energy in absence of resonances. From all the above reasoning, the cross section is defined as

$$\sigma(E) = \frac{S(E)}{E} \exp(-b/\sqrt{E}), \tag{2.10}$$

with a $1/E$ dependence coming from the de Broglie wavelength component of the cross section, and the exponential term from the tunnelling effect.

The reaction rate will then be integrated over the whole gas properties. We know the probability of reaction for a given relative velocity between two particles, or equivalently for a given energy. In a gas this needs to be integrated over all possible energies the gas can have at a temperature T. Assuming a relative velocity with a Maxwellian distribution (no direction privileged), the reaction rate is

$$r_{\mathrm{AB}} = N_{\mathrm{A}} N_{\mathrm{B}} \langle \sigma v \rangle_{\mathrm{AB}} = N_{\mathrm{A}} N_{\mathrm{B}} \int_O^\infty \sqrt{\frac{8}{\mu\pi}} \frac{1}{(kT)^{3/2}} S(E) \exp\left(-\frac{E}{kT} - \frac{b}{\sqrt{E}}\right) \mathrm{d}E. \tag{2.11}$$

With $S(E)$ varying slowly with the energy, $S(E) \approx S_0$, and using the method of steepest descend (or Laplace method) to get an approximate of the integral gives

$$r_{\mathrm{AB}} = N_{\mathrm{A}} N_{\mathrm{B}} \sqrt{\frac{8}{\mu\pi}} \frac{S_0}{(kT)^{3/2}} \exp(-\frac{E_0}{kT} - \frac{b}{\sqrt{E_0}}) \int_0^\infty \exp\left(-\frac{3}{4} \frac{1}{E_0 kT} \frac{(E - E_0)^2}{2}\right) \mathrm{d}E, \tag{2.12}$$

where all we have done is approximating the exponential term as a Gaussian function in order to be able to integrate it, with a common maximum to the exponential term at $E_0 = \left(\frac{bkT}{2}\right)^{2/3}$

and of width $\Delta = \frac{4}{\sqrt{3}}(E_0 kT)^{1/2}$. This can be done because only the points around the maximum participate significantly to the integral, and this method corresponds to perform a second order Taylor expansion of the term in the exponential. To show how temperature-dependent this integral is, we can evaluate it roughly (keeping in mind that I will use the results of more accurate methods in the present work when it comes to actually use reaction rates in accretion disks).

$$r_{\mathrm{AB}} \approx N_{\mathrm{A}} N_{\mathrm{B}} \sqrt{\frac{8}{\mu\pi}} \frac{S_0}{(kT)^{3/2}} \exp\left(-\frac{E_0}{kT} - \frac{b}{\sqrt{E_0}}\right) \sqrt{\frac{8\pi E_0 kT}{3}}, \tag{2.13}$$

Rearranging,

$$r_{\mathrm{AB}} \approx N_{\mathrm{A}} N_{\mathrm{B}} \sqrt{\frac{8}{\mu\pi}} \frac{S_0}{(kT)^{3/2}} \exp\left(-\frac{3E_0}{kT}\right) \sqrt{\frac{8\pi E_0 kT}{3}}, \tag{2.14}$$

We see from this that reaction rates are extremely temperature dependant. It is responsible for the differences of reaction speeds at different temperatures. The temperature is therefore going to play a major role in the present work. In practice, the cross sections and the astrophysical S factor are either computed numerically or measured in experimental laboratories. The later being very challenging in most cases (some rates provided for neutron reactions for example), astrophysicists working with nuclear reaction often have no other choice than using the cross sections predicted by theory and integrated numerically. The results give a certain number of data points for $\langle \sigma v \rangle$ for different temperatures. The cross sections are then interpolated in different exponential and power laws for completeness. This gives a direct analytical expression to use in order to find a reaction rate for a given reaction, which will be very useful in Section 5.1.

The reaction rate of a given reaction tells how fast this reaction happens and is thus linked to the production rate of new elements. In the reaction in Equation 2.5, one nucleus of species A reacts with one nucleus of species B. We say, for terminology, that A and B are burning (not to confuse with the chemical reactions in combustion).

A different reaction to consider than the one described by Equation 2.5 is the following reaction, described in Figure 2.2.

$$\mathrm{A} + \mathrm{A} \longrightarrow \mathrm{C} + \mathrm{D}. \tag{2.15}$$

In that case, the two particles reacting are of the same species. Another description of the same reaction is

$$2\mathrm{A} \longrightarrow \mathrm{C} + \mathrm{D}. \tag{2.16}$$

The number of pairs of particles here is $\frac{N_{\mathrm{A}} \times (N_{\mathrm{A}} - 1)}{2} \approx \frac{N_{\mathrm{A}}^2}{2}$ as N_{A} is large because nuclear reactions occur in dense environments. And the factor two in the denominator appears because in this reaction, projectile and target are not differentiable, so we should avoid counting the same pair twice. The corresponding reaction rate is

$$r_{\mathrm{AB}} = \frac{N_{\mathrm{A}}^2}{2} \langle \sigma v \rangle_{\mathrm{AA}}, \tag{2.17}$$

More generally, if instead of two particles A reacting, there were three of them (triple reaction): $3\mathrm{A} \longrightarrow \mathrm{C} + \mathrm{D}$, again projectiles and targets would not be differentiable, so a factor 6 would appear in the denominator (6 possible permutations of projectile/target): the same reaction of the same triplet could occur in six different orders: (123),(132),(213),(231),(312),(321)).

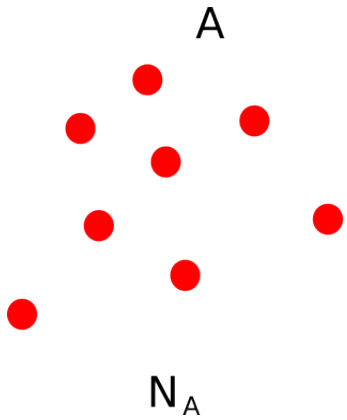

Figure 2.2: Schematic view of the reaction described by Equation 2.16 where the projectile nuclei and the target nuclei are of the same species, and the number of pairs that can react is approximately $N_{\mathrm{A}}^2/2$.

Some reactions may involve a different fraction of each species. More generally,

$$a\mathrm{A} + b\mathrm{B} \longrightarrow c\mathrm{C} + d\mathrm{D} \tag{2.18}$$

where a, b, c and d are the number of each nucleus of each species involved in the reaction. The rate at which this reaction occurs is denoted r_{AB}. It is the probability per unit time that a nuclei A react with b nuclei B. This probability is the ratio of "number of outcomes which make the event occur" and the "total number of possible outcomes". As two particles of the same species are identical, they are not labelled, there exist $a!b!$ different configurations of reaction involving the same particles and giving the same outcome, where $x! = x(x-1)(x-2)....$ In a formalism of probability theory, this is the number of all possible permutations. If nuclei were differentiable, r_{AB} would correspond to the sum over all individual probabilities. Independently from the reaction configuration, once a reaction has occurred, the particles which were involved in the reaction have reacted once, not $a!b!$ times. Therefore, the rates at which the species A and B burn are respectively

$$\dot{N}_{\mathrm{A}} = -\frac{a}{a!b!} N_{\mathrm{A}} N_{\mathrm{B}} \langle \sigma v \rangle_{\mathrm{AB}}, \tag{2.19}$$

,

$$\dot{N}_{\mathrm{B}} = -\frac{b}{a!b!} N_{\mathrm{A}} N_{\mathrm{B}} \langle \sigma v \rangle_{\mathrm{AB}}, \tag{2.20}$$

while the new elements C and D are produced at a rate

$$\dot{N}_{\mathrm{C}} = \frac{c}{a!b!} N_{\mathrm{A}} N_{\mathrm{B}} \langle \sigma v \rangle_{\mathrm{AB}}, \tag{2.21}$$

$$\dot{N}_{\mathrm{D}} = \frac{d}{a!b!} N_{\mathrm{A}} N_{\mathrm{B}} \langle \sigma v \rangle_{\mathrm{AB}}. \tag{2.22}$$

Due to the dependence of r_{AB} on N_{A} and N_{B}, the two first equations are differential equations. Due to the exponential dependence on the temperature, they are called "stiff" differential equations. Repeating this reasoning on a complete ensemble of nuclear reactions leads to a set of differential equations called a nuclear network. This is going to be described in the following section.

2.2 Nuclear networks

A nuclear network is a set of differential equations describing how fast abundances vary through nuclear reactions. Until now, we have used for simplicity the number density of species i, N_i. In a gas of mass density ρ, it is more convenient to work in units of molar fraction than keeping track of the total number of particles or the partial densities ρ_i.

The mass fraction X_i and the molar fraction Y_i for a nuclear species i are defined as.

$$X_i = \frac{N_i A_i}{\sum_j N_j A_j} = \frac{\rho_i}{\rho}, \tag{2.23}$$

$$Y_j = \frac{X_i}{A_i} = \frac{N_i}{\rho N_\mathcal{A}} \mathrm{molg}^{-1}, \tag{2.24}$$

where A_i is the number of nucleons in the nucleus, but also the molar weight in g/mol of a species. $N_\mathcal{A}$ is the Avogadro number. The differential equation 2.19 becomes

$$\dot{Y}_\mathrm{A} = -Y_\mathrm{A} Y_\mathrm{B} \rho \frac{a}{a!b!} N_\mathcal{A} \langle \sigma v \rangle_\mathrm{AB}. \tag{2.25}$$

It quantifies how fast the molar fraction of A varies if A only reacts with B, the reaction 2.18. But A may be involved in more reactions with other elements. How many more reactions burn A? Of these, is there any reaction that can be neglected? The reaction rates are actually so temperature dependant that at a given temperature, they differ of many order of magnitude, leaving a few dominating. Therefore, where a given set of reactions takes place, a lot more reactions are negligible. I am going to use this argument in the rest of this thesis to model nucleosynthesis and choose which reactions to include when it comes to building a simple nuclear reaction network. Examples of two reactions in two different networks (pp chain (proton proton chain) and CNO cycle (carbon nitrogen oxygen cycle)) burning the same elements, hydrogen to helium are given in Figure 2.3. Depending on the temperature, several orders of magnitude separate the two, which makes one completely dominating the other. It seems then appropriate to neglect the slowest reaction.

I am now going to describe a few reaction networks important in an astrophysical context: the pp-chain, CNO cycle and alpha chain. As explained, the high dependency on temperature allows us to sort different types of nuclear networks, depending on the temperature range. At temperatures lower than $10^7 K$, nuclear fusion does not occur significantly. There is no way to vanquish Coulomb repulsion. But above approximately this temperature, the lightest elements, such as hydrogen, (which contain less positive charges) can undergo fusion. The reactions occurring at the lowest temperatures are involved in the pp-chain. The set of reactions involved is:

$$\begin{cases} p + p \longrightarrow d + e^+ + \nu_e + \gamma \\ d + p \longrightarrow {}^3\mathrm{He} + \gamma \\ {}^3\mathrm{He} + {}^3\mathrm{He} \longrightarrow {}^4\mathrm{He} + 2p \\ {}^4\mathrm{He} + {}^3\mathrm{He} \longrightarrow {}^7\mathrm{Be} + \gamma \\ {}^7\mathrm{Be} + e^- \longrightarrow {}^7\mathrm{Li} + \nu \\ {}^7\mathrm{Li} + p \longrightarrow 2\,{}^4\mathrm{He} \\ {}^7\mathrm{Be} + p \longrightarrow 2\,{}^4\mathrm{He} + e^+ + \nu + \gamma \end{cases} \tag{2.26}$$

The first of these reactions is extremely slow (about 10^{10}yr, (Prialnik, 2010)) as it requires a proton to transform into a neutron while colliding with another proton, which is unlikely.

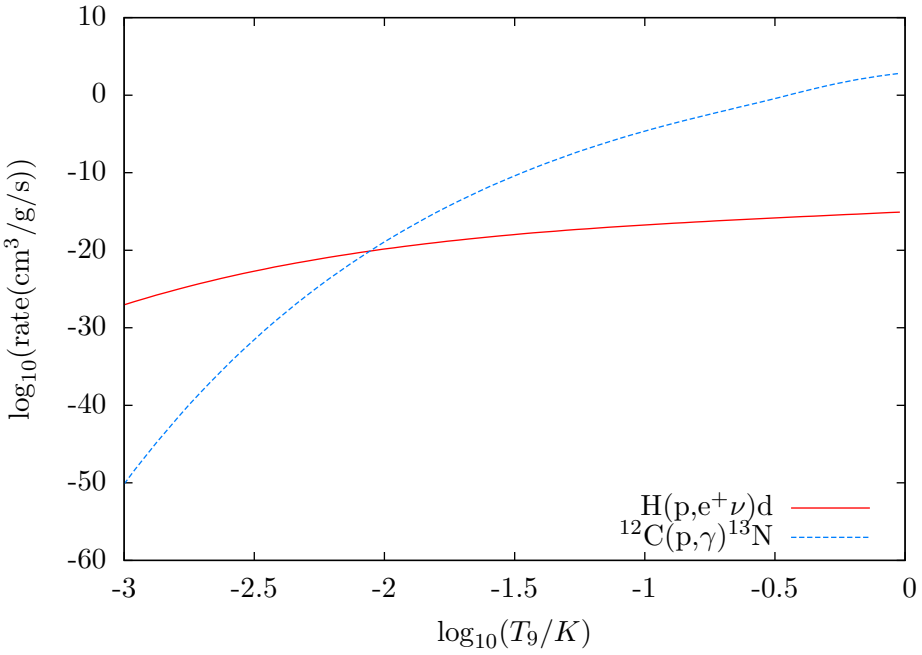

Figure 2.3: Reaction rates for two different reactions in function of temperature, with $T9 = T/10^9$K. The first steps of the pp-chain (red line), and the CNO cycle (blue dashed line) are plotted. Both networks burn hydrogen in helium. At low temperatures, the dominant reactions are pp-chain reactions, whereas at higher temperatures they are negligible (many order of magnitude lower) compared to the CNO cycle.

The CNO cycle involves a succession of proton captures (the nucleus catches a proton, seeing its charge Z and atomic number A increase of 1) by carbon and nitrogen and β^+ decays of unstable nitrogen and oxygen. Without changing the quantities of C, N and O, it transforms hydrogen into helium. The difference with the pp-chain is that it is more effective at higher temperatures.

The alpha chain is a repetition of capture of helium nuclei. This is an important reaction network as it produces heavier elements, as described by the diagonal network in Figure 2.4 (the two right angle lines describe other reactions, carbon and oxygen burning). The ideal temperature range for alpha reactions is approximately $[5 \times 10^8, 10^{10}]$K.

The networks described above have a common point: isotopes are involved in multiple reactions. The variation of the molar fraction of an isotope will therefore be a sum of the rates over all the reactions in which it plays a role, either as a reactant or a product. More generally, an element A reacting with the species i and being produced by other species j and k satisfies the differential equation

$$\dot{Y}_A = -\sum_i \rho Y_A Y_i \langle \sigma v \rangle_{Ai} + \sum_{j,k \geq j} \rho Y_i Y_j \langle \sigma v \rangle_{jk}. \tag{2.27}$$

Each of the terms corresponds to a specific reaction. All the reactions have a different temperature dependency, but the rates still vary very fast with temperature. This point is extremely important because it is responsible for a numerical challenge in the integration of these differential equations, qualified of "stiff". The numerical treatment to solve such equations is

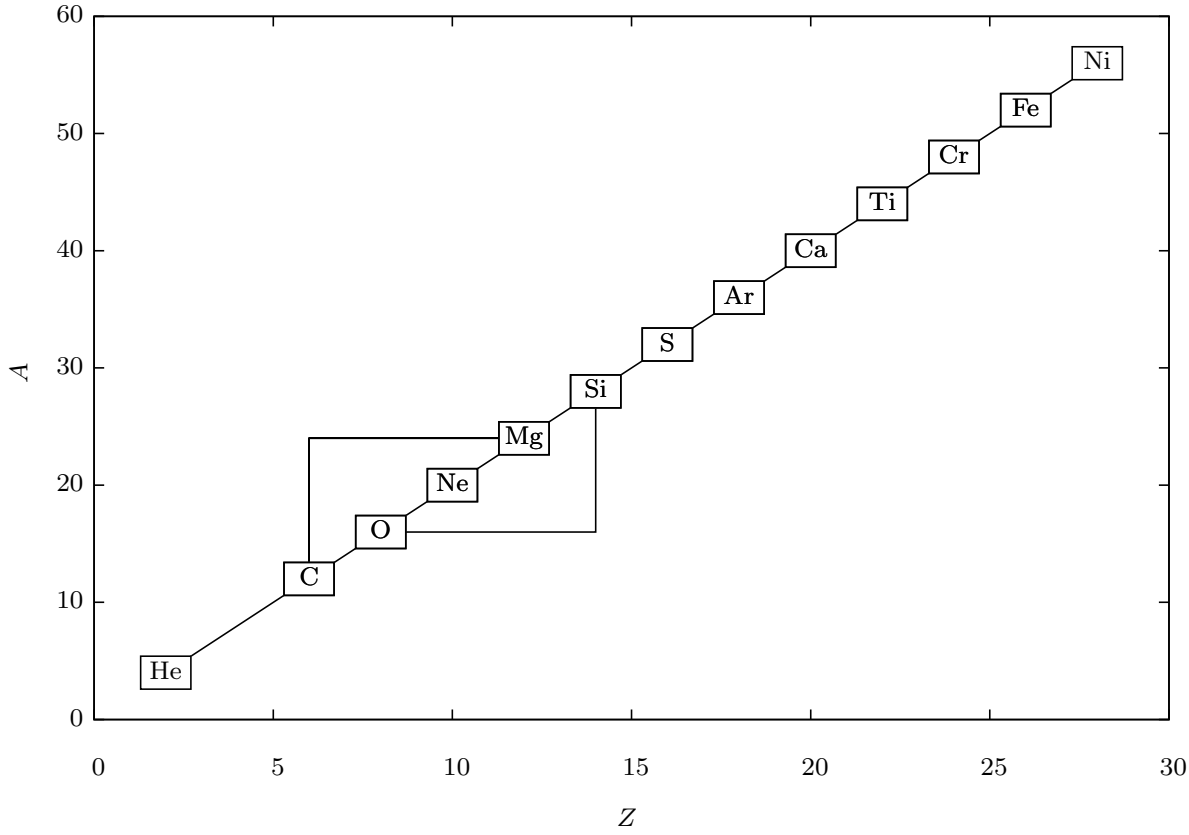

Figure 2.4: Alpha chain network. Atomic number A in function of the atomic charge Z of elements. Each element is produced by the reaction of the closest element of lower mass with an alpha particle, except for the following cases: the first step from helium to carbon occurs through the triple alpha reaction involving three helium nuclei fusing together. Carbon also reacts with itself, producing magnesium. Oxygen, when reacting with itself, produces silicon.

described in detail in the Appendix A. There are as many different differential equations as species involved in the nuclear network. For example, 13 isotopes are involved in the network describing the alpha chain in Figure 2.4, so there is a set of 13 differential equations describing the evolution of such systems.

2.3 Big Bang

Current cosmology theories agree on that the Universe used to be hotter and denser than it is now. In 1929, Edwin Hubble measured the redshift of galaxies, giving their radial velocity with respect to us and their distances (Hubble, 1929). Lundmark also did in 1925 (Lundmark, 1925). They found that the velocity increases with the distance which separate them from us. These observations together with the cosmic microwave background give strong evidence for a primordial explosion, named Big Bang. During this explosion, the universe was dense and hot enough for nuclear reactions to occur.

The big bang is characterized by very large temperatures and densities, but they are decreasing very fast with time t(s), as

$$T_9 = 13.8 t^{-1/2} \mathrm{K} \tag{2.28}$$

$$\rho = 3.3 \times 10^4 \eta T_9^3 \mathrm{g/cm^3}, \tag{2.29}$$

where η is the baryon to photon ratio (e.g. MacDonald & Mullan, 2009).

Starting with protons and neutrons emerging from the primordial quark soup, the equilibrium between protons and neutrons is provided by protons forming neutrons through collisions between electrons and neutrinos, while neutrons decay into protons. When the density decreases, the neutrinos decouple and the balance is not maintained: the neutrons decay faster. But we still find neutrons today. Not all of them decayed. When they are bound in an atomic nucleus, they are more stable. The first nucleus to be synthesised during the Big Bang is the deuterium, composed of a proton and a neutron, saving the neutrons which will build heavier elements. Later are synthesised isotopes of helium, lithium, beryllium and boron (Vangioni-Flam et al., 2000). Then, density and temperature are too low to build more elements. Fortunately, gravitation will help supplying denser and hotter environments in objects such as stars.

2.4 Stars

After the Big Bang, at a redshift of about $z = 20$ (Schneider, 2015), the first stars form. Emerging from clouds of gas which underwent self gravitational collapse, they are subject to their own gravity and supported by gas pressure. The temperature in their core is very high and allows nuclear fusion. Through their evolution, stars undergo different burning stages: main sequence, where they spend most of their life time with hydrogen burning slowly in the core, then hydrogen burning in a shell, red giant branch, core helium burning, and finally heavy elements burning, up to iron for the most massive stars. As star form from the self gravitational collapse of a gas cloud, the first stars have the same composition as the material they were formed of: the big bang elements, hydrogen and helium.

During the main sequence, hydrogen burns in helium through two processes: the pp chain and CNO cycle, one dominating the other in function of the temperature of the stellar core, i.e. depending on the mass of the star, see Figure 2.3. The life time of a star on the main sequence is $\propto M^{-2}$. Low mass stars spend a very long time on the main sequence whereas massive stars evolve faster because their cores are hotter, so nuclear fusion is more rapid. Old stars have low mass, and their composition reflects the composition of the past universe. They are metal poor. Helium burning starts when hydrogen in the stellar core is exhausted. The core contracts and heats, allowing the next burning stage (helium burning) to take place. Carbon is produced in the core from the triple alpha reaction, which is the step from helium to carbon in Figure 2.4. Oxygen is produced as well. The mass of the star determines the next processes: low mass stars, due to their limited core temperature, cannot go on the next burning stages and become white dwarfs, containing mainly carbon and oxygen. Massive stars burn carbon and oxygen and produce heavier elements. Stars more massive than about $8 M_\odot$ end their lives in a core collapse supernova. They synthetised heavy elements up to iron, the most stable element. During this energetic explosion, more nucleosynthesis happens: most of the core elements are photodisintegrated and produce a lot of neutrons, active in s- and r-processes which produce elements heavier than iron. Whether s- and r- process elements observed today come from supernovae or other processes is not

well known. The ejected material is released to the ISM. In particular, the outer layers of the star, containing all the products of the stellar nucleosynthesis are expelled. The aim of the current thesis is to see how accretion disks around black hole could compete against such enrichment. A direct consequence of stellar evolution is that since the composition of the atmosphere of a main sequence star keeps traces of the medium in which the star was born, the first generation stars and the next generation stars do not have the same composition (abundances in elements). While the first generations are metal poor, younger stars contain more heavy elements released by the former stellar generations, and are metal rich.

Chapter 3

Accretion disks physics

Does nucleosynthesis happen in accretion disks? To answer this question, we need to know what determines the temperature and the density in accretion disks. What is the physics involved in accretion disks and what heats them? In this chapter, I explain qualitatively and quantitatively what makes an accretion disk hot and dense, based on Frank et al. (2002). A key to high density and high temperature in accretion disks is the compactness of the central object, because of the tidal forces it provides, leading to large differential velocities responsible for viscous heating. I show the derivation of the equations of the disk model I used, namely the Shakura & Sunyaev (1973) disk model. This knowledge on disks will help us to answer the nucleosynthesis question in the next chapter.

3.1 Accretion physics

We saw in the previous sections that nuclear reactions take place in hot environment. We described the origin of high temperatures during the Big Bang (initial explosion) and in stars (virial temperature). Another mechanism increasing the temperature is the dissipation of mechanical energy energy into heat. This process happens in accretion disks through viscous dissipation. We observe this process in X-ray binaries, containing a star transferring mass to its neutron star companion, to which it is gravitationally bound. Material from one star flows onto the other. As it generally has angular momentum, the material first forms a disk and then accretes onto the other star. The inner disk is heated such that the corresponding black body peak (wavelength at which the thermal emission of radiation is maximum) is located in the X-ray. This heating can be quantified: the gas orbiting an accreting object undergoes a differential rotation: the gas closer to the central object rotates faster than the gas further, exerting torques. A general description of accretion disks can be obtained from mass and angular momentum conservation laws.

A first approximation of gas orbiting a central object of mass M, from a distance R, is to assume it has a Keplerian angular velocity $\Omega = \Omega_{\rm K}$, which means no other forces than gravity are exerted on the gas

$$\Omega = \sqrt{\frac{GM}{R^3}}, \tag{3.1}$$

where G the gravitational constant. Mass conservation in the disk is expressed with the

surface density $\Sigma = \rho H$ where ρ is the mass density and H is the scale-height:

$$R\frac{d\Sigma}{dt} + \frac{\partial}{\partial R}(R\Sigma v_R) = 0, \tag{3.2}$$

with v_R the radial velocity of the gas, characterising the accretion. Angular momentum is exchanged between neighbouring disk rings because viscous torques $\mathcal{T}$ originate from turbulent motion characterised by a random velocity $\tilde{v}$ on a length scale λ in the disk. Turbulent motion leads disk particles to move radially and transport their angular momenta J at another radius. If we consider a ring of gas, there will be on average a flux of angular momentum, from both the outer ring and the inner ring, with each ring characterised by its own angular momentum. The flux of angular momentum J from the outer ring to the inner ring will be $\frac{\mathrm{d}J}{\mathrm{d}t} = \dot{J} = 2\pi R\rho\tilde{v}HR^2\Omega$. The net flux from each side of this ring can be written as $\dot{J}_{\mathrm{net}} = 2\pi R\rho\tilde{v}HR^2\frac{\mathrm{d}\Omega}{\mathrm{d}R}\mathrm{d}R$. And as this happens on the typical scale λ, we finally have an expression for the torque:

$$\mathcal{T}(R) = \dot{J} = 2\pi R\rho\tilde{v}HR^2\lambda\frac{\mathrm{d}\Omega}{\mathrm{d}R}. \tag{3.3}$$

The quantity $\nu = \lambda\tilde{v}$ is the kinematic viscosity. The final expression for the viscous torques is therefore given by

$$\mathcal{T}(R) = 2\pi R\nu\Sigma R^2\frac{\mathrm{d}\Omega}{\mathrm{d}R}. \tag{3.4}$$

We can now write the angular momentum conservation equation. This is the same equation as for mass conservation, but the presence of a torque induces a change in angular momentum:

$$R\frac{\partial}{\partial t}(\Sigma R^2\Omega) + \frac{\partial}{\partial R}(R\Sigma v_R R^2\Omega) = \frac{1}{2\pi}\frac{\partial}{\partial R}(2\pi R^3\Sigma\nu\frac{d\Omega}{dr}) = \frac{1}{2\pi}\frac{\partial\mathcal{T}}{\partial R}. \tag{3.5}$$

If one develops this expression, simplifies it using the mass conservation equation above, assuming a Keplerian orbital velocity, and inserting the expression for the viscous torques $\mathcal{T}(R)$, one finds

$$R\frac{\partial\Sigma}{\partial t} = -\frac{\partial}{\partial R}(R\Sigma v_{\mathrm{R}}) = -\frac{\partial}{\partial R}\left(\frac{1}{2\pi(R^2\Omega)'}\frac{\partial\mathcal{T}}{\partial R}\right), \tag{3.6}$$

where $x' = \frac{\mathrm{d}x}{\mathrm{d}R}$. The radial derivative of the torque is

$$\frac{\partial\mathcal{T}}{\partial R} = -3\pi\frac{\partial}{\partial R}(\nu\Sigma R^2\sqrt{GMR}) \tag{3.7}$$

So the mass continuity equation becomes

$$\frac{\partial\Sigma}{\partial t} = \frac{3}{R}\frac{\partial}{\partial R}\left(\sqrt{R}\frac{\partial}{\partial R}(\nu\Sigma\sqrt{R})\right) \tag{3.8}$$

This equation is very general and represents the evolution of the disk surface density. It is solvable analytically in a certain number of different conditions, explained in the next section.

The radial velocity due to viscous dissipation is

$$v_{\mathrm{R}} = \frac{3}{\Sigma\sqrt{R}}\frac{\partial}{\partial R}(\nu\Sigma\sqrt{R}). \tag{3.9}$$

In addition to the gas dynamics going on in the disk, interaction between electromagnetic radiation and matter plays a major role. Through the viscous processes, the material in

the disk drifts inwards. Gravitational energy is transformed into heat by dissipation. This induces heating, responsible for a temperature rise. If all this energy is emitted as a black body radiation, the disk becomes luminous, with a luminosity equal to the gravitational power of material accretion. If the central object accretes at a rate $\dot{M}$, the accretion power is

$$L_{\rm acc} = \frac{GM\dot{M}}{R}. \tag{3.10}$$

How this energy is transported (radiation, advection) depends on disk models and will be discussed in the next sections.

Imagining that all this energy is emitted in radiation, we can introduce the useful concept of Eddington maximum accretion rate. Electrons are affected by electromagnetic radiation and undergo Thomson scattering. They experience a force $\sigma_{\rm T}S/c$ where $\sigma_{\rm T}$ is the Thomson cross section, S is the radiation flux and c the speed of light. This force is in the radial direction and directed outwards, and is proportional to the radiation flux. Let us consider a disk of which the material is dominated by ionized hydrogen. As electrons are negatively charged, they drag protons in their motion outwards, through the Coulomb force. At a given distance from the central object, there exists therefore an electromagnetic flux (or a luminosity) for which this force will overcome the gravitational force, directed inwards. There exists therefore a threshold luminosity above which material from the gas will not be gravitationally bound, and thus not be accreted any more. This limit is called Eddington Luminosity, and one finds it by equating the gravitational force inwards to the radiation pressure force outwards: $\frac{\sigma_{\rm T}L_{\rm Edd}}{R^2} = \frac{GM\dot{M}}{R^2}$. The luminosity threshold is therefore equal to $L_{\rm Edd} = \frac{4\pi GMm_{\rm p}c}{\sigma_{\rm T}}$. Luminosities greater than this limit are qualified of "super-Eddington". Although many assumptions were made to describe the Eddington Luminosity, this reasoning is of particular importance to argue about outflows. If the systems considered in the next chapters have super-Eddington accretion, then one should expect outflows from the disk. These outflows depend on the opacity of the material when the disk is not made of protons and electrons only.

Equating the accretion power $L_{\rm acc}$ to the Eddington luminosity $L_{\rm Edd}$, we find an accretion rate threshold, the Eddington accretion rate:

$$\dot{M_{\rm Edd}} = \frac{4\pi R_* m_{\rm p} c}{\sigma_{\rm T}}, \tag{3.11}$$

where R_* is the central object radius, $m_p = 2\times10^{-27}$kg, $c = 3\times10^8$ms^{-1}, $\sigma_T = 7\times10^{-29}$m^2. A higher accretion rate is thought to power winds. Material cannot be accreted faster onto the central object. Observational evidence for outflows powered by super Eddington accretion is provided for the black hole system SS433, discovered by Stephenson & Sanduleak (1977), with supercritical accretion leading to powerful winds (Fabrika, 2004).

When the central object is a black hole, the surface is not well defined and we estimate the gravitational potential energy loss from infinity to its event horizon radius (which is the Schwarzschild radius in the Schwarzschild metric, for non rotating black holes) $R_{\rm SCH} = \frac{2GM_{\rm BH}}{c^2}$. This radius defines the distance from the black hole centre where the escape speed is the speed of light. Not all the gravitational energy will necessarily be radiated, some could be retained by the black hole. Therefore, we introduce the factor η which quantifies the fraction of energy radiated. It usually takes the value 0.1 (Frank et al., 2002).

$$L = \eta\frac{GM\dot{M}}{R_{\rm SCH}} \tag{3.12}$$

The Eddington accretion rate is therefore

$$\dot{M}_{\rm Edd} = \frac{4\pi G M_{\rm BH} m_{\rm p}}{\eta \sigma_{\rm T} c} \approx 2 \times 10^{-8} m_{\rm BH} M_\odot {\rm yr}^{-1} \tag{3.13}$$

where $m_{\rm BH}$ is the black hole mass in units of solar mass.

3.2 Steady accretion disk models

To describe an accretion disk analytically, the previous equations need to be simplified. Simplifications consist in identifying which physical processes dominate in different regimes, and assume other processes can be neglected. Several simplifications exist in the literature, leading to different models. Three of them are introduced quickly below.

3.2.1 Thin, or Shakura-Sunyaev model

This disk model was developed by Shakura & Sunyaev (1973), and describes a geometrically thin disk (small scale height H), neglecting pressure forces. In this model, gas loses angular momentum according to a viscosity prescription such that λ, the typical scale for turbulent eddies, is less than the scale height H of the disk, and the typical velocity of these turbulent eddies $\tilde{v}$ is less than the sound speed $c_{\rm s}$ of the disk material. As a result, it is written that the viscosity is $\nu = \alpha c_{\rm s} H$ where α is a constant less than 1. This prescription permits to solve the equations above. Additionally, kinetic energy due to this turbulence becomes heat in the disk, and this heat is re-emitted as a black body radiation.

3.2.2 Slim disk

These disk models are similar solutions to above, except from the energy equation. They describe super-Eddington accretion better than the thin disks because they take advection of energy into account whereas thin disks do not (Abramowicz et al., 1988). At high accretion rates, the drift time-scale becomes shorter than the radiation time-scale. Not all the energy coming from viscous heating is radiated away. A fraction of it is transported by the material during its motion.

3.2.3 Advection Dominated Accretion Flows

ADAFS, or Advection Dominated Accretion flows, are completely dominated by advection. These disk models take into account pressure forces, in particular radiation pressure. The gas is sub-Keplerian and geometrically thick. The temperature is almost virial. They do not apply for extremely high accretion rates (Narayan & Yi, 1994).

The three models described in these three sections present disks in different regimes. The thin disk provides the simplest physics and is what the present thesis is based on. But other models exist which could describe better other regimes, depending on the accretion rate for example.

3.3 The Thin disk Model

In this section, I establish the equations used in the accretion disk model which my results will be based on. The derivation is going to be detailed, following Frank et al. (2002) and Pringle

(1981) leading to the solution of Shakura & Sunyaev (1973), to allow a deep discussion of the results and assumptions made later-on. The thin, steady disk is the simplest existing model and leads to an analytical solution thanks to the alpha prescription. I used in my program this solution in order to reduce complexity and computational time.

Vertical component: The thin approximation, assuming a Keplerian disk velocity and that the pressure gradient is vertical, permits the decoupling of vertical and radial structure of the disk. Therefore, writing the hydrostatic equilibrium in the z direction of cylindrical coordinates leads us to an expression for the mass density in the disk in function of the isothermal sound speed $c_\mathrm{s} = P/\rho$ and the orbital velocity v_ϕ,

$$\rho(z) = \rho_\mathrm{c} \exp\left(-\frac{z^2}{2H^2}\right), \tag{3.14}$$

where the scale-height is such that $H^2 = c_\mathrm{s}^2 \frac{R^3}{GM_*} = R^2 c_\mathrm{s}^2 / v_\phi^2$.

Mass and angular momentum conservation laws If the disk parameters change slower than changes affect the disk structure (time-scale of radial inflow), then an assumption of steady state (cancelling time derivatives) is a good approximation. The term $R\Sigma v_R$ is then constant in Equation 3.2 and defines a steady accretion rate characterizing mass conservation:

$$\dot{M} = 2\pi R \Sigma v_R, \tag{3.15}$$

where $\dot{M}$ is the accretion rate, the flow of mass through a surface of constant radius. The angular momentum conservation Equation 3.5 can be integrated over the radius as

$$R\Sigma v_\mathrm{R} R^2 \Omega = \frac{\mathcal{T}}{2\pi} + \frac{C}{2\pi} = R^3 \Sigma \nu \frac{\mathrm{d}\Omega}{\mathrm{d}R} + \frac{C}{2\pi}, \tag{3.16}$$

where $\mathcal{T}$ is the viscous torque exerted on the disk, and the constant C characterises the torque exerted by the central object onto the inner edge of the accretion disk. In the example of a possibly rotating star as a central object, the material at the surface of the star rotates slower than its Keplerian angular velocity. If further from the star, the disk material is Keplerian, then it will need to slow down before reaching the star surface (for continuous boundary conditions). If this happens at radius r_slow, then

$$\frac{\mathrm{d}\Omega}{\mathrm{d}R}(r_\mathrm{slow}) = 0. \tag{3.17}$$

We can use this argument in Equation 3.16 to find

$$\Sigma v_R \Omega(r_\mathrm{slow}) r_\mathrm{slow}^3 = \frac{C}{2\pi}, \tag{3.18}$$

which gives us an expression for C. If this boundary layer between the star surface and r_slow is thin, then $r_\mathrm{slow} \approx R_*$ and we may rewrite C as

$$C = 2\pi \Sigma v_\mathrm{R} \Omega_\mathrm{K}(R_*) R_*^3, \tag{3.19}$$

where Ω_K stands for the Keplerian rotation velocity. Using the continuity equation 3.15 for the accretion rate, this can be rewritten as

$$C = -\dot{M}\sqrt{GMR_*}. \tag{3.20}$$

The angular momentum conservation equation 3.16 is finally

$$-\nu\Sigma\frac{\mathrm{d}\Omega}{\mathrm{d}r} = -\Sigma\Omega V_{\mathrm{R}} - \frac{\dot{M}}{2\pi R^3}\sqrt{GM_* R_*}. \tag{3.21}$$

If the gas rotates at a Keplerian velocity, then $\Omega = \Omega_K = \sqrt{\frac{GM_*}{R^3}}$ and we can rearrange this equation as the viscous surface density equation:

$$\nu\Sigma = \frac{\dot{M}}{3\pi}\left(1 - \sqrt{\frac{R_*}{R}}\right). \tag{3.22}$$

Energy equation: The thin disk model assumes that heating of the disk comes from viscous dissipation, and that the cooling mechanism is emission of radiation, close to black body. The energy production term is noted as Q_{visc} and the cooling term Q_{rad}. The viscous dissipation rate responsible for the heating process is provided by the work of the viscous torque given by

$$\Omega\frac{\partial\mathcal{T}}{\partial R}\mathrm{d}R = \left(\frac{\partial}{\partial R}(\mathcal{T}\Omega) - \mathcal{T}\frac{\mathrm{d}\Omega}{\mathrm{d}R}\right)\mathrm{d}R. \tag{3.23}$$

The local rate of energy loss per unit surface D corresponds the second term in the parenthesis $\mathcal{T}\frac{\mathrm{d}\Omega}{\mathrm{d}R}\mathrm{d}R = 2\times 2\pi R D(R)\mathrm{d}R$, where the factor 2 comes from the presence of two sides of the disk. Therefore, the dissipation rate per unit surface is

$$D(R) = \frac{\mathcal{T}}{4\pi R}\frac{\mathrm{d}\Omega}{\mathrm{d}R} = \frac{9}{8}\nu\Sigma\frac{GM_*}{R^3}. \tag{3.24}$$

where we assumed a Keplerian disk for the last equality. We can use 3.22 to replace $\nu\Sigma$ and completely determine the dissipation rate as a function of central body mass, accretion rate and radius:

$$D(R) = \frac{3GM_*\dot{M}}{4\pi R^3}\left(1 - \sqrt{\frac{R_*}{R}}\right). \tag{3.25}$$

The energy loss per unit surface through one face of the disk is:

$$Q_{\mathrm{visc}} = D(R) = \frac{3GM_*\dot{M}}{8\pi R^3}\left(1 - \sqrt{\frac{R_*}{R}}\right). \tag{3.26}$$

The cooling term by radiation is given by the flux of electromagnetic radiation through an horizontal surface (z constant in cylindrical coordinates). Integrated from the mid plane ($z = 0$) to one face of the disk, it is

$$F = \frac{4\sigma}{3\tau}T_{\mathrm{c}}^4 = Q_{\mathrm{rad}} \tag{3.27}$$

with σ is the Stefan-Boltzmann constant, τ is the optical depth of the gas in the mid-plane and T_{c} is the mid-plane temperature. If these are the mechanisms of energy transfer, then we can write $Q_{\mathrm{visc}} = Q_{\mathrm{rad}}$ and find

$$\frac{4\sigma}{3\tau}T_{\mathrm{c}}^4 = \frac{3GM_*\dot{M}}{8\pi R^3}\left(1 - \sqrt{\frac{R_*}{R}}\right). \tag{3.28}$$

Equation of state (EOS): The equation of state relates the thermodynamical variables P, ρ, T to each other. The force contributing to the pressure are normally the gas pressure $P_{\rm gas} = \frac{\rho k T}{\mu m_{\rm H}}$, where k is the Boltzmann constant, μ the molecular mass, m_H the mass of hydrogen and the radiation pressure. The radiation pressure term is neglected in the present model (Shakura & Sunyaev, 1973): $P = P_{\rm gas}$. This assumption is part of the thin disk approximation: as we neglect pressure coming from radiation, we assume the gas is optically thick, comforting the near black body assumption.

Opacity law and α prescrition: The optical depth τ is defined as $\tau = \Sigma\kappa_{\rm R}$ where $\kappa_{\rm R}$ is the mean Rosseland opacity. It is an average over the wavelength. We therefore neglect variations of opacity with the wavelength and assume the disk material reacts identically to all wavelengths. If the opacity is dominated by ionization of atoms (bound-free absorption) and by free electron scattering (free-free absorption), then Kramer's law for opacity is adopted:

$$\kappa_{\rm R} = 5 \times 10^{24} \rho T^{-7/2} {\rm cm}^2 {\rm g}^{-1} \tag{3.29}$$

For the viscosity, the thin model uses the Shakura & Sunyaev (1973) prescription. As written in Section 3.1, the kinematic viscosity is $\nu = \lambda\tilde{v}$ where λ is a characteristic scale for the turbulence (size of turbulent eddies), and $\tilde{v}$ is the velocity of random motions. The argument of Shakura & Sunyaev (1973) is that the size of the turbulent eddies should not be greater than the scale height of the disk: $\lambda < H$ and that in the absence of shocks, the turbulent motion velocity should not be greater than the sound speed: $\tilde{v} < c_{\rm s}$. Therefore we can constrain the product of these two quantities giving kinematic viscosity as

$$\nu = \lambda\tilde{v} < H c_{\rm s}, \tag{3.30}$$

so we can introduce the dimensionless paramter $\alpha < 1$:

$$\nu = \alpha c_{\rm s} H. \tag{3.31}$$

Another approach of this parametrisation is that locally, the problem is not dimensional: looking at Equation 3.4, the torques per unit volume depend only on the orbital angular velocity Ω: the torque density is equal to $\frac{3}{2}\rho\nu\Omega$, (Brandenburg et al., 1995), hence the scaling with α.

Disk radial structure: All the above equations permit to find an analytical solution for the radial structure of the disk. Taking Equation 3.28 and doing some algebra using the expression of the previous paragraph for the optical depth and the EOS, using $\Sigma = \rho H$, $H/R = c_{\rm s}/v_\phi$ and $c_{\rm s} = \sqrt{kT/(\mu m_{\rm p})}$, we find a relation between the surface density and the temperature.

$$T = D(R)^{1/8} \Sigma^{1/4} M_*^{1/16} R^{-3/16} A^{-1/8} \tag{3.32}$$

with $A = \frac{5\sigma}{3\times5\times10^{20}}\sqrt{\frac{k}{G\mu m_{\rm p}}}$. Injecting this expression in Equation 3.22 and using $\nu = \alpha c_{\rm s} H$ and the expression for H as above,

$$\Sigma^{5/4} = \frac{\dot{M}}{3\pi} f^{7/2} \alpha^{-1} C B^{-1/8} A^{1/8} M_*^{1/16} R^{-15/16} G^{1/2}, \tag{3.33}$$

where we named the constants $B = \frac{3H}{8\pi}$, $C = \frac{\mu m_{\rm p}}{k}$ and $f = \left(1 - \sqrt{\frac{R_*}{R}}\right)^{1/4}$. The surface density is now completely determined as a function of central object mass, accretion rate, α and radial position. Replacing the constants A, B and C by their expression, one finally gets

$$\Sigma = \left[\frac{4 \times 8\sigma}{3 \times 3 \times 3 \times 5 \times 10^{20}}\right]^{1/10} G^{1/4} \left(\frac{\mu m_{\rm p}}{k}\right)^{3/4} (3\pi)^{-7/10} M_*^{1/4} \dot{M}^{7/20} \alpha^{-4/5} f^{14/15} R^{-3/4}. \tag{3.34}$$

Following Frank et al. (2002), we introduce the dimensionless quantities $m_1 = M_*/M_\odot$ $R_{10} = R/10^{10}$cm and $\dot{M}_{16} = \dot{M}/10^{16}$g/cm^3

$$\Sigma = \left[\frac{32\sigma}{27 \times 5.10^{20}}\right]^{\frac{1}{10}} G^{\frac{1}{4}} \left(\frac{\mu m_{\rm p}}{k}\right)^{\frac{3}{4}} (3\pi)^{-\frac{7}{10}} m_1^{\frac{1}{4}} M_\odot^{\frac{1}{4}} \dot{M}_{16}^{\frac{7}{20}} (10^{13})^{\frac{7}{20}} \alpha^{-\frac{4}{5}} f^{\frac{14}{15}} R_{10}^{-\frac{3}{4}} (10^8)^{-\frac{3}{4}}. \tag{3.35}$$

Replacing all constants by their numerical values and taking the mean molecular weight $\mu \approx 0.615$ (ionized solar-like composition) gives the expression for the surface density in Equation 3.36. Injecting this expression into the temperature Equation 3.32 gives directly the temperature. The scale height H follows directly. The midplane density $\rho = \Sigma/H$. The radial drift velocity is deduced from the mass conservation Equation 3.15.

$$\begin{cases} \Sigma = 5.29\alpha^{-4/5} \dot{M}_{16}^{7/10} m_1^{1/4} R_{10}^{-3/4} f^{14/5} & \text{g/cm}^2 \\ H = 1.7 \times 10^8 \alpha^{-1/10} \dot{M}_{16}^{3/20} m_1^{-3/8} R_{10}^{9/8} f^{3/5} & \text{cm} \\ \rho = 3.1 \times 10^{-8} \alpha^{-1/10} \dot{M}_{16}^{11/20} m_1^{5/8} R_{10}^{-15/8} f^{11/15} & \text{g/cm}^3 \\ T_{\rm c} = 1.4 \times 10^4 \alpha^{-1/5} \dot{M}_{16}^{3/10} m_1^{1/4} R_{10}^{-3/4} f^{6/5} & \text{K} \\ \tau = 190\alpha^{-4/5} \dot{M}_{16}^{1/5} f^{4/5} & \\ \nu = 1.8 \times 10^{14} \alpha^{4/5} \dot{M}_{16}^{3/10} m_1^{-1/4} R_{10}^{3/4} f^{6/5} & \text{cm}^2/\text{s} \\ v_{\rm R} = 2.7 \times 10^4 \alpha^{4/5} \dot{M}_{16}^{3/10} m_1^{-1/4} R_{10}^{-1/4} f^{-14/5} & \text{cm/s} \\ f = \left(1 - \sqrt{\frac{R_*}{R}}\right)^{1/4} & \end{cases} \tag{3.36}$$

These are the equations governing the thin accretion disk solution. Using them and doing some algebra, I worked-out useful homology relations. Noting first that the temperature decreases as the radius increases, we can expect the limiting cases to host nuclear burning at the inner edge of the disk. It is therefore convenient to write the radius in units of Schwarzschild radii $R_{\rm SCH}$, natural limiting scale of the inner disk edge. $R_{\rm SCH} \propto m_1$. Similarly, as the limiting case of mass accretion rate is the Eddington limit rate rate $\dot{M}_{\rm Edd}$, Equation 3.13, it is also convenient to work in units of$\dot{M}_{\rm Edd}$. For a given disk viscosity α, the disk temperature scales as

$$T \propto \left(\frac{M_{\rm BH}}{M_\odot}\right)^{-1/5} \left(\frac{\dot{M}}{\dot{M}_{\rm Edd}}\right)^{3/10} \left(\frac{R}{R_{\rm SCH}}\right)^{-3/4} \text{K}, \tag{3.37}$$

and the density scales as

$$\rho \propto \left(\frac{M_{\rm BH}}{M_\odot}\right)^{-7/10} \left(\frac{\dot{M}}{\dot{M}_{\rm Edd}}\right)^{11/20} \left(\frac{R}{R_{\rm SCH}}\right)^{-15/8} \text{g/cm}^3. \tag{3.38}$$

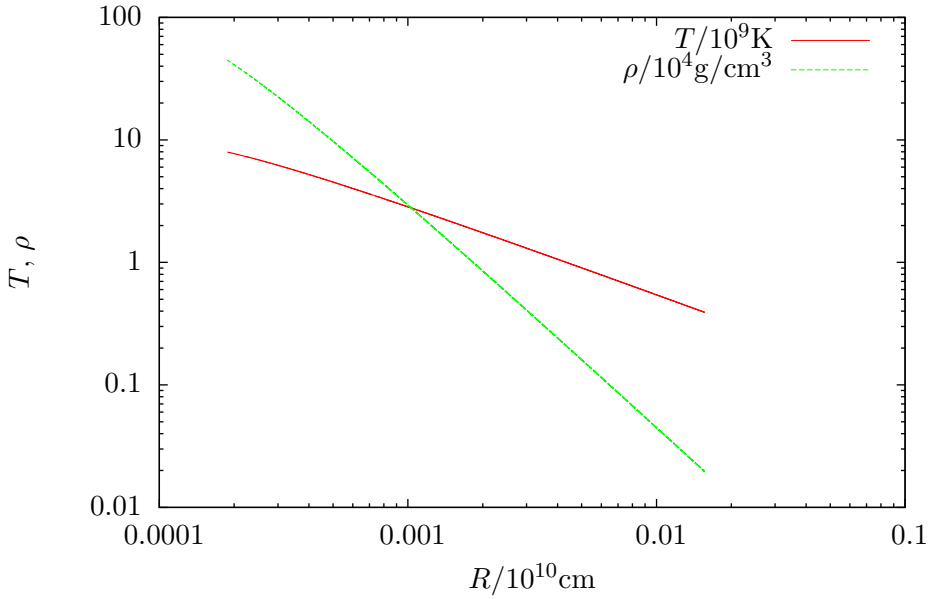

Figure 3.1: Temperature and density in an accretion disk around a $3M_\odot$ black hole, with an accretion rate of $10^6\dot{M}_{\rm Edd}$ and a viscosity parameter $\alpha = 0.01$.

At a given radius, say a few Schwarzschild radii, the temperature increases with increasing accretion rate and decreasing black hole mass. Same goes for the density. To get a first idea regarding nuclear reactions, a simple question to consider is: for a given black hole mass, what order of magnitude of accretion rate is needed for nucleosynthesis to happen? I worked-out a rough estimate with a black hole of $10M_\odot$, which is a common mass, measured for black holes in X-ray binaries (Özel et al., 2010), and a radius of about $3R_{\rm SCH}$. With a viscosity of $\alpha = 10^{-2}$ and an arbitrary burning temperature of about $5 \times 10^9 K$ (with these high temperatures, nucleosynthesis should, if fast enough compared to the accretion, happen in the disk), then the accretion rate needed is $10^6\dot{M}_{\rm Edd}$. The temperature and density profiles are plotted in Figure 3.1 in such conditions. This consideration tells us that the temperatures in the accretion disk can reach ignition temperatures, but the accretion rate is overwhelmingly large. Such an event is not impossible and is a sign of very powerful disk outflows. We can already have the intuition that the events hosting nucleosynthesis will happen rarely, for specific cases only. Favourable conditions are there in principle, but whether burning actually happens or not will depend on the accretion time-scale as well: does the gas burn faster than it accretes? This question is treated in details in the next chapter.

Chapter 4

Which disks host nucleosynthesis?

In this chapter, two theoretical experiments are described. I carried them out in order to determine which systems in general, and which accretion disks in particular, host nucleosynthesis and should be simulated in detail. Firstly, I determined the two competing, characteristic time-scales of black hole accretion and nucleosynthesis: the viscous time-scale (Equation 4.1) and the nuclear burning time-scale (Equation 4.2). With this, I investigated the burning conditions in the disk of one specific theoretical black hole accretion disk, with a given black hole mass and a given accretion rate. I studied in detail the evolution of a blob of gas being accreted and chose to compare the results obtained to the best nucleosynthesis factories we know for heavy elements: stellar cores. From this simulation, I determined the important variables necessary for nuclear reactions to happen: temperature and density. Then, I investigated the burning conditions in a large range of black hole masses and accretion rates; and determined which pairs $(M, \dot{M})$ are favourable to nucleosynthesis. Finally, I considered the mechanisms producing these accretion rates, namely
(1) accretion of matter by a black hole from a companion star,
(2) spherical accretion by a black hole inside a gas cloud (Bondi accretion),
(3) accretion disk and black hole formed from the merger of compact objects.
Once these systems were determined, I studied them separately and concluded whether nucleosynthesis could take place or not.

4.1 Time-scales: Nucleosynthesis versus accretion

The density and the temperature of a material determines nucleosynthesis (Chapter 2). In an accretion disk, nuclear burning is significant only if it burns an important fraction of the disk material before it gets accreted or leave the disk in winds. There is therefore a competition between two time-scales: the nuclear burning time-scale, and the accretion time-scale. The accretion, characterised by a radial velocity, is driven by viscosity. The characteristic viscous time-scale at a specific radius R is given by R/v_R. This is roughly the characteristic time $\tau_{\rm visc}$ it takes the material at radius R to be accreted onto the central object.

$$\tau_{\rm visc} = \frac{R}{v_R} \tag{4.1}$$

The competing mechanism, which changes the composition of the disk Y_i (molar fraction of species i) comes from the nuclear burning.

$$\tau_{\rm burn} = \frac{Y_i}{\dot{Y}_i} \tag{4.2}$$

If the burning time-scale is shorter than the viscous time-scale, then burning occurs faster than accretion. The material will then undergo nuclear fusion before leaving the disk. The burning time-scale depends strongly on the temperature of the disk, and on the type of nuclear reaction. To go further, we need to choose which nuclear reactions to consider.

To be interesting in terms of competition with the abundances in stellar winds, the material in the disk needs to produce heavy elements such as carbon and oxygen. Heavier elements production often involves alpha chain reactions. We can therefore investigate the densities and temperatures needed for reactions such as the triple alpha reaction, carbon burning, oxygen burning to happen. These temperatures lie around $5 \times 10^8 - 10^9 K$. Attaining such high temperatures by viscous heating will require, from Equation 3.36, super Eddington accretion rates, probably around $10^5 - 10^7 \dot{M}_{\rm Edd}$. And if these reactions occur, are they fast enough? Considering that the highest temperatures are located at the inner edge of the disk, we expect most of the nucleosynthesis to take place there. The inner edge of the disk is defined as the closest distance to the black hole at which the gas can still have a circular orbit around the black hole. This is the innermost stable circular orbit (innermost stable circular orbit (ISCO)), closest distance to the black hole where the effective potential has a gradient equal to zero. Around a black hole, the effective gravitational potential is relativistic and the innermost stable orbit is located (for non spinning black holes) at (Schutz, 2009)

$$R_{\rm ISCO} = 6\frac{GM_{\rm BH}}{c^2}{}_3 R_{\rm SCH}. \tag{4.3}$$

There, at the super-Eddington accretion rates that we may consider, typical viscous time-scales are of the order of $\tau \approx 10^{-2}$s. Nuclear reactions become significant at equality between burning and viscous time-scales ($\tau_{\rm visc} = \tau$). This equality is illustrated for helium, carbon and oxygen burning by the blue, red and green lines in the temperature-density plane, Figure 4.1. At temperatures and densities greater than those defined by these three lines, the respective reactions take place. So where is located an accretion disk on the temperature–density plane? Where are located the core of stars? To consider these questions, I carried-out a simple numerical experiment which will be generalised later-on.

Let us consider a simple accretion disk described by Shakura-Sunyaev solution with, as central object, a $3M_\odot$ black hole and an accretion rate of $\dot{M} = 10^7 \dot{M}_{\rm Edd}$. Let us follow the evolution of a blob of gas while it is being accreted, from a radius of $R = 150 R_{\rm SCH}$ because this is where temperatures starts being interesting, around $10^9 K$, where heavier elements burn, see Figure 4.1. These values are arbitrary, I chose them here because they provide an interesting comparison with stars. An investigation for a much broader range of systems will be considered in the next section. The gas density and temperature are initially low, which means the gas blob will starts its journey on the bottom left part of the temperature-density plane, see Figure 4.1. When the material gets closer to the central black hole while spiralling in, its temperature and density increase. Using Equations 3.36, I estimated the slope determining the evolution of a blob of gas through the disk in the $\rho - T$ plane:

$$\log_{10}(\rho) \propto 2.5 \log_{10}(T). \tag{4.4}$$

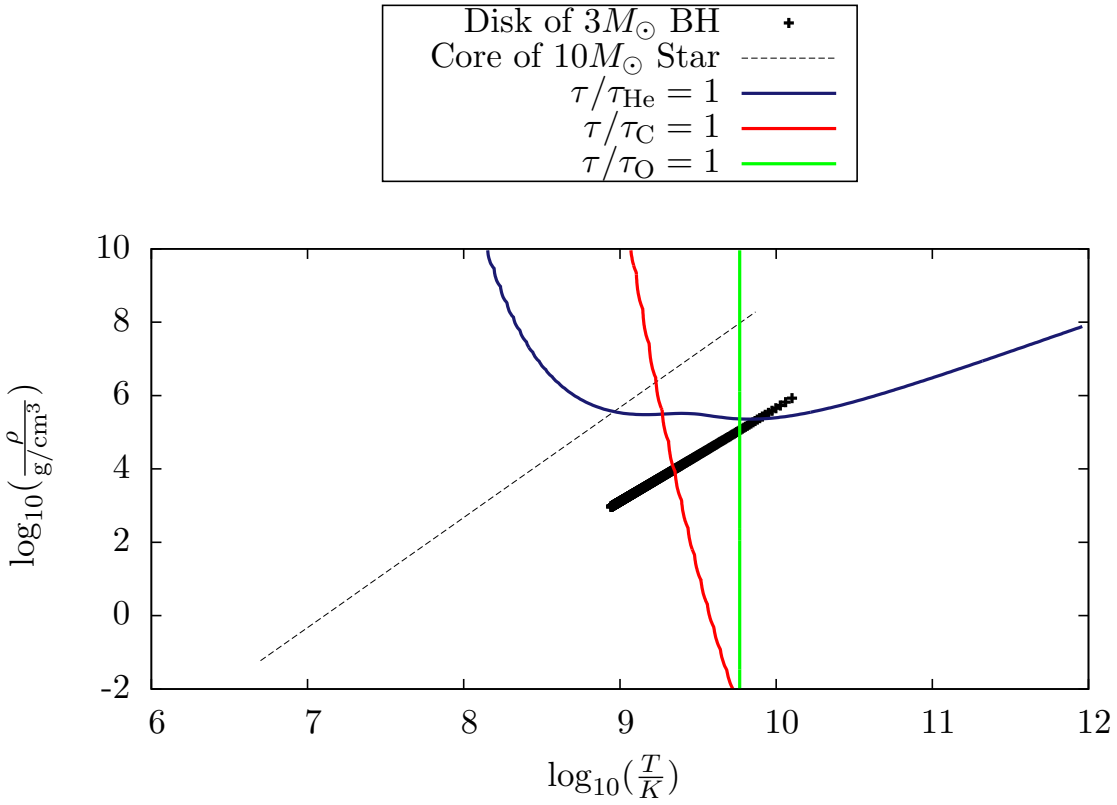

Figure 4.1: Temperature-density plane. The thick 'plus' line represents the trajectory of a blob of gas through an accretion disk in the temperature-density plane. The disk model here is a $3M_\odot$ black hole accreting at a highly super Eddington rate of $10^7\dot{M}_{Edd}$. The dashed line represents the trajectory of the centre of a star of $10M_\odot$ during its life time. The additional blue, red and green curves represent the threshold for burning of helium (triple alpha), carbon and oxygen, in competition with a time-scale of $10^{-2}s$, duration between two 'plus', corresponding to the viscous time-scale close to the inner edge of the disk. Nucleosynthesis occurs above the blue line, and on the right of the red and green lines.

Such a line is drawn in Figure 4.1 as a thick line of 'plus' signs. Regarding stellar interiors, the nuclear reactions mainly happen in the core of the stars or a shell surrounding it. These reactions are determined by the temperature and density of the stellar core. During the evolution of the star, the density-temperature scaling relation follows (Prialnik, 2010):

$$\log_{10}(\rho) \propto 3\log_{10}(T). \tag{4.5}$$

Clearly, even with accretion rates as high as $10^7\dot{M}_{Edd}$, the density of the disk is low compared with the centre of a star. The triple alpha reaction depends more on the density than other reactions because it is a three-body reaction. Therefore, it can hardly happen in an accretion disk. Helium burns a lot more easily in stars. Producing heavy elements in a disk will be much easier if the initial disk composition contains elements heavier than helium, such as carbon or oxygen.

A second difference between a stellar core and an accretion disk is that a star has millions of years to burn its material, whereas a blob of gas spends a limited amount of time in the

burning region of the disk, of the order of the minute to hour, and the time spent in the inner disk is even shorter. The burning rates need therefore to be higher in accretion disks than in stars to change significantly the disk composition. For this reason, a higher temperature is needed in an accretion disk compared to a star.

The heating process in an accretion disk originates from the differential velocity of material. It undergoes viscous heating. At a given position $R/R_{\rm SCH}$, the Keplerian orbital motion of a test particle has a stronger gradient for a low mass central black hole than for a massive black hole, because low mass black holes are more compact. This is due to the fact that the Schwarzschild radius is proportional to the black hole mass. We therefore expect, at a given radius in Schwarzschild units, to see the maximum temperature increase when the black hole mass decreases. Taking the temperature in Expression 3.36 and the Schwarzschild radius $R_{\rm SCH} \propto m_1$,

$$T \propto m_1^{-1/2} \alpha^{-1/5} \dot{M}_{16}^{3/10} \left(\frac{R}{R_{\rm RSCH}} \right)^{-3/4} . \tag{4.6}$$

We can therefore already expect lower mass black holes to be more effective at providing nuclear burning conditions.

4.2 The mass - accretion rate plane ($\mathbf{M\dot{M}}$)

As we now know the conditions necessary for nuclear burning in terms of temperature and density, we can use our knowledge of accretion disks to translate these conditions in terms of black hole mass and accretion rate. The temperature and density are highest in the inner disk. I therefore perform an experiment at this location, and, for various ranges of black hole masses, from asteroid mass to super-massive black hole (SMBH), and accretion rates, answer the question: is nuclear fusion possible? I first investigate the possibility of a simple network of two reactions:

$$\alpha + \alpha + \alpha \longrightarrow \gamma + {}^{12}C \tag{4.7}$$

$${}^{12}C + \alpha \longrightarrow {}^{16}O + \gamma \tag{4.8}$$

To know if black hole accretion disks can compete with stars, we want to know if heavier elements than helium can be produced. This is the reason behind the choice of these two reactions.

In the inner disk, I compute the temperature, the density, and the burning and viscous time-scales using Equations 4.1 and 4.2. Scaling relations follow roughly

$$\tau_{\rm visc} \propto \alpha^{-4/5} m_1^{6/5} \left(\frac{\dot{M}}{M_{\rm Edd}} \right)^{-3/10} \left(\frac{R}{R_{\rm SCH}} \right)^{5/4} \tag{4.9}$$

for the viscous time-scale. For the burning time-scale, I computed the exact expression in equation 4.2, evaluating the variation of carbon due to the simple reaction network described above. The triple alpha reaction is the slowest, so it limits the reaction rate of the above network and determines the production of heavier elements such as oxygen. Following the carbon production through the triple alpha reaction can be done with the following scaling relation:

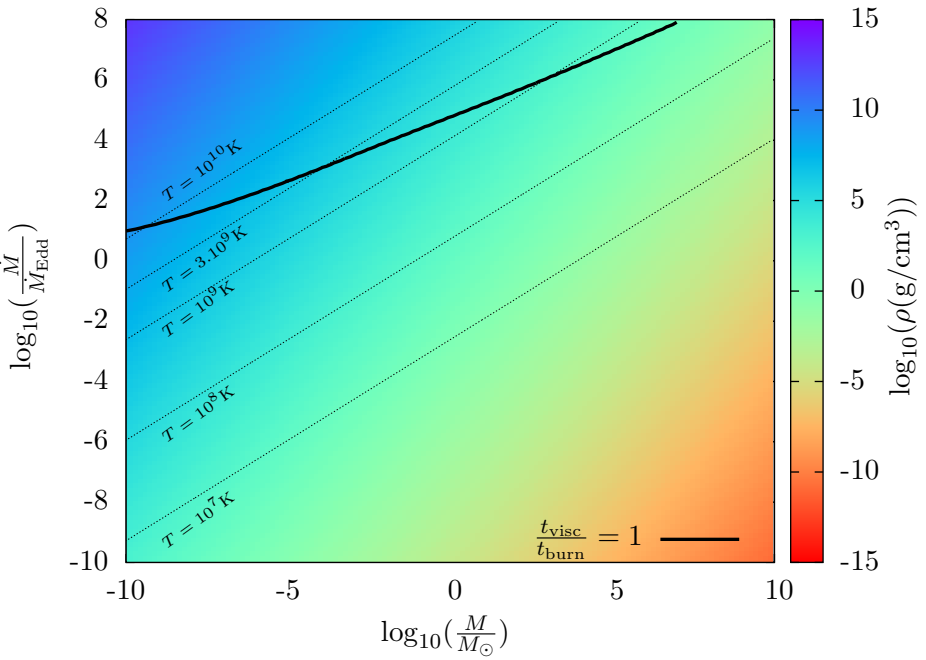

Figure 4.2: Black hole mass - accretion rate plane. The black hole mass varies from asteroid mass to SMBH (super-massive black hole), and the accretion rate from $10^{-10}\dot{M}_{\rm Edd}$ to $10^{8}\dot{M}_{\rm Edd}$ to consider a large range. System composed of a Black hole accretion disk composed of 20% helium, 40% carbon and 40% oxygen, isotopes of which reactions are being investigated. Isolines of highest disk temperature are plotted in dotted lines. An isoline characterising an equality between viscous time-scale and nuclear burning time-scale is plotted in black. The color indicates the highest disk density in g/cm^3.

$$\dot{Y_{\rm C}} \propto \rho^2 Y_\alpha^3 \langle\sigma v\rangle_{3\alpha} \tag{4.10}$$

with, writing $T_9 = T \times 10^9 K$,

$$\langle\sigma v\rangle_{3\alpha} \propto T_9^\beta, \tag{4.11}$$

with $\beta \approx 41$ for $T_9 \approx 0.1$, $\beta \approx 11$ for $T_9 \approx 0.3$ and $\beta \approx 1.4$ for $T_9 \approx 1$ and β decreases slowly at greater temperatures. As seen in the temperature-density plane (Figure 4.1), most of the nuclear burning occurs at temperatures between 10^9K and 10^{10}K, so taking $\beta = 1$ is a good approximation here.

$$\tau_{3\alpha} \propto \frac{Y_{\rm C}}{Y_\alpha^3} \alpha^{1-\beta/5} \left(\frac{\dot{M}}{\dot{M}_{\rm Edd}}\right)^{-\frac{11+3\beta}{10}} m_1^{\frac{7+\beta}{5}} \left(\frac{R}{R_{\rm SCH}}\right)^{\frac{15+3\beta}{4}} \tag{4.12}$$

Nuclear burning is significant if the viscous time-scale is equal or greater than the burning time-scale at a few Schwarzschild radii. Setting these two time-scales equal led me to find a relation between the accretion rate and the black hole mass:

$$\left(\frac{\dot{M}}{\dot{M}_{\rm Edd}}\right) \propto m_1^{\frac{1+\beta}{5}} \approx m_1^{2/5} \tag{4.13}$$

On a logarithmic scale, 2/5 is a good approximation of the slope of the black line of the $M\dot{M}$ plane in Figure 4.2.

I did these computations more rigorously numerically for a range of black hole mass from asteroid-mass black hole ($\approx 10^{-10} M_{\odot}$) to approximately the most massive black holes known in Active Galactic Nuclei at the centre of galaxies ($\approx 10^{10} M_{\odot}$). The accretion rate is investigated on a very wide range between 10^{-10} to 10^{8} Eddington limits. Nuclear burning occurs significantly when the burning and inner disk viscous time-scales are comparable, i.e. $\frac{\tau_{visc}}{\tau_{burn}} = 1$. This means a significant fraction of the inner disk composition has changed before it was accreted into the black hole. This inequality corresponds to the plain black line plotted in Figure 4.2. Any pair $(M\dot{M})$ such that $\frac{\tau_{visc}}{\tau_{burn}} > 1$ is satisfied is favourable to nuclear burning. This equality is satisfied above the plain black line in Figure 4.2. I assumed the initial composition of the disk to be 20% helium, 40% carbon and 40% oxygen since they are the elements involved in the above nuclear reactions.

The outcome is that highly super-Eddington accretion rates are needed to allow nuclear burning. And the accretion rate needed for this reaction network increases with the black hole mass. This result is visible in Figure 4.2 where the systems favourable to nuclear burning sit above the black line. The high temperature is provided by viscous heating. It depends on differential rotation, greater close to low mass black holes than to massive black holes because of the proportionality relation between the Schwarzschild radius and the black hole mass. Said differently, for super-massive black holes, the interesting temperatures are enclosed in the Schwarzschild radius. At this point, we realise that the "best way" to satisfy the nuclear burning conditions is to be able to approach the centre of the black hole as much as possible. This distance is limited by the innermost stable orbit, which is $3R_{\rm SCH}$ for non rotating black holes. But rotating black holes, described by a Kerr metric, have a different potential and a different innermost stable orbit, which can be closer to the event horizon of the black hole. If the spin characterised by the parameter $a = \frac{J}{M_{\rm BH}c}$ where J is the angular momentum of the black hole. J is constrained by the upper limit $\frac{GM_{\rm BH}}{c^2} M_{\rm BH} c$, so a must be less than $\frac{GM_{\rm BH}}{c^2}$. The ISCO is given by (Frank et al., 2002):

$$\frac{GM}{c^2}\left(3 + A_2 - \sqrt{(2 - A_1)(3 + A_1 + 2A_2)}\right) \tag{4.14}$$

with $A_1 = 1 + \left(1 - \frac{a^2}{\frac{GM_{\rm BH}}{c^2}}\right)^{1/3}\left[\left(1 + \frac{a}{\frac{GM_{\rm BH}}{c^2}}\right)^{1/3} + \left(1 - \frac{a}{\frac{GM_{\rm BH}}{c^2}}\right)^{1/3}\right]$, $A_2 = \sqrt{\frac{3a^2}{(\frac{GM_{\rm BH}}{c^2})^2 + A_1^2}}$ and is plotted in Figure 4.3. As the black hole spin increases, the ISCO moves towards the event horizon of the black hole. If getting closer to the black hole really allows the disk to reach higher temperatures, the black hole spin should have an effect on the nucleosynthesis and the plain black line of the $M\dot{M}$ plane should move down. This is visible in Figure 4.4. This result might be interesting as lower accretion rates, such as $10^4 \dot{M}_{\rm Edd}$ in the limit for stellar mass black holes, permit nuclear burning. Such a rate could, in principle, be provided by stable mass transfer from a white dwarf to a $3M_{\odot}$ black hole for example.

4.3 Possible systems leading to nucleosynthesis in black hole accretion disks

The results of the numerical experiment in Section 4.2 and illustrated in Figure 4.2 show that the number of possibilities for nucleosynthesis in black hole accretion disks is quite restricted.

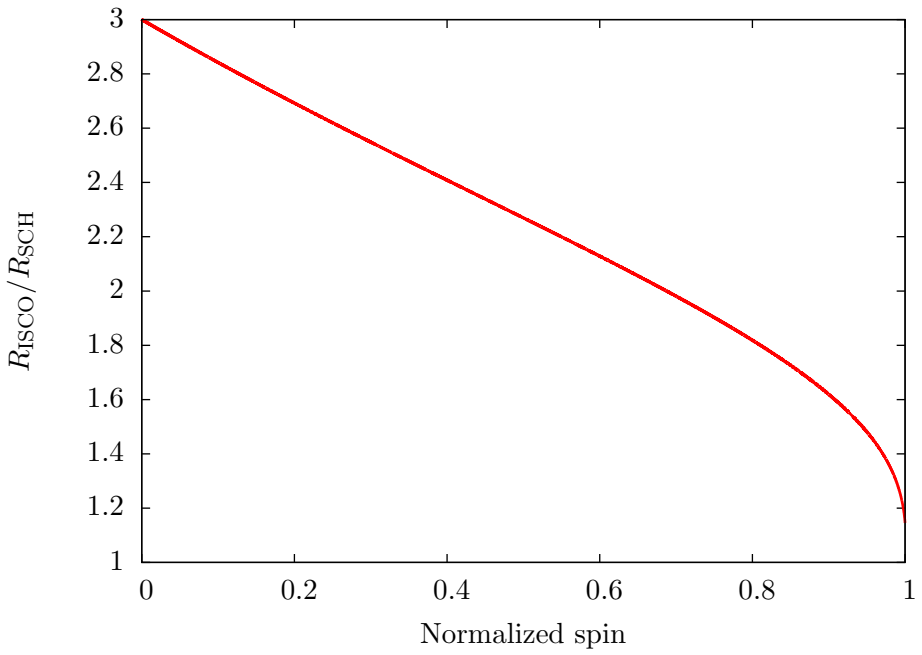

Figure 4.3: Inner most stable orbit as a function of normalised black hole spin. As the spin approaches its maximum value the innermost stable circular orbit (ISCO) moves to the Schwarzschild radius. For a spin zero, we find again the ISCO of 3 Schwarzschild radii, solution for non rotating black holes.

For an accretion disk to burn helium and carbon significantly, the possible ranges are reduced to highly Eddington accretion rates and low mass black holes, corresponding to the area above the black line in Figure 4.2, so the top left corner. Low mass black holes are the best candidates. I will review first the different black hole (BH) families, and then consider the possible companion stars.

4.3.1 Black hole families

The black holes with a mass within $[\ 10^{-10},\ 10^{-5}]M_{\odot}$ belong to the primordial black holes category. They are mainly candidates to dark matter. There is currently no observational evidence for their existence. Many upper limits on their contribution to dark matter exist (Carr et al., 2016). I will mention their possible role in nucleosynthesis in Chapter 7. From Figure 4.2, they are our best candidates for nucleosynthesis as accretion at super-Eddington rates is conceptually challenging and these black holes are the less demanding in terms of feeding. We could imagine then accreting material spherically through Bondi accretion, and see if the material is dense enough to give large accretion rates. See Chapter 7.

The black holes with masses within $[\sim 3, \sim 30]M_{\odot}$ which formed from stellar evolution channels are called astrophysical black holes. Massive stars $(20 - 150M_{\odot})$ evolve very fast and are thought to end their lives in a core collapse. This formation channel has been under debate since the LIGO gravitational waves detection in September 2016 (Abbott et al., 2016). I will focus on these systems as these black holes are the only family which we have confirmed observations from either X-ray sources or gravitational wave detections (Abbott

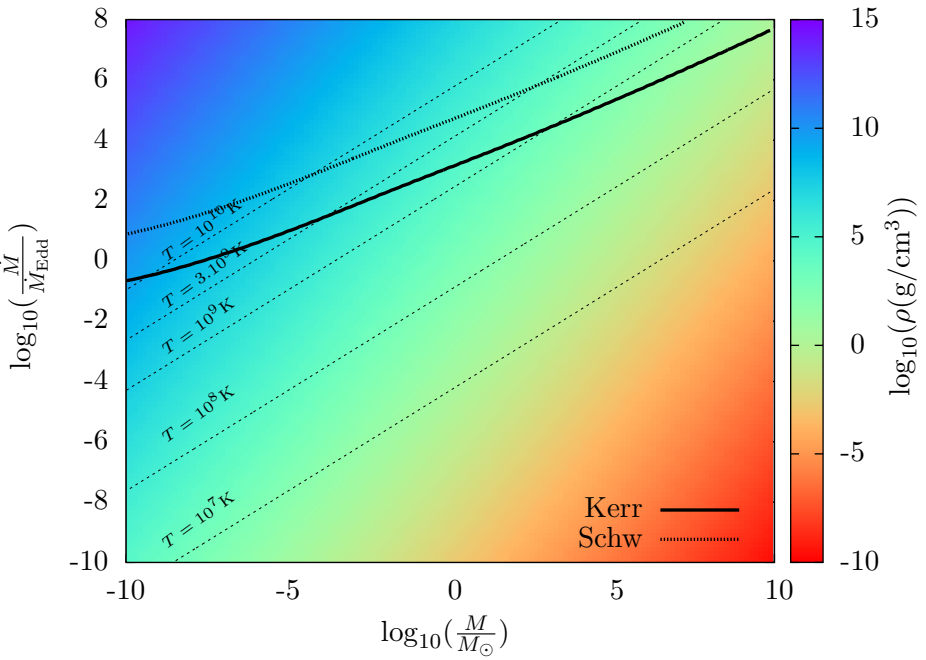

Figure 4.4: Black hole mass - accretion rate plane. System composed of a black hole accretion disk composed of 20% helium, 40% carbon and 40% oxygen. Isolines of temperature are plotted in dotted lines. An isoline characterising an equality between viscous time-scale and nuclear burning time-scale is plotted, for a non-rotating black hole described by a Schwarzschild metric, in thick dotted line, and a rotating black hole described by a Kerr metric. The color indicates the highest disk density in g/cm^3.

et al., 2016). One can read from Figure 4.2 that super-Eddington accretion is required to allow nucleosynthesis. I discuss possible systems providing so high accretion rates in the next section.

Black hole masses in the range $[10^2, 10^5]M_\odot$ characterize the intermediate mass black hole (IMBH) family. They are thought to be found in stellar clusters as they make the bridge between stellar mass BHs and SMBHs, though there is no direct evidence for their existence. The arguments for their existence come from galactic evolution. From the $M\dot{M}$ plane (Fig 4.2), they seem to play a minor role in nucleosynthesis. However, if they do play a role and produce new elements, nuclear reactions taking place in their hypothetical accretion disk could, in principle, produce observable gamma rays. It would provide a way to detect these IMBHs.

Black holes with masses above 10^5 are SMBHs. They are thought to lie a the centre of most galaxies. Observational evidence we have consists in the stellar dynamics ongoing at the centre of the Milky Way and observation of quasars at the centre of other galaxies. In the Milky Way, stars have been observed orbiting very fast around a central compact object called Sagittarius A, of which the mass was inferred to be about $4 \times 10^6 M_\odot$ (Schödel et al., 2009; Gillessen et al., 2009). This mass and compactness rules-out all known astrophysical objects, except for black holes. In the $M\dot{M}$ plane, these black holes require the highest accretion rates.

4.3.2 Companion star

Stellar mass black holes are the black holes we have most observational evidence for. And not only do we have evidence, but the nature of the observation confirms they accrete material: what is actually seen is their accretion disk, shining in the X-ray wavelengths. The gas in their accretion disk is provided by a companion star transferring mass. Under which conditions is the mass transfer rate greater than $10^6 \dot{M}_{\rm Edd}$? In binary systems on circular orbit, mass transfer is governed by the gravitational field. In the co-rotating frame, we can write the effective potential felt by a point mass. For a BH mass of $M_{\rm BH} = M_1$, its companion M_2 and the mass ratio $q = M_2/M_1$, lines of equipotential are drawn in Figure 4.5. Each of these lines define to which object a point mass is bound. Where the equipotentials cross, between the two stars, is located the Lagrangian point L_1 where a particle is bound to both stars. If a particle initially bound to the secondary star reaches this points, it might be transferred to the primary. The surface defined by these equipotential lines is the Roche lobe, and there is mass transfer if one of the stars occupies the volume within its Roche lobe. A good approximation is to assume this surface spherical and compare the radius of the star to the radius of the sphere of equal volume as the volume of the Roche lobe (Roche radius). If the radius of the star is larger, the outer material is not bound to it. There should then be mass transfer through the inner Lagrangian point. How fast does this mass transfer occur? Can it reach high accretion rates? The answer to this question depends on the reaction of (1) the size of the Roche lobe of the transferring star and (2) the response of star to the mass loss. If the star radius grows fast enough compared to the size of its Roche lobe during the mass transfer, it will become unstable.

A good approximation of the Roche radius of the secondary star in function of the mass ratio and the separation is given by Eggleton (1983)

$$\frac{R_{\rm L}}{a} = \frac{0.49 q^{2/3}}{0.6 q^{2/3} + \ln(1 + q^{1/3})} \approx 0.462 \left(\frac{M_2}{M_1 + M_2} \right)^{1/3} \tag{4.15}$$

In conservative mass transfer, all the mass lost by the secondary goes to the primary and the total angular momentum of the system is conserved. The separation varies as

$$\frac{\dot{a}}{a} = -2\dot{M} \left(\frac{M_2 - M_1}{M_1 M_2} \right) \tag{4.16}$$

From this equation, we see that if $M_2 < M_1$, then the separation between the two stars increases. And the Roche radius is proportional to the separation. This contributes to an increase of the Roche radius, while the fact that the mass ration decreases contributes to decrease the Roche Radius. The Roche lobe response can be quantified:

$$\zeta_L = \frac{\partial \log R_L}{\partial \log M_2}, \tag{4.17}$$

and the response of the star is

$$\zeta_2 = \frac{\partial \log R_2}{\partial \log M_2}. \tag{4.18}$$

The question of unstable mass transfer is sorted by comparing these two quantities. Stars for which ζ_2 is negative are objects of which the size increases as their mass decreases. Such objects exist, for example a white dwarf (WD) has a mass radius relation $R \propto M^{-1/3}$.

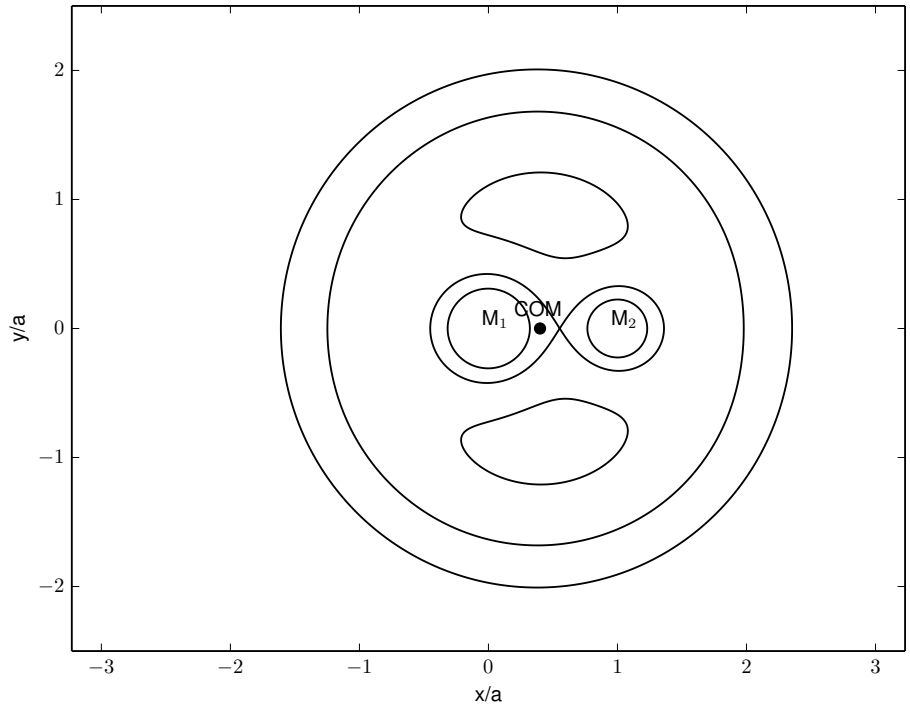

Figure 4.5: Lines of equipotential in the orbital plane of a circular binary system of mass ratio $q = \frac{M_1}{M_2} = 0.6$, where the primary star is located at the origin, and the secondary is located at a separation of a on the x axis.

WDs are interesting for further simulations: if they do not provide the needed accretion rates, then main sequence stars, which become smaller as their mass decrease, will not either. Additionally, most common white dwarfs contain carbon and oxygen. Recalling the difficulties in igniting helium (this is not impossible as we will see), white dwarfs present additional interesting properties: they provide already some heavier elements to the accretion disk, and potentially high accretion rates. WDs seem to be an ideal starting point to investigate nucleosynthesis in black hole accretion disks.

Chapter 5

Black hole – white dwarf

I wrote independently a computer program in `C++` simulating nucleosynthesis in a black hole accretion disk, specifically designed for BH–WD binaries as WD disruptions provide the super Eddington mass transfer rates needed for nucleosynthesis. In this chapter, I describe the model I implemented, using the framework introduced in the first chapters. Nuclear networks are a set of stiff differential equations, introducing reaction rates which may differ of many orders of magnitudes. This stiffness is numerically challenging as forward integration methods are then unstable (Press et al., 2007). I overcame this problem by using an implicit differentiation scheme. It is less straightforward to implement because it consists in evaluating the derivatives one step forward, but numerically stable. I then performed a set individual runs to investigate how nucleosynthesis in black hole disks varies within the mass ranges, accretion rates and white dwarf types leading to nucleosynthesis. I finally obtained and compared the yields from my simulations to expected stellar yields from models in the literature (Nomoto et al., 2013).

5.1 Thin disk model

I implemented the one dimensional thin (or Shakura-Sunyaev) disk model using the analytical solutions described in Equation 3.36. This allows the code to execute computations fast, as no integration of the gas dynamics equations need to be performed numerically. The thermodynamic variables such as density and temperature are simple functions of radius, mass and accretion rate. The drift velocity v_{R} is also known. Practically, I simulate the path followed by a blob of gas from the outer disk to the inner disk (Lagrangian approach). The position of the gas blob at different times is numerically integrated.

Independently from the disk, I implemented the nuclear burning network of the alpha chain described in Figure 2.4. I am going to describe the method briefly and refer the reader to the appendix for more details about the integration of the network. Given the temperature ranges and the composition rich in alpha elements (He, C, O, Ne) in a disk produced by the disruption of a white dwarf described in the previous section, the 13 isotopes alpha chain illustrates well the dominating nuclear reactions. Ideally, one should consider all possible nuclear reactions. But this is extremely heavy computationally, so I chose a set of nuclear reactions for which the rates are significantly greater than for other nuclear reactions. And this is the alpha chain. In this network, 13 differential equations of the same type as described in Chapter 2 are to be solved, one per isotope. Due to the high dependency in temperature,

many different scales are introduced in the burning rates. These differential equations are stiff and challenging for numerical integration (Press et al., 2007). To give an example, we can consider in detail the neon isotope and see in which nuclear reactions it is involved, and write fully the differential equation to solve, keeping in mind that this has to be done for each of the 13 elements involved in the nuclear network. Neon is produced by an alpha reaction with oxygen. It is also involved in an alpha reaction producing magnesium. In addition, the reverse reactions might occur as well. This implies a total of four reactions to consider.

$$\begin{aligned} {}^{16}\mathrm{O} + \alpha &\rightleftharpoons \gamma + {}^{20}\mathrm{Ne} \\ {}^{20}\mathrm{Ne} + \alpha &\rightleftharpoons \gamma + {}^{24}\mathrm{Mg}. \end{aligned} \tag{5.1}$$

The variation of the molar fraction of neon will therefore be

$$\dot{Y}_{\mathrm{Ne}} = Y_{\mathrm{O}} Y_{\mathrm{He}} \rho N_{\mathcal{A}} \langle \sigma v \rangle_{O\alpha} - Y_{Ne} \langle \sigma v \rangle^{\mathrm{rev}}_{O\alpha} - Y_{\mathrm{Ne}} Y_{\mathrm{He}} \rho N_{\mathcal{A}} \langle \sigma v \rangle_{Ne\alpha} + Y_{Mg} \langle \sigma v \rangle^{\mathrm{rev}}_{Ne\alpha}. \tag{5.2}$$

The quantities $\langle \sigma v \rangle$ are measured in laboratories at different temperatures or integrated numerically. The results are interpolated as functions of temperature. I use the interpolation functions resulting from these studies. References for each reaction used are given in Table D.1 in Appendix D. For instance, the reaction rate of the alpha reaction with oxygen (first term of Equation 5.2) is given by

$$\begin{aligned} \langle \sigma v \rangle_{\mathrm{O}\alpha}(T_9) = 2.68 \times 10^{10} T_9^{-2/3} \exp\left[-39.76 T_9^{-1/3} - (T_9/1.6)^2\right] + 51.1 T_9^{-3/2} \exp(-10.32/T_9) \\ + 616.1 T_9^{-3/2} \exp(-12.2/T_9) + 0.41 T_9^{2.966} \exp(-11.9/T_9), \end{aligned} \tag{5.3}$$

where $T_9 = T/10^9 K$. This reaction rate was taken from Angulo et al. (1999). The general form of this expression (exponentials and powers) emphasise the stiff character of the differential equation 5.2. The reaction rates of the second reaction involving neon and the alpha particle has a similar expression, but its own temperature dependency. In order to solve these 13 differential equations and preserve numerical stability, I implemented an implicit Euler scheme, which consists in evaluating the derivative at $t + h$ instead of t where h is the time-step. This method is a general method used for solving stiff differential equations, and has shown its efficiency (Press et al., 2007). If we were to solve them numerically with an explicit Euler scheme, then we would simply write

$$Y_{\mathrm{Ne}}(t + h) = Y_{\mathrm{Ne}}(t) + h \dot{Y}_{\mathrm{Ne}}(t). \tag{5.4}$$

But this integration method is numerically unstable: for a given time-step, the integration results may not be only have an error, but tend to infinity very quickly, which means that not only the error (which goes at $\mathcal{O}(h)$) sets a constrain on the time-step, but also the stability of the solution. One might, at some point, need an infinitely small time-step. An example of an explicit integration is shown in Figure 5.1 together with the same integration and with the same parameters (initial conditions, time-step). This figure shows the mass fraction of elements produced by nuclear reactions in the disks, as a function of radius. This integration was performed for a carbon oxygen donor. We can note the explicit scheme is unstable and diverges from a certain radius. To overcome this problem, the use of an implicit scheme allows

me to get rid of the stability constrain on the time-step. This means that instead of using the time derivative at time t, one evaluates the time derivative at $t + h$:

$$Y_{\rm Ne}(t + h) = Y_{\rm Ne}(t) + h\dot{Y}_{\rm Ne}(t + h). \tag{5.5}$$

But $\dot{Y}_{\rm Ne}(t+h)$ is not directly known. I use the equation 5.2 linearised at time $t+h$. The molar fraction of each element $Y(t+h)$ can be expanded as $Y(t+h) \approx Y(t)+h\dot{Y}(t)$. Neglecting the terms in $\mathcal{O}(h^2)$, this leads to a linear equation to solve, and allows one to estimate $\dot{Y}_{\rm Ne}(t+h)$. This involves all nuclear species affected in the reactions with neon. The whole set of linear equations can be written in the form of a matrix relating the derivatives of molar fraction of each element at time t to their derivative at $t + h$. And the problem is reduced to inverting the matrix in question. To do this in C++, I use the linear algebra package `LAPACK++` recommended in Press et al. (2007). The whole nuclear network integration method and the use of the `LAPACK++` package are described in detail in the Apendices A and B.

Given initial conditions and boundaries, my programs solve the equations governing the state of the accretion disk: we fully know the density, temperature and abundances at any position and time. In the BH–WD scenario, the accretion disk is provided by mass transfer through Roche lobe overflow of the white dwarf, where the binary has negligible eccentricity (I leave arguments for circular orbit to the next chapter, where I discuss how these systems can form). Assuming for now that by some mechanism, a binary BH–WD comes to contact (mass transfer), then what are the dimensions of the accretion disk? The size of the Roche lobe around the white dwarf when the binary separation is a and the mass ratio $q = M_{\rm WD}/M_{\rm BH}$ is given by Eggleton (1983)

$$\frac{R_{\rm L}}{a} = \frac{0.49q^{2/3}}{0.6q^{2/3} + \ln(1 + q^{1/3})}. \tag{5.6}$$

At the onset of the mass transfer the separation $a_{\rm RLOF}$ is such that the white dwarf fills its Roche lobe, $R_{\rm L} = R_{\rm WD}$. Material from the WD is transferred to the BH. For the white dwarf radius, I used the mass-radius relation of Verbunt & Rappaport (1988)

$$\frac{R_{\rm WD}}{R_\odot} = 0.0114\sqrt{\left(\frac{M_{\rm WD}}{M_{\rm ch}}\right)^{-2/3} - \left(\frac{M_{\rm WD}}{M_{\rm ch}}\right)^{2/3}} \times \left[1 + 3.5\left(\frac{M_{\rm WD}}{M_{\rm p}}\right)^{-2/3} + \left(\frac{M_{\rm p}}{M_{\rm WD}}\right)\right]^{-2/3}, \tag{5.7}$$

where $M_{\rm ch} = 1.44M_\odot$ is the Chandrasekhar mass of the WD and $M_{\rm p} = 0.00057M_\odot$ is a numerical factor. If the mass transfer is unstable, then the white dwarf gets shredded on a dynamical time-scale, only a few orbits and the white dwarf material piles up at a favoured radius. As in Frank et al. (2002), we approximate this mass transfer by a quick change of "binding body" conserving angular momentum. This allows us to define the circularisation radius: the distance from the BH at which the material orbiting it has the same specific angular momentum as the system at the onset of the mass transfer. At the onset of the mass transfer, the angular momentum of the system is

$$J = M_{\rm BH}M_{\rm WD}\sqrt{\frac{Ga}{(M_{\rm BH} + M_{\rm WD})}}. \tag{5.8}$$

At the circularisation radius, the angular momentum of the $1M_{\rm WD}$ of gas is

$$J_{\rm circ} = M_{\rm WD}v_\phi R_{\rm circ} \tag{5.9}$$

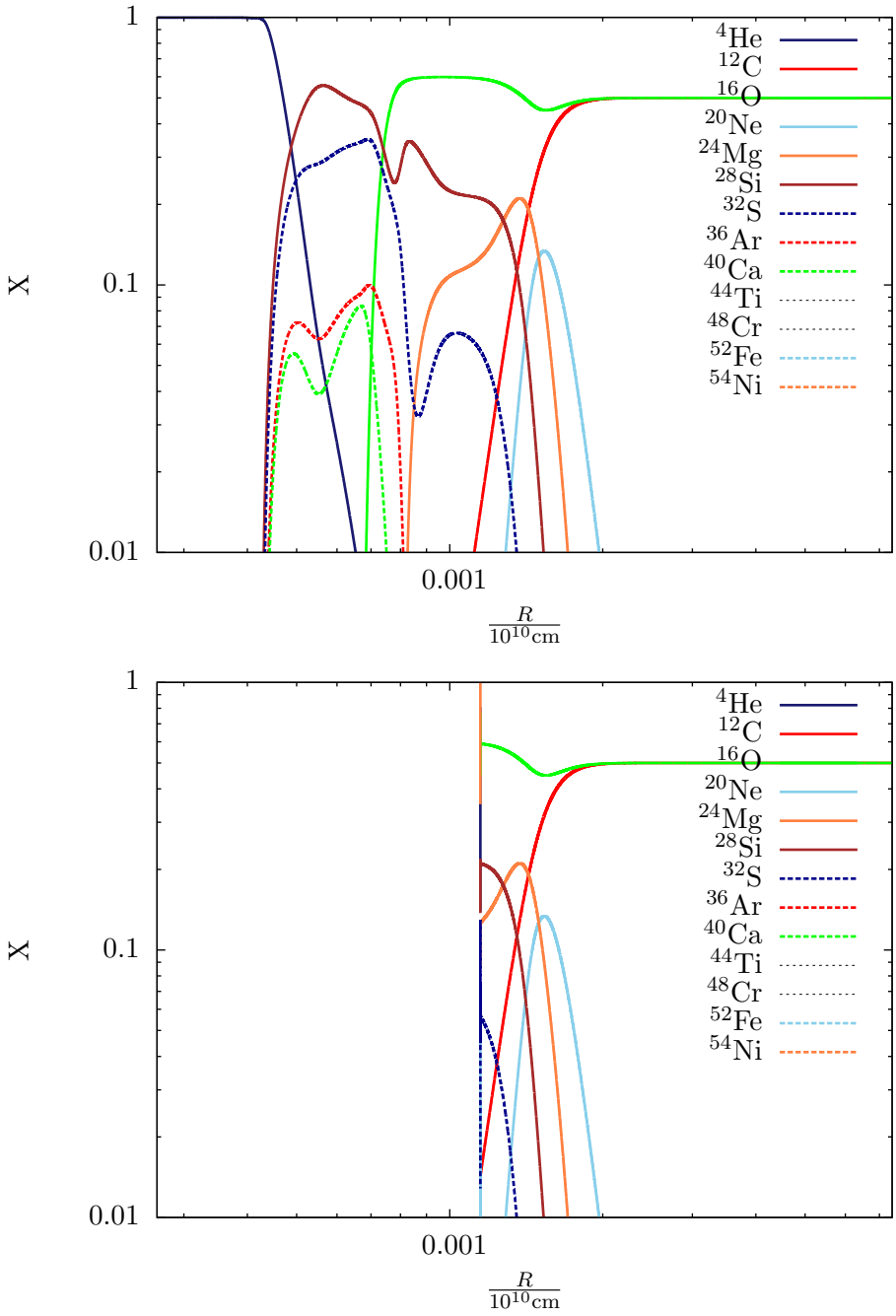

Figure 5.1: Demonstration of the difference in explicit and implicit integration of stiff differential equations in the nuclear network of alpha chain. Mass fractions of the different isotopes produced in the thin disk around a $3M_{\odot}$ black hole accreting at $10^{6}\dot{M}_{\rm Edd}$ from a carbon oxygen donor. *Upper panel:* Explicit scheme. *Bottom panel:* implicit scheme.

If the gas settles at the circularisation radius on a circular orbit, then $v_{\phi} = \sqrt{\frac{GM_{\rm BH}}{R_{\rm circ}}}$ and its angular momentum is

$$J_{\rm circ} = \sqrt{GM_{\rm BH}R_{\rm circ}}M_{\rm WD} \tag{5.10}$$

If angular momentum is conserved during this phase of mass transfer from the WD to the BH, equating Equations 5.8 and 5.10 when the WD fills its Roche lobe, we find where the gas settles, the circularisation radius

$$R_{\rm circ} = \frac{a_{\rm RLOF}}{1+q}, \tag{5.11}$$

where $a_{\rm RLOF}$ is the separation of the binary at which mass transfer takes place. $R_{\rm circ}$ is roughly the size of the newly formed accretion disk.

The inner boundary of the disk is also constrained, by the BH potential. The disk goes as close to the black hole as where it can be on a circular orbit. Due to the compactness of black holes, relativistic effects are not negligible. The relativistic effective potential presents minima and maxima, depending on the angular momentum of particles orbiting the BH and this sets a minimum distance from which a particle can have a circular orbit. For a sufficiently large angular momentum (which we assume the gas has, since we consider accretion disks), the innermost stable orbit (ISCO) around a non rotating black hole lies at $3R_{\rm SCH}$. This defines the inner edge of the accretion disk. At lower radii, the motion of the gas is not circular and it either falls into the BH rapidly or escapes in a powerful outflow. If the BH is rotating, then the ISCO has a different form (e.g. Frank et al. (2002)) which I took into account when I considered spinning BHs.

An additional boundary condition, which affects the nucleosynthesis in the accretion disk, is the initial composition of the disk, determined by the composition of the object shredded into the BH. Different cases have been considered in this work, namely carbon oxygen (CO) WDs, carbon oxygen helium (COHe) WDs, pure helium (He) WD and more massive oxygen neon (ONe) WDs. At the circularisation radius, I imposed the initial composition of the disk to be the composition pf the donor object. I have not considered in the present work cases where nuclear burning starts occurring before the formation of the disk (e.g. thermonuclear disruptions of white dwarfs) or spatially outside from the accretion disk.

5.2 A windy disk

Accretion rates as high as $10^6 \dot{M}_{\rm Edd}$, power outflows from the disk (King & Muldrew, 2016). The inner edge of the disk has a luminosity of at least the Eddington luminosity, so radiation pressure prevents most of the gas from in-falling. A more sensible question is on the outflow profile: where is most of the mass ejected? Before considering qualitatively the complex physics involved in winds, I will describe how I computed the mass of each element produced in my accretion disk program. The total mass m_i of element i produced is the integration of its mass fraction X_i from the inner disk to the outer disk, weighted by the density as a function of radius.

$$m_i = \int_{\rm ISCO}^{R_{\rm d}} 2\pi \rho_i(R) X_i(R) R H(R) dR \tag{5.12}$$

So it would correspond to the area under all the curves in Figure 5.3 for example, weighted by the density in the disk. How much of it is expelled? A first approximation, ignoring any physical interaction producing it, is to consider a uniform wind profile: the mass expelled at each radius is the same. Additionally, we can reasonably assume that the central black hole is accreting at its Eddington limit. So the fraction of material ejected is $\frac{\dot{M}-\dot{M}_{\rm Edd}}{\dot{M}}$. This fraction is very close to 1 considering the highly Eddington accretion I considered. If a mass

m_i of element i were produced in the disk, then the mass of i released to the ISM would be $\frac{\dot{M}-\dot{M}_{\rm Edd}}{\dot{M}} m_i = \frac{10^6-1}{10^6} m_i \approx m_i$.

There are several reasons for which the wind profile should be different from uniform. Firstly, the inner edge of the disk is more luminous than the rest as it is more heated due to greater differential rotation. So the source of radiation pressure should be at the inner edge of the disk, and the outlfows should be greater at the inner edge of the disk (Watarai & Fukue, 1999). This consideration should not affect my results for heavy elements (and helium coming from photodisintegration), synthetised at the disk inner edge. But less "primitive elements" coming from the white dwarf, which do not undergo nucleosynthesis, would be expelled.

Secondly, I have not considered any magnetic field in the disk. But this is very unrealistic: the disk is highly ionized, so there should definitely be a magnetic field. Magnetic fields can drive outflows under the form of disk winds and powerful jets (Blandford & Payne, 1982).

Thirdly, the model does not account for the nuclear energy generated by nucleosynthesis. Does it have a dynamical effect on the disk? Could it power winds? This is discussed in Section 5.3.4.

5.3 Explore the parameter space

5.3.1 Effect of the black hole mass

The mass of the black hole is of particular importance for nuclear burning efficiency. A black hole too massive (of mass above approximately $10^5 M_\odot$) swallows the white dwarf without disrupting it. But more constrains come from the accretion disk. For boundary conditions, the nuclear burning should happen within the disk size because this is where the simulation starts. This issue is more of a technical than scientific nature, if a particular disk model predicts that nuclear burning should happen from outside the disk, one should also simulate in detail the mass transfer from the white dwarf to the black hole. The present work is focused on nucleosynthesis within disks rather than mass transfer in binaries. For the calculations to stay consistent, I determined where the boundaries of the systems I can consider lie.

Let us define the "burning zone" as the range of radii where the temperature is more than 10^9K. This is a rough approximation as the burning depends also a little on the density, but it provides interesting constrains on the black hole mass limits. The radii at which the temperature is 10^9K for a fixed accretion rate in Eddington units scales as

$$\frac{R_{T9}}{R_{\rm SCH}} \propto m_1^{-4/15} \tag{5.13}$$

with the temperature. Scaling with the circularisation radius $R_{\rm circ} \propto m_1^{1/3}$ for black hole masses greater than the white dwarf mass,

$$\frac{R_{T9}}{R_{\rm circ}} \propto m_1^{11/5}. \tag{5.14}$$

Equation 5.13 tells us that as the black hole mass increases, the event horizon grows faster than the burning threshold radius. Therefore, there exist a black hole mass above which the temperature in the inner disk is too low. This description corresponds exactly to the temperature isolines in the $M\dot{M}$ plane. But a more accurate threshold for burning is provided by the burning and accretion time-scales comparison line in the $M\dot{M}$ plane. On the other

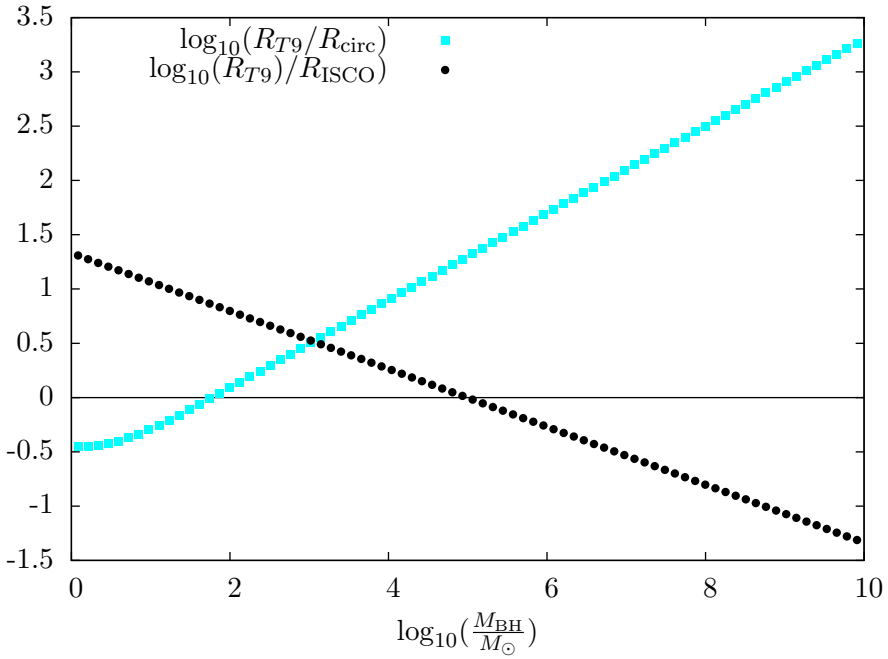

Figure 5.2: Radius at which the temperature is equal to 10^9K (approximate burning threshold for carbon), in units of innermost stable orbit in black dots and in units of circularisation radius in blue squares. The black line must be above the zero line for the inner disk to be hot enough for nuclear burning and corresponds approximately to the burning threshold of the $M\dot{M}$ plane. The blue line must be below the zero line for the outer disk to be cold enough for boundary conditions. This is accretion rate dependant. These are conditions when $\dot{M} = 10^7 \dot{M}_{\rm Edd}$. Where the two lines cross, the system dimensions become unphysical: the circularisation radius becomes less than the innermost stable orbit. This corresponds to the configuration where the white dwarf is swallowed by the black hole.

hand, some new information is brought by Equation 5.14. This shows that as the black hole mass increases, the burning region also increases. And for boundary conditions explained above, we need this ratio to be less than unity, so that burning occurs well within the accretion disk. See Figure 5.2, where a particular example at $\dot{M} = 10^7 \dot{M}_{\rm Edd}$ is taken, and where we see the maximum BH mass is about $100 M_\odot$, where the blue line crosses the zero line.

As a consequence of these two effects, increasing the black hole mass up the order of $100 M_\odot$ (for the particular case of $\dot{M} = 10^7 \dot{M}_{\rm Edd}$) moves the burning zone towards the BH, see Figure 5.3 and 5.4. These two figures show the radial structure of their respective accretion diks, with a few elements dominating at specific radii. For a $3 M_\odot$ BH, the inner disk is dominated by helium resulting from the photo-disintegration of heavier elements, and an outer disk dominated by the WD composition (constrain I have imposed explicitly in the beginning of this section), a more massive black hole produces a lot less helium than a lower mass black hole as the inner disk is cut due to the growth of the event horizon proportional to the BH mass. Other elements dominating in the inner disk might also be produced in lesser proportions. This can be visualised by comparing the Figures 5.3 and 5.4, showing the mass of elements produced in function of their atomic mass A. The difference in yields resulting from these effects is presented in Figure 5.5.

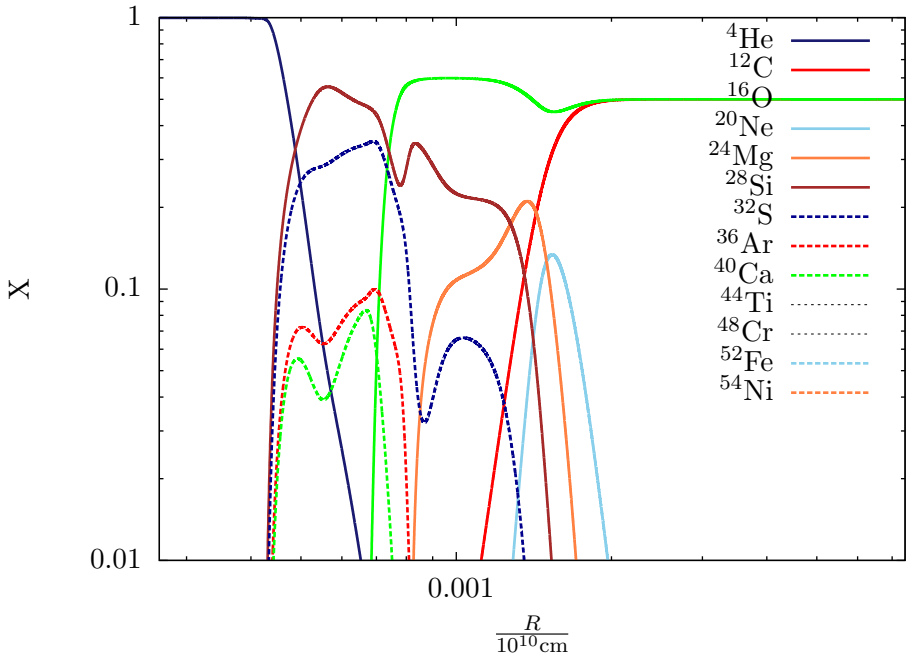

Figure 5.3: Mass fraction of elements in a disk from a carbon oxygen donor to a $3M_{\odot}$ black hole, at an accretion rate of $10^{6}\dot{M}_{\text{Edd}}$.

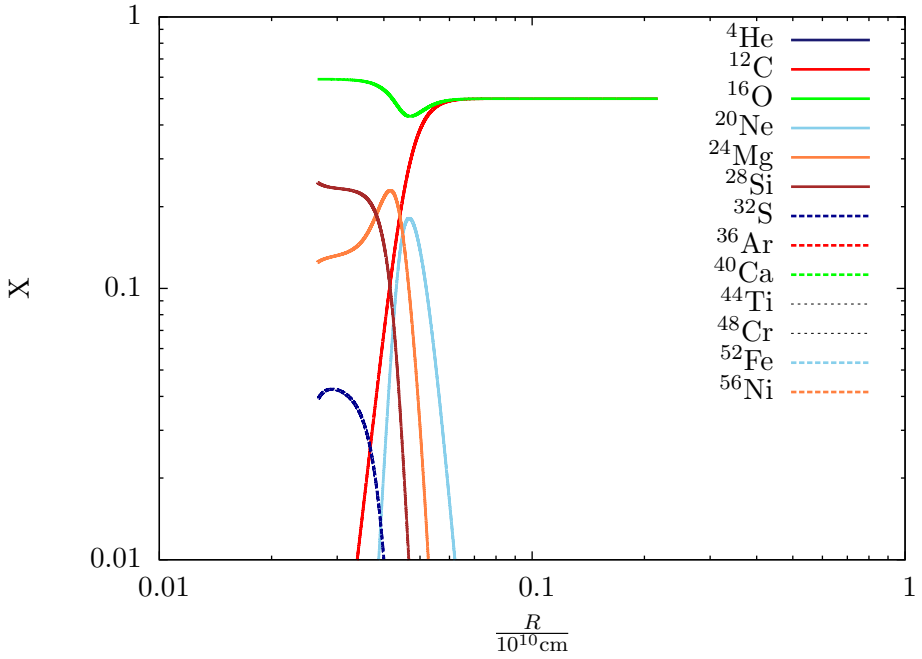

Figure 5.4: Mass fraction of elements in a disk from a carbon oxygen donor to a $300M_{\odot}$ black hole, at an accretion rate of $10^{6}\dot{M}_{\text{Edd}}$.

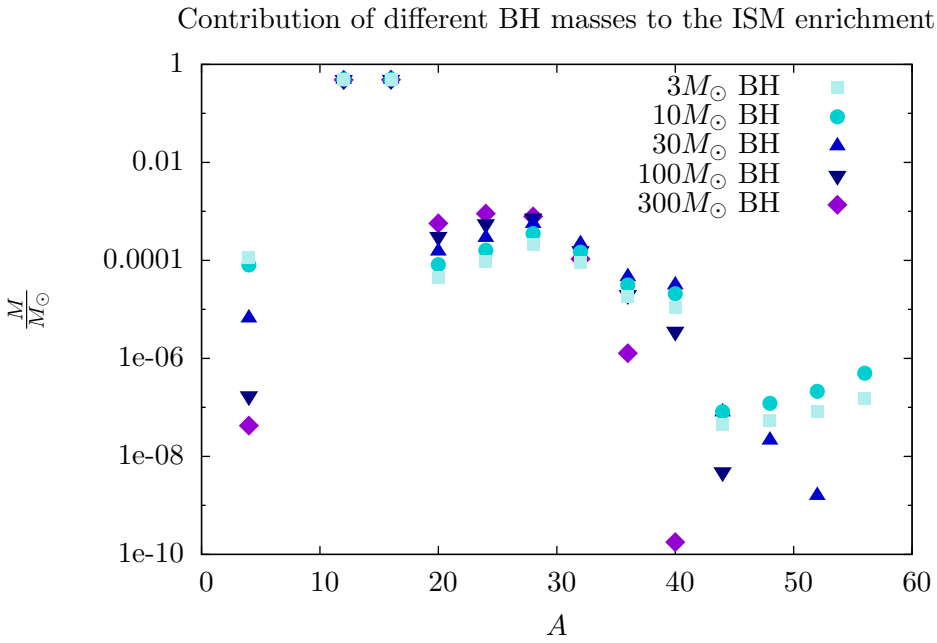

Figure 5.5: Mass ejected in winds in $M_\odot$ in function of element atomic mass A, for different black hole masses, from $3M_\odot$ in red to $300M_\odot$. The companion is a $0.6M_\odot$ CO white dwarf and accreting at $10^6 \dot{M}_{\rm Edd}$. As the black hole mass increases, the produced mass of helium (A=4) and heavy elements decreases because these elements are produced at the highest temperatures, located in the inner disk radius, proportional to the black hole mass.

As seen in the previous section, since the highest temperature of an accretion disk decreases with increasing black hole mass, and since this highest temperature is reached at the inner edge of the disk, for a given accretion rate, the nucleosynthesis location moves towards the inner edge as the black hole mass increases. For a given accretion rate, there exist a maximum black hole mass permitting nuclear fusion. This is due to the large size of the event horizon of massive black holes, letting the "high temperature location" be within the Schwarzschild radius.

A further consequence is that the elements which are most affected by a change of black hole mass are the elements synthesised at the inner edge of the black hole disk, namely helium and the heavier elements such as titanium, chromium, iron and nickel, as we can see very clearly in Figure 5.5. This remark is extremely important if we consider the problem in a slightly different angle than the direct topic of my thesis (ISM enrichment). A question under ongoing research is: can we detect the presence of intermediate mass black holes from the electromagnetic counter parts of a tidal disruption of a white dwarf? (e.g Law-Smith et al. (2017)). If such a tidal disruption allows the production of the four elements listed above, then the answer will tend towards a "yes", because these four elements are unstable so their decay could produce a light curve, which would perhaps be observable. This statement would need further investigations before drawing any conclusion. But if the disruption of a white dwarf does not produce these radioactive elements, then probing the presence of an IMBH through a tidal disruption could be more challenging, since it would reduce the observations to electromagnetic emission from the gas heated during the disruption: the amount of time

during which the event shines is more limited.

5.3.2 Effect of the accretion rate

Given a black hole mass, the accretion rate determines the temperature in the disk. For the alpha chain, optimum burning occurs between 10^9 and $10^{10}K$. As the accretion rate increases, the highest temperature attained in the disk increases too, and the burning location moves towards the outer disk. While running simulations for different systems and increasing the accretion rate, I realised that at some point, the "burning sweet spot" had moved outside of the disk. But if nuclear reactions start occurring already at the outer edge of the disk, I cannot integrate rigorously the burning network in the disk, as nuclear reactions would start already in the gas flow before forming the disk. This is not unphysical, but it would cause boundary conditions problems which are not treated in the present work. To investigate where the limits of the systems I can study stand, I calculated, as in the previous section, where exactly the $T = 10^9$K location stands, for different black hole masses and different accretion rates. As the outer edge of the disk, defined by the circularisation radius, depends on the size of the companion star, I did this computation for three different white dwarf masses: (1) $1.4M_\odot$, which represents the Chandrasekhar limit, maximum mass for degenerate electron pressure supported bodies (e.g. white dwarfs), and massive white dwarfs often contain oxygen and neon; (2) $0.6M_\odot$, typical CO white dwarf; and (3), $0.35M_\odot$ for a white dwarf which most likely contains helium. This consists in doing the same calculation as to produce Figure 5.2, but where the accretion rate is also varied a number of times, and for each accretion rate, the BH mass needs to be less than where the blue line of Figure 4.1 is under zero (i.e. the outer disk is not too hot for nucleosynthesis to have started further than the disk edge). The results are plotted in Figure 5.6 with red for a $1.4M_\odot$ WD, blue for a $0.6M_\odot$ WD and yellow for a $0.35M_\odot$ WD. Burning happens within the disk only for accretion rates located under these lines.

It is visible here that massive white dwarfs pose a problem in most situations, as for stellar mass black holes, the accretion rate is limited to $10^8\dot{M}_{\rm Edd}$. In unstable mass transfer, the accretion rate goes in a runaway process where it might exceed this limit. Lower mass white dwarfs are not concerned by this issue. The reason for which this maximum accretion rate allowed for the simulation is dependant on the white dwarf mass comes from the following: The disk size depends on the separation between the black hole and the white dwarf at the moment of the disruption. And this separation depends on the separation at Roche lobe overflow of the white dwarf, which is proportional to the white dwarf size. Now, remembering the mass radius relation of white dwarfs, $R_{\rm WD} \propto M_{\rm WD}^{-1/3}$, massive white dwarfs are more compact, smaller, than less massive white dwarfs. The size of the accretion disk is therefore less than for white dwarfs of lower masses.

5.3.3 Effects of the companion composition

Different types of white dwarfs exist, with different compositions, namely He, CO, ONe, ONeMg depending on the evolution of their progenitors. The nucleosynthesis in the accretion disk is inevitably affected by this difference in initial composition. In addition, the mass transfer might also be different as white dwarfs of different compositions may have different masses, and mass-radius relations. (Panei et al., 2000). Helium white dwarf have lower masses than CO white dwarfs, which have lower masses than ONe white dwarfs, as a result

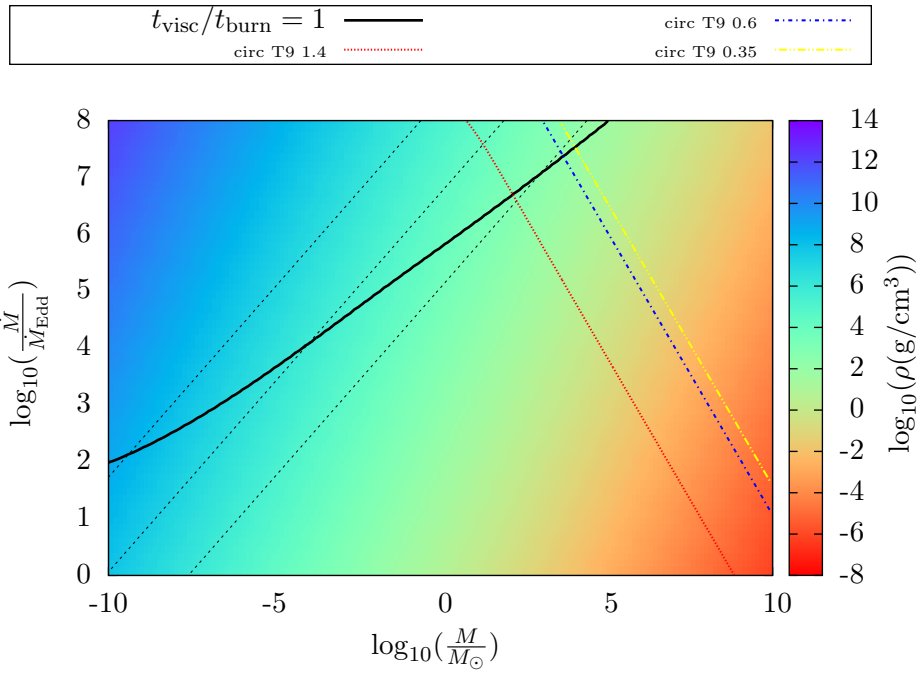

Figure 5.6: $M\dot{M}$ plane, where the black hole (BH) mass varies from asteroid mass to supermassive black hole, and the accretion rate from the Eddington limit to $10^8\dot{M}_{\rm Edd}$. Nuclear burning is allowed in the disk for the pairs $(M, \dot{M})$ located above the plain black line characterising an equality between burning and viscous time-scales. The three colored lines represent the limiting conditions for which the temperature of 10^9K is already attained at the outer edge of the disk (circularisation radius), for different white dwarf masses, with $1.4M_\odot$ in red, $0.6M_\odot$ in blue and $0.35M_\odot$ in yellow. The pairs $(M, \dot{M})$ must be located on the left of these lines for the nuclear burning to start inside the accretion disk.

of the growth of the burning core in stellar evolution. In Figure 5.7 we can note how different the disks are. Mainly, ONe white dwarfs have four different dominant elements in function of the position in the disk: ONe in the outer disk, then OMg as go inwards, Si and S, and finally helium provided from photodisintegration at higher temperatures. A He WD leads to a different outcome where Helium is always dominating, but a lot of nickel, iron, chromium and titanium are also produced. The reason for which a ONe WD does not produce such heavy elements is due to a lack of helium, needed for the alpha chain to take place. Therefore, any advanced nucleosynthesis needs wait for the heavier elements to undergo phtodisintegration, providing alpha particles and allowing nucleosynthesis to continue. But this happens when the temperatures are already high, so only very little time is available to produce heavier elmements. He white dwarfs do not have this problem as helium is very abundant. Another issue is that a disk composed of only helium needs to go through the triple alpha reaction to build heavier elements. And this reaction is very slow. We therefore need to wait to reach densities high enough to trigger the rest of the nuclear burning chain. As soon as the triple alpha reaction has started, then the rest of the burning goes very fast and many helium nuclei are available to produce heavy elements up to nickel, see Figure 5.7. Then, as in the case of the ONe WD, the disk undergoes photo disintegration when it reaches the high temperatures at the inner disk edge. A comparaison of the yields id plotted in Figure 5.8, where one can

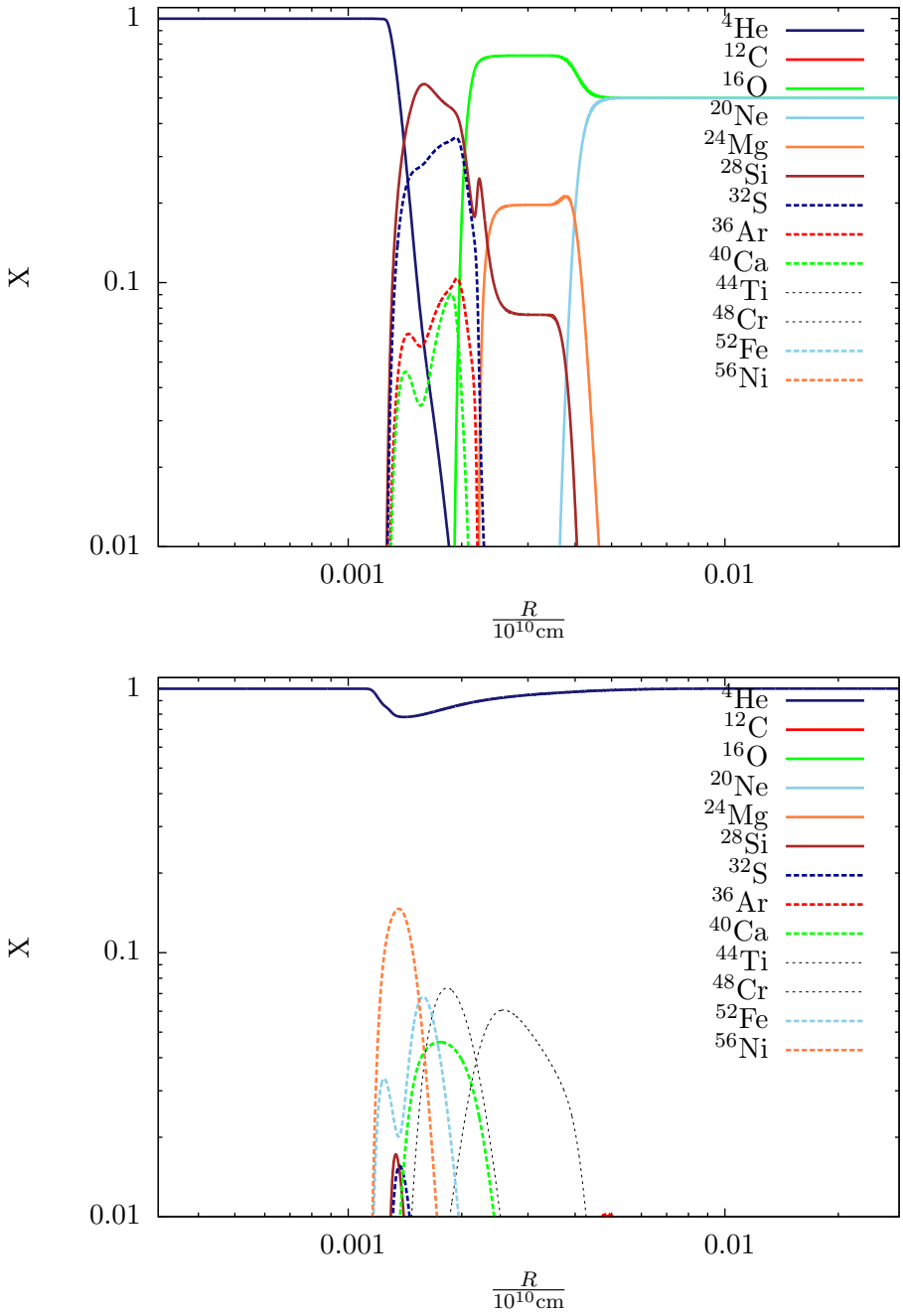

Figure 5.7: Chemical composition (mass fraction) of a thin disk for two different donor compositions: *upper panel*: oxygen neon and *lower panel*: helium, to a $3M_{\odot}$ black hole accreting at a rate of $10^{7}\dot{M}_{\text{Edd}}$. The elements dominating the disk are very different in function of the donor composition, so in function of the white dwarf type.

note that lack of helium in disks limits the production of heavier elements.

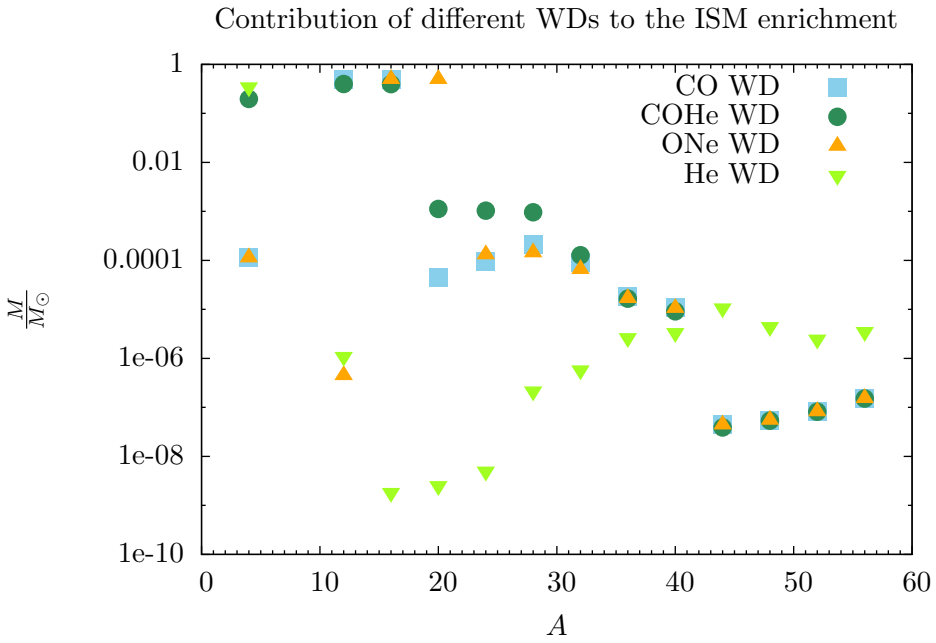

Figure 5.8: Mass of elements ($M_\odot$) ejected in winds from the disk around a $3M_\odot$ black hole accreting at $10^6\dot{M}_{\rm Edd}$ in in function of element atomic mass A, for different white dwarf types.

5.3.4 Effect of nuclear energy

The Shakura-Sunyaev solution I implemented has the advantage be computationally light. But it is an analytical solution which holds only under a large set of assumptions. By considering such high accretion rates, responsible for high temperatures and therefore nuclear reactions, the assumption that the only source of heating was of a viscous origin, and that the unique cooling mechanism was radiation, was broken because of energy coming from nuclear reactions. To know if this energy has a significant effect on the accretion disk, I computed the nuclear power in function of radius (position in the disk) and compared it to the viscous dissipation rate, characteristic to the disk. I also compare it to the gravitational energy release rate (which should be of same order of magnitude as the viscous dissipation rate since this is exactly the assumption under the thin disk model) in order to see if the release of energy could be enough to power winds.

One nuclear reaction produces (or uses) an amount of energy $Q = \Delta mc^2$ which correspond to the mass difference between the reactant nuclei and products. Given a nuclear reaction rate, the energy production rate by a two body reaction such as 2.5 will be:

$$\dot{Q} = Y_{\rm A} Y_{\rm B} \rho < \sigma v >_{\rm AB} N_{\mathcal{A}} Q_{\rm AB} {\rm MeV/g/s} \tag{5.15}$$

Where I took arbitrary units. To compare it with the viscous energy released in accretion disks $D(R)$ (Equation 3.25), I express it in Joules and per unit surface per unit time. Therefore,

$$\dot{Q} = Y_{\rm A} Y_{\rm B} \rho < \sigma v >_{\rm AB} N_{\mathcal{A}} Q_{\rm AB} \Sigma {\rm J/cm^2/s} \tag{5.16}$$

In a ring $(R, R + dR)$ in the disk, more than one reaction occur. Considering them all, the total energy production rate is the sum of the production of all these reactions. We call the

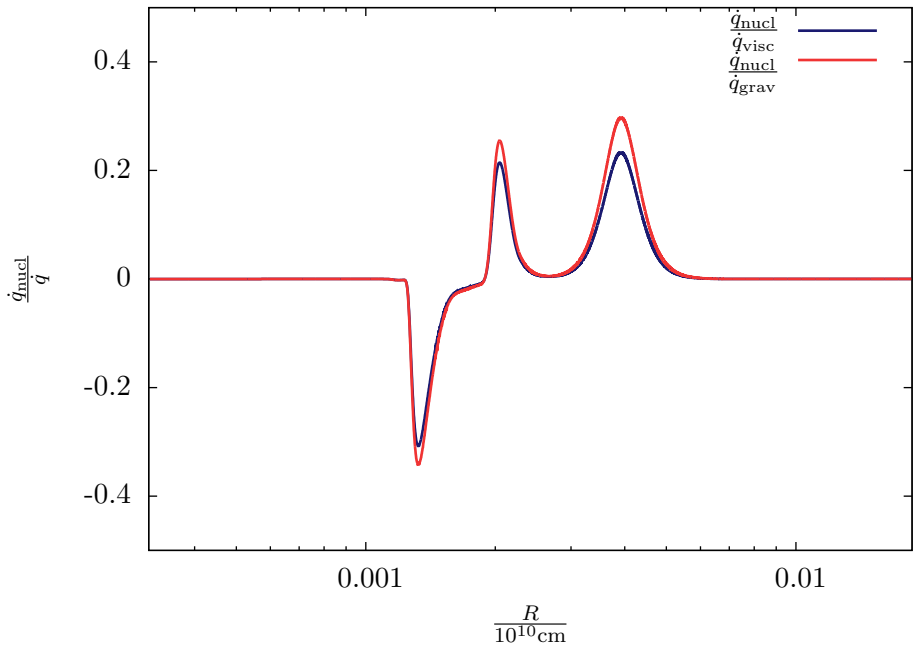

Figure 5.9: *Blue:* Ratio of nuclear energy generation to viscous dissipation as a function of position in the disk. As I assumed the only heating source of the disk was of a viscous origin, nuclear energy becomes significant when this ratio comes close to 1 in absolute value. This happens at three locations where the ratio is about a third. Carbon burning generates a significant amount of energy on the right hand side. In the middle, oxygen burning is the source of nuclear energy. On the left, the energy generation is negative because this corresponds to photodisintegration of heavier nuclei. Photodisintegration is endothermal, taking internal energy from the disk. *Red:* Ratio of nuclear energy generation to gravitational energy release as a function of position in the disk. A low ratio indicates that even if the nuclear energy were entirely absorbed, this is not enough to escape the potential well of the BH.

energy release rate $\dot{q}_{\rm nucl}$.

$$\dot{q}_{\rm nucl}(R) = \sum_{\rm A,B} Y_{\rm A}(R) Y_{\rm B}(R) \rho(R) N_{\mathcal{A}} < \sigma v >_{\rm AB} (R) N_{\mathcal{A}} Q_{\rm AB} \Sigma(R) {\rm J/cm^2/s} \tag{5.17}$$

The fraction of nuclear power to viscous heating is plotted in Figure 5.9 in blue. To compare the nuclear energy release rate to the gravitational energy release rate, we can compare $\dot{E}_{\rm nucl} = \Delta m c^2$ to $\dot{E}_{\rm grav} \approx \dot{M} c^2$. This quantity is plotted in red in Figure 5.9.

In most of the disk, the ratio is zero and nuclear energy is negligible. However, carbon and oxygen burning release a lot of energy, almost a third of the viscous heating, so almost a forth of the total energy release should come from nuclear burning in these two hot spots of the disk. Additionally, photodisintegration is endothermic and uses a lot of energy from the inner disk. How these gamma rays actually interact with the material in the accretion disk should be investigated. As these investigations require to shift to an hydrodynamical code or implement one in order to account for nuclear burning in the energy equation, which is (1) computationally expensive, (2) time demanding for learning it and running it, I will

only speculate qualitatively how the results can be affected. In this optically thick disk, the photons are in equilibrium with the gas through scattering. The disk temperature should therefore rise. Two effects are noticeable from an increase in temperature. Firstly, different nuclear reactions can occur, and at different rates. So the disk composition should change. Secondly, this internal energy could help powering winds. This aspect is discussed in the last chapter.

Now that the parameter space is explored, to infer any conclusions, one needs to know what the parameter space looks like in Nature: how often does, for example, a system with a $10M_{\odot}$ BH with a CO WD form?

Chapter 6

Production and event rates

In this chapter, I summarise the proposed formation channels of BH–WD binaries and find the rate at which they are produced. We are particularly interested in the BH – WD binaries wich are exchanging mass. Such systems are categorized as Ultra Compact X-ray Binaries (UCXBs). About 16 of them are known, of which 10 are in the Galactic field (Nelemans & Jonker, 2010) and 6 are in globular clusters (Chen & Podsiadlowski, 2016; Cartwright et al., 2013; Bahramian et al., 2017). They are a subcategory of low mass X-ray binary (LMXB)s. Most LMXBs in the Galactic field are thought to form through stellar binary evolution while in globular clusters, the favourite scenario is dynamical interaction, due to high stellar density. The proportions of observed LMXBs per unit mass in globular clusters relative to the Galactic field are considerably higher. Verbunt & Hut (1987) find that there are of the order of thousand times more LMXBs per unit mass in clusters than in the Galactic field. Known LMXBs are thought to contain a neutron star accretor. To date, all detected LMXBs are confirmed neutron stars. But recent observations of the system 47 Tuc X9 could suggest there is a candidate which might host a black hole and a carbon oxygen donor (Bahramian et al., 2017), but it is not confirmed. As a result of this lack of observational evidence, working-out the production scenarios is done theoretically and with numerical simulations, together with many assumptions, leading to large uncertainties.

6.1 Collision in globular cluster

Compact binaries (binary systems made of compact objects) can form in dense globular clusters (Verbunt & Hut, 1987). The formation channels of neutron star (NS)-WD binaries through dynamical interactions have been investigated in Ivanova et al. (2008). A NS entering in direct collision with a red giant (RG) can form a compact binary with the RG's degenerate core, resulting in a NS-WD binary (Davies et al., 1992). The cross section is significant due to the large radius of a RG. This scenario can also be envisaged for stellar mass black holes instead of neutron stars (Ivanova et al., 2010).

The collision cross section between a black hole of mass $M_{\rm BH}$ and a RG of mass $M_{\rm RG}$ at a relative velocity at infinity v_∞ can be worked out as

$$\sigma_{\rm col} = \pi r_{\rm max}^2 \left(1 + \frac{2G(M_{\rm BH} + M_{\rm RG})}{r_{\rm max} v_\infty^2}\right), \tag{6.1}$$

where the second term in the parenthesis is gravitational focussing. The quantity $r_{\rm max}$ is the maximum separation that will lead to a collision. If stars were solid balls, $r_{\rm max} = R_{\rm RG} + R_{\rm BH}$.

But we are interested in the maximum separation that will allow the formation of a BH–WD binary compact enough for mass transfer to start. The maximum separation $r_{\max}$ can be determined with accuracy with SPH simulations as it was done in Lombardi et al. (2006) for NSs. For a notation in units of RG radius we can introduce the dimensionless parameter $f_{\rm p}$ such that $r_{\max} = f_{\rm p} R_{\rm RG}$. For NSs, the results of the simulations gave $f_{\rm p} = 1.3$. Other SPH simulations for $15 M_\odot$ BHs apparently resulted with $f_p = 5$ (unpublished). To know if this value was reliable, I contacted N. Ivanova who confirmed the results from several SPH simulations of her and collaborators. As the size of a RG star evolves during its life time, not all RGs in the cluster have the same size, depending on their evolution stage (so depending on their birth mass). So the total collision rate of BHs and RGs is the integral over the RG radius. This is equivalent to using Equation 6.1 with a mean RG radius $\langle R_{\rm RG} \rangle$, which can be calculated with a prescription for the size evolution of the RG or a stellar evolution codes (Ivanova et al., 2005). The collision rate of black holes and RGs in a volume V is

$$r_{\rm col} = N_{\rm BH} N_{\rm RG} \sigma_{\rm col} v_\infty \frac{1}{V}. \tag{6.2}$$

The number of RGs $N_{\rm RG}$ is approximately $n f_{\rm RG} V$ where n is the number density of stars in the volume V, and $f_{\rm RG}$ is the fraction of RGs.

To find an upper limit on this collision rate, we can consider the number density of stars n where it is maximum, in the core of a globular cluster. Ivanova et al. (2010) provides typical values for the fraction of RG stars, the core star density, and the mean radius of RGs. Strader et al. (2012) discovered two stellar mass black holes in the globular cluster M22 and performed a statistical analysis to conclude there should be between 5 and 100 black holes in this cluster. The upper limit on the collision rate is calculated with a maximum of 100 stellar mass black holes in a globular cluster. See table Table 6.1 for the values.

n	$f_{\rm p}$	$f_{\rm RG}$	$R_{\rm RG}$	$r_{\max}$	v_∞	$N_{\rm BH}$
$10^5 {\rm pc}^{-3}$	5	0.008	$\sim 3.7 R_\odot$	$5 R_{\rm RG}$	10km/s	$5 - 100$

Table 6.1: Values of the number density of stars in the core of a globular cluster,the maximum distance for ,the fraction of RGs, the averaged radius of RGs over time, the maximum radius for mass transfer to start, the velocity dispersion of stars in the cluster (Ivanova et al., 2010), and the number of black holes (Strader et al., 2012).

The collision rate is

$$r_{\rm col} = N_{\rm BH} f_{\rm RG} n \pi f_{\rm p}^2 \langle R_{\rm RG} \rangle^2 \left(1 + \frac{2G(M_{\rm BH} + M_{\rm RG})}{f_{\rm p} R_{\rm RG} v_\infty^2} \right) v_\infty, \tag{6.3}$$

With a typical black hole mass of about $10 M_\odot$ we find a rate of 10 collisions /Gyr per cluster. When such interactions happen, mass transfer from the reg giant can, if rapid enough, generate a common envelope phase. During this phase, the black hole and the RG core both orbit around their common centre of mass within the envelope provided by the reg giant. The binary heats the gas in the envelope through tidal draf forces and looses energy. This results in a more tight binary system. This procedure continues until the envelope has evaporated. If enough energy is transferred to the envelope, it will become unbound and the outcome system might be a BH–WD binary. Depending on the separation between the two bodies at this moment, two different outcomes can be envisaged. If the binary is very tight, with a period

of the order of tens of minutes, the system looses angular momentum through gravitational radiation, and this might result in mass transfer or tidal disruption of the white dwarf by the black hole. If the separation is larger, then the merger would happen in more than Hubble time if no external boost takes angular momentum from the system (e.g. interaction with a third body). In the common envelope phase, if not enough energy is transferred to the common envelope, the shrinking of the separation between the black hole and the white dwarf does not stop, and this results in a merger. This mechanism of common envelope evolution phase is not well understood, and still subject to research. Therefore, the production rate of the BH–WD X-ray binaries has large errorbars. The amount of energy transferred from the binary $\Delta E_{\rm Orb}$ to the envelope $\Delta E_{\rm env}$ can be written as

$$\Delta E_{\rm env} = \alpha_{\rm CE} \Delta E_{\rm Orb} \tag{6.4}$$

(e.g. Postnov & Yungelson (2014)), where $\alpha_{\rm CE}$ is called the common envelope efficiency, and characterises the fraction of energy transferred from the shrinking binary to the envelope. Empirical values for this parameter have been measured by Zorotovic et al. (2010), studying post common envelope evolution systems. And a real question is that it is not known what determines $\alpha_{\rm CE}$ (for example, it is unknown whether it depends on the mass of the system, which makes its application to black holes uncertain). Thus all rates of events inferred from common envelope evolution are questionable (e.g Toonen (2017) for the rate of supernovae type Ia, coming from mass transfer onto white dwarfs). Therefore a rate of BH–WD UCXB formation inferred from common envelope evolution will, at best, be an order of magnitude. Sorting with common envelope evolution between systems which will lead to BH–WD mass transfer and systems which will not lead to BH–WD mass transfer within a Hubble time reduces the rate of about 10% (Ivanova et al., 2010), leading to finally about 1.5 UCXB per Gyr per cluster. From this production mechanism, due to the energy loss to the gas, the orbit of the stars is close to circular, so the assumptions of circular orbits made in the previous chapters is correct.

6.2 Dynamical interaction in globular cluster

More mechanisms can lead to the formation of an UCXB in a globular cluster. Kuranov et al. (2001) argue on the formation of low mass X-ray binaries from triple systems. Ivanova et al. (2010) estimate the number of three-body encounters by black holes in a cluster, and conclude three body encounters are not significant enough to account for the observed rates of BH–WD X-ray binaries. A hierarchical three body system, made of a pre existing binary BH–WD and an additional star, which undergo Kozai mechanism can result in binary mass transfers. Kozai mechanism describes secular interaction when the two orbital planes of the system are not aligned, where the eccentricity and relative inclination start oscillating. If the system becomes eccentric enough, this could trigger mass transfer.

6.3 Binary stellar evolution channel

Ultra-compact X-ray binaries are observed in the Galcactif field (Nelemans & Jonker, 2010), so there must be other mechanism than dynamical interactions to form them, such as binary interaction. When two stars form close to each other and stay gravitationally bound, they form a binary system where the stars orbit their common centre of mass and may exchange

material, depending on their size, mass ratio (ratio of their masses) and separation. This configuration is particularly frequent for massive stars (Sana et al., 2012) which are thought to be progenitors of BHs. We can therefore question the possibility of evolution of these binary systems towards a BH–WD compact binary.

To study how binary stars evolve, a first approximation (which may be inaccurate) is to assume that our description of single stellar evolution is correct in the binary case, and include mass transfer, responsible for changes in the mass ratio and separation. This is what many population synthesis codes are based on and currently used in the community. In the current project, I envisaged performing a population synthesis using realistic initial distributions of binary stars (mass, mass ratio, separation, metallicity) and then investigating the production rate of BH–WD systems with the stellar evolution code `BSE` (Hurley et al., 2002). This would have allowed me to track the production rate for different BH masses and WD types, since we have seen the production of different elements depends strongly on the white dwarf composition. However, I learned that uncertainties in such models would be too large to estimate these properly and the code might lead to mergers instead (S.E. de Mink, private conversation). To have a general order of magnitude of the number of BH–WD systems (without specifying possible types), I instead studied work in the literature. Belczynski & Taam (2004) performed a population synthesis of UCXBs in a very similar way, proposed different formation channels for these systems, and compared their relative contributions.

A first formation scenario for BH–WD binary systems can be provided by the evolution of a massive star of about $8M_\odot$ with a lower mass companion, of about $4-7M_\odot$. The primary evolves until the asymptotic giant branch, with an oxygen-neon-magnesium core, and loosing its envelope due to expansion. More massive, it cedes some mass to the secondary, and the separation between them shrinks. The mass transfer is unstable: the mass loss rate is too large for the transfer to be conservative. Material piles-up around the two stars, leading to a common envelope phase (CE). Losing angular momentum, the system cedes energy to the envelope and, if a merging event is avoided, ends with an ONeMg WD in a binary with a main sequence star (MS). When the secondary uses its nuclear fuil and expands, a second CE phase occurs, and the system eventually becomes an ONeMg WD in binary with a He star or a WD., of comparable mass. The secondary star comes to fill its Roche lobe once more, due to orbit shrinkage from gravitational waves emission, and stable mass transfer occurs into the primary WD. The primary degenerate companion comes to exceed its critial mass, the Chandrasekhar limit, and collapses to a neutron star (NS) or BH . This event is named accretion induced collapse (AIC). This is where the mass of the secondary becomes important: if it is less than about $4M_\odot$, no mass transfer occurs and the systems remains as it is. If the secondary is of the range described above, $4-7M_\odot$, mass transfer goes on and the neutron star undergoes a second AIC event and collapses to a black hole. The secondary becomes a low mass (about $3.5M_\odot$) HeCO WD. About 7.5% of BH–WD UCBs are formed through this channel with a period of less than 80 min. A similar scenario consists again of two common envelope phases, but each of them followed by stable mass transfer. 4.4% of UCBs form to reach these systems with a period less than 80 min.

The most famous scenario to form a BH through stellar evolution is the implosion of a massive star during a type II supernova. This direct formation does not form UCXB according to Belczynski & Taam (2004), although massive stars in their systems can undergo type II supernovae to form neutron stars, which then form black holes through AIC. This formation process is the least efficient due to the potential supernova kick applied to the neutron star during its formation. About 3.8% of BH UCXBs with period less than 80 min are thought

to form according to this scenario. If the supernova occurs after a phase of mass transfer, another 3.1% of BH UCXBs are produced with short periods.

The total number of short period BH UCXBs produced in the Galactic field in 10 Gyr is estimated to 90, where 95% of the donors are HeCO white dwarfs and 5% are CO white dwarfs (Belczynski & Taam, 2004).

Chapter 7

Other systems

Other systems can provide nucleosynthesis conditions in accretion disks. Nuclear reactions which need lower temperatures than nuclear fusion between two charged nuclei, such as neutron capture, can happen in neutron-rich disks. Or perhaps, very low mass black holes, on the left side of Figure 4.2, could allow nuclear burning if they can accrete at a rate of about their Eddington limit.

7.1 Neutron star - neutron star and black hole - neutron star

Many mechanisms have been thought of to form black holes in the literature. One scenario is the merger of two neutron stars. The total mass exceeding the Chandrasekhar mass limit, it would produce either a very fast rotating neutron star or a central black hole and a dense accretion disk rich in neutrons. The nucleosynthesis in such an event produces many neutron capture elements (Wu et al., 2016; Fernández & Metzger, 2016). Neutron capture permits to synthetise elements heavier than iron by successive increases the number of neutrons of a nucleus and radioactive decays to a more stable atom. Two process exist, the s-process (slow) when the decay occurs faster than the neutron capture, and the r-process (rapid) when the neutron capture occurs faster than the radioactive decay. This last mechanism is thought to happen in neutron star mergers. Two main observations could be explained by this mechanism. Firstly, neutron star mergers consist in one of the many model which could explain the observed short gamma ray bursts, which are very bright events seen in gamma rays, with a duration of less than 2 seconds (Levan et al., 2016). These observations help putting constraints on models, using event rates, light curves from radioactive elements, spectra, produced elements and other signatures. Secondly, neutron capture elements are observed in old metal poor stars (Sneden et al., 2008). It was proposed that the explosions of early massive stars release r-process elements, which would now be contained in old low mass stars (Sneden et al., 2008). Such scenario would provide an excellent framework to study the first supernova: nature of produced elements, use of radioactive elements to date their production and thus find at what time the earliest supernovae occurred, for example. But if some of these r-process elements come from neutron star mergers, one needs to identify which elements, and in which fractions.

7.2 Primordial black holes

Black holes outside from the stellar mass range must form differently from stellar evolution. Those which do not form from stars but are present in the early Universe are called primordial black holes, and can be candidates for dark matter In this section, I study the effect of black holes of masses from $10^{-10} - 10^{-1} M_\odot$. Considering nucleosynthesis in accretion disks around such black holes can be extremely interesting. Firstly, they could enrich the ISM in the early Universe, at very high redshift, and if they did, then the first stars could already contain metals. Another interesting consequence of nucleosynthesis in their accretion disks is that this could allow us to detect their presence. Asteroid mass black holes can heat gas, when they travel through material, because they accrete material through spherical Bondi accretion. The temperature of the accreted gas depends on the accretion rate into the black hole. The Bondi accretion rate depends on the gas density. Densities as high as stellar core or big bang conditions are needed to reach temperatures allowing nucleosynthesis.

For a black hole travelling through material (ISM for example) at a relative velocity $v_{\rm rel}$, in the rest frame of the BH, the total energy per unit mass of the gas is

$$E = E_{\rm K} + E_{\rm P} + U, \tag{7.1}$$

where U is its internal energy and involves a term of sound speed $c_{\rm s}$. The specific energy (energy per unit mass) of the gas will be respectively

$$E_{\rm K} = \frac{v_{\rm rel}^2}{2}, \tag{7.2}$$

$$U = \frac{c_s^2}{\gamma - 1}, \tag{7.3}$$

$$E_{\rm P} = -\frac{GM_{\rm BH}}{r}. \tag{7.4}$$

We define R_0, the radius within which the material is bound to the black hole. It corresponds to the iso-surface where $E = 0$. Then neglecting factors of the order of unity, the black hole accretes the following amount of mass during a time Δt:

$$\Delta M_{\rm BH} = \pi R_0^2 \rho \sqrt{v_{\rm rel}^2 + c_{\rm s}^2} \Delta t \tag{7.5}$$

Replacing R_0 by its expression and taking the limit $\Delta t \to 0$, this gives an approximation of the accretion rate into the BH,

$$\dot{M} = \frac{4\pi\rho (GM_{\rm BH})^2}{(v_{\rm rel}^2 + c_{\rm s}^2)^{3/2}}. \tag{7.6}$$

In terms of Eddington limit, this gives

$$\frac{\dot{M}}{\dot{M}_{\rm Edd}} = \frac{\rho \sigma_{\rm T} G M_{\rm BH}}{2(v_{\rm rel}^2 + c_{\rm s}^2)^{3/2} m_{\rm p} c} \tag{7.7}$$

where $m_{\rm p}$ is the mass of the proton, and c is the speed of light. For a given relative velocity, and if we demand the accretion rate to have a certain value (since we are interested in high accretion rates providing conditions favourable to nucleosynthesis), this gives us constrains on the density of the material. We get

$$\rho = \frac{2m_{\rm p}c}{\sigma_{\rm T}GM_{\rm BH}}(v_{\rm rel}^2 + c_{\rm s}^2)^{3/2}\frac{\dot{M}}{\dot{M}_{\rm Edd}}, \tag{7.8}$$

approximately

$$\rho \approx 10^{-13}(v_{\rm rel}^2 + c_{\rm s}^2)^{3/2}\left(\frac{M_\odot}{M_{\rm BH}}\right)\left(\frac{\dot{M}}{\dot{M}_{\rm Edd}}\right){\rm g/cm^3}. \tag{7.9}$$

To maintain a given accretion rate, a low mass black hole will need a denser environment than a more massive black hole. So very low mass black holes, of asteroid mass, will need to accrete from inside something very dense. From what kinds of mediums can a black hole accrete about its Eddington limit? Using the previous equation, and letting on the left-hand side of the equation all the properties which are intrinsic to the material, for example the sound speed (together with the relative velocity), we can write

$$\frac{\rho}{(v_{\rm rel}^2 + c_{\rm s}^2)^{3/2}} \approx 10^{-13}\left(\frac{M_\odot}{M_{\rm BH}}\right)\left(\frac{\dot{M}}{\dot{M}_{\rm Edd}}\right){\rm g/cm^3}. \tag{7.10}$$

And let us go through different types of objects, compute the quantity $\frac{\rho}{(v_{\rm rel}^2+c_{\rm s}^2)^{3/2}}$ in the most optimistic condition ($v_{\rm rel} = 0$), and see what the corresponding black hole mass should be. We can consider molecular clouds, main sequence stars, more compact objects such as white dwarfs. If white dwarfs, which are the densest bodies of this list, do not provide the necessary conditions, then considering molecular clouds and main sequence stars will not be relevant. So let us start with white dwarfs:

The density ρ of a white dwarf is roughly $8 \times 10^5{\rm g/cm^3}$. And the sound speed is of the order of $c_{\rm s} = kT/m_{\rm p}$. Then, $\frac{\rho}{c_{\rm s}^3} = 3 \times 10^{-8}{\rm gs^3cm^{-3}m^{-3}}$. This corresponds to the case where a primordial black hole of mass $M_{\rm BH}$ sits, at rest, inside a white dwarf. But this case it not very realistic: how do such systems form? There should be a relative velocity between the black hole and the white dwarf medium. If, now, we say this velocity is of the order of the orbital velocity at the surface of the white dwarf, then $\frac{\rho}{c_{\rm s}^3} = 3 \times 10^{-14}{\rm gs^3cm^{-3}m^{-3}}$. We can now plot this in function of the black hole mass, see Figure 7.1. In this figure, the density must be greater than the one illustrated by the red line for the corresponding black hole to accrete at its Eddington limit. In the same plot, I show where white dwarfs stand, for the two relative velocities just considered (zero and orbital). In the case a black hole at rest inside a white dwarf, the black hole mass must be greater than about $3 \times 10^{-5}M_\odot$. For a black hole moving at the orbital velocity right at the surface of the white dwarf, then the mass must be greater than a Solar mass. It is not surprising to find, for an orbital velocity, a similar result as for the Roche mass transfer considered in previous chapters. But this mass is too large and we have already considered stellar mass black holes. It now seems irrelevant to consider less dense bodies which will lead us to find that only black holes of masses above stellar mass can accrete at the interesting accretion rates.

A scenario could be imagined where a primordial black hole crosses a white dwarf at a large velocity, close to its escape velocity (thus not accreting much), but loosing energy, and crossing back the white dwarf a certain number of times, loosing energy each time. Subsequently, the black hole would be trapped inside the white dwarf and see its velocity decreasing, up to a point where it can accrete fast enough to ignite. Now, this is very speculative. And if there were ignition, what would happen? Well inside the white dwarf, it would be difficult to release the nucleosynthesis products to the ISM. Or, could the burning inside the white dwarf trigger

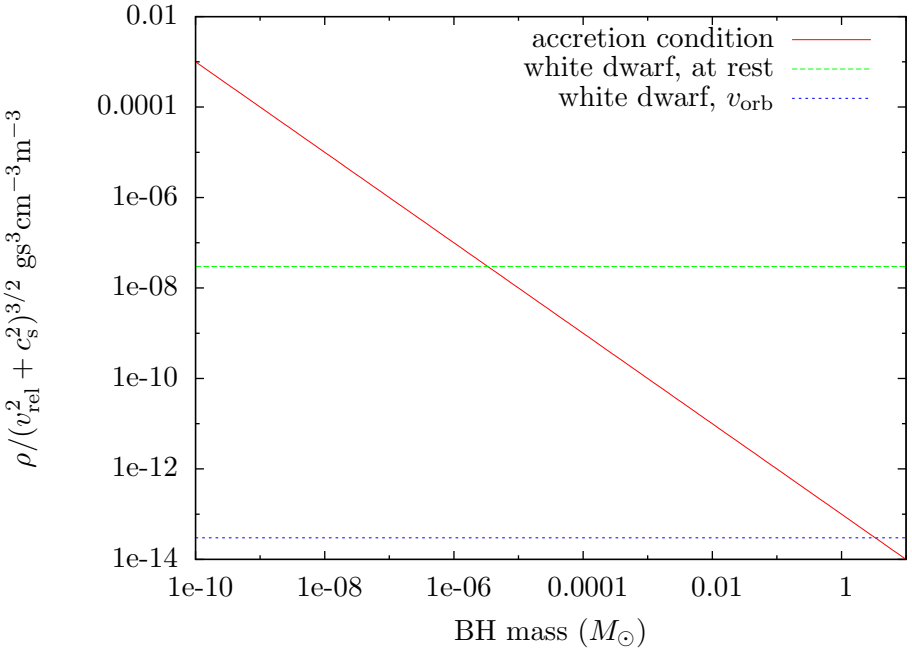

Figure 7.1: *Red*: Condition on the density of matter surrounding a black hole such that the black hole accretes the material at its Eddington limit. *Green*: corresponding value for the matter inside a white dwarf, when the relative velocity between the black hole and the medium inside the white dwarf is zero, $v_{\rm rel} = 0$. *Blue*: corresponding value for the matter inside a white dwarf, when the relative velocity between the black hole and the medium inside the white dwarf is the orbital velocity, $v_{\rm rel} = \sqrt{GM_{\rm WD}/R_{\rm WD}}$.

a carbon ignition and an event similar to a type Ia supernova? To answer this question, one could consider the number of primordial black holes that can exist today (many constraints are fixed, by microlensing for example, see Figure 3 in Carr et al. (2016)) and work-out the rate at which these events happen. But conditions to see a thermonuclear explosion of a white dwarf triggered by nuclear burning due to a primordial black hole inside it are rather difficult to infer and not the purpose of the present work.

Chapter 8

Interstellar medium enrichment

The nucleosynthesis products from the white dwarf disruption around a black hole are mainly alpha elements. Stars release alpha elements in two different processes. Low mass stars ($3-6M_{\odot}$) (Nomoto et al., 2013) release carbon during the 3rd dredge up stage, blowing off a carbon-rich atmosphere in winds. Massive stars ($13-50M_{\odot}$) which end their lives in supernova explosion expell all the outer layers containing the burning products of stellar evolution, up to iron, see Figure 8.1. How do these stars compare to the accretion disk products? I first estimate how individual objects compare, compute roughly the relative contribution between each system, and in a second section, I account for the distribution of each of these systems.

8.1 Nucleosynthesis yields

In this section, I compare my predictions of the individual nucleosynthesis yields of BH–WD tidal disruptions to expected yields from stellar evolution models, which I take from Nomoto et al. (2013). The main sources of alpha elements are stars low mass stars ($3-6M_{\odot}$) experiencing dredge up and releasing mainly carbon and s-process elements, and massive stars ($13-50M_{\odot}$), exploding in supernova. The $8-13M_{\odot}$ stars mostly experience "faint supernovae" (Nomoto et al., 2013) and do not release many metals. One BH–WD system releases approximately 100 times more carbon than one dredge up star, and the dredge up star does not release other alpha elements. See Figure 8.2. A $13M_{\odot}$ star releases, in comparison, about 10 times more of carbon and oxygen, and a hundred to a thousand times more of the other alpha elements as it can be read from Figure 8.1. I can comment already on the content of this figure which shows the yields from a $13M_{\odot}$ star. The elements that I chose to include in the burning network are also the elements which dominate the production of these stars. In other words, in this plot, for stars (black plus and red crosses), the elements which are not the alpha elements (A = 4, 12, 16, 20 etc) are produced in smaller quantities than alpha elements. This difference is of serveral orders of magnitudes. Looking at the temperature-density plane, Figure 4.1, we see that the path of the stellar core and accretion disk follow a similar pattern as soon as they pass carbon burning. We therefore expect similar nucleosynthesis yields for heavier elements. This indicates that the burning network I implemented is a good "first approximation" for the burning network of the star in Figure 8.1. Or said differently, the correct reactions were neglected for the nuclear burning in the accretion disk.

One single event produces, at best, a hundred times less heavy elements than a $13M_{\odot}$ star, except for carbon and oxygen which did not burn in the outer disk and are over produced

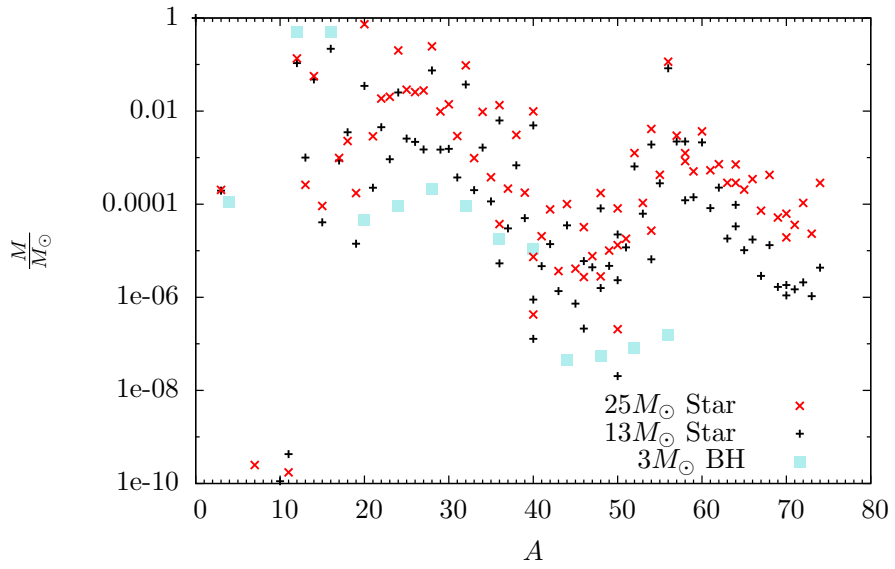

Figure 8.1: Mass ejected in winds in $M_\odot$ in function of element atomic mass A, for a $3M_\odot$ BH disrupting a $0.6M_\odot$ CO WD and accreting at $10^6\dot{M}_{\rm Edd}$. The black pluses are the elements produced and ejected during the evolution of a $13M_\odot$ star, and the red crosses are the elements produced and ejected during the evolution of a $25M_\odot$ star.

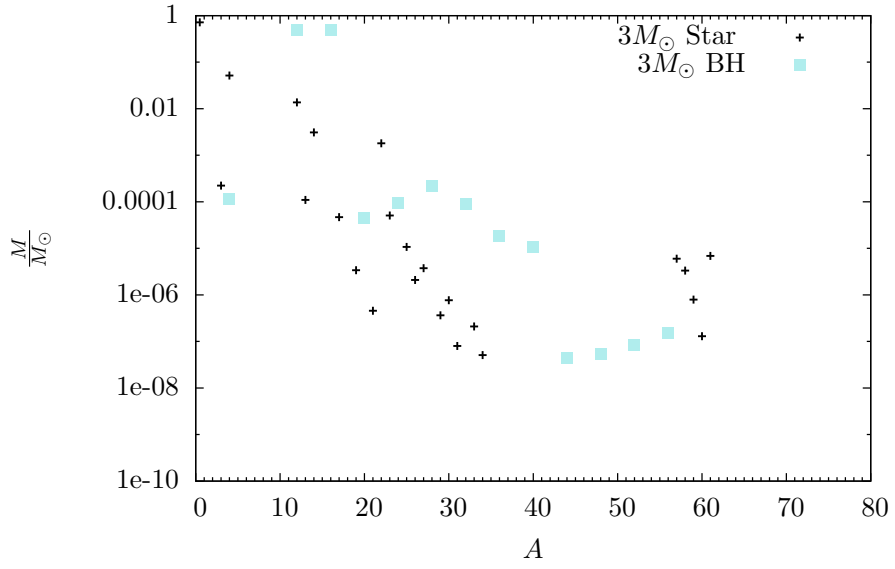

Figure 8.2: Mass ejected in winds in $M_\odot$ in function of element atomic mass A, for a $3M_\odot$ BH disrupting a $0.6M_\odot$ CO WD and accreting at $10^6\dot{M}_{\rm Edd}$. The black pluses are the elements from the evolution of a $3M_\odot$ star.

in the BH–WD disk of a factor 10. This difference increases for heavier elements ($A > 40$). And the excess of carbon produced by BH disks may be compensated by dredge up stars. To know whether it is compensated or not, one should consider the number of dredge up stars per thight BH–WD system. I have done it and it is described in the next section.

8.2 Relative enrichment: black hole disks versus stars

The fraction of BHs which ends up in UCXBs is roughly known for both globular clusters and the Galactic field, from Chapter 6. The contribution of one UCXB relative to one massive star and to one low mass star is also known, from the previous section. To finally know the total relative contribution to the Milky-Way content, the only missing piece the ratio black holes to these stars. I compute them separately as follows.

Assuming that the mass of stars determine the outcome of their evolution, for example main sequence stars below $8M_\odot$ finish their lives as white dwarfs, stars between $8-25M_\odot$ become neutron stars after a supernova explosion, and stars between $25-50M_\odot$ become black holes, then a simple calculation can be made to estimate the fraction of UCXBs. Using the distribution of masses at which stars are born, the Initial Mass Function (IMF), one can derive the fraction of BH to stars. I used the IMF of Kroupa (2001) giving a distribution

$$\zeta(m)\mathrm{d}m = \zeta_0 m^{-\alpha}\mathrm{d}m, \tag{8.1}$$

where $\alpha = 2.3$. The integral of ζ over a given mass range gives the number of stars forming in this mass range, if ζ_0 is known. The number of stars between $M1$ and $M2$ is

$$N(M1, M2) = \zeta_0 \int_{M1}^{M2} m^{-\alpha} dm = \zeta_0 \left[\frac{M2^{1-\alpha} - M1^{1-\alpha}}{1-\alpha}\right]. \tag{8.2}$$

This calculation is very simple and may not necessarily apply to massive stars because first, not all stars in the mass range $[25-50]M_\odot$ become necessarily black holes (Janka, 2012), and since many massive stars are born in binary systems or become bound in binary systems later in their evolution, the unique outcome per stellar mass predicted by single stellar evolution might not be the best estimate of the number of black holes. But this is somewhat useful to compute a simple estimate.

Ratio UCXBs to massive stars in globular clusters And the fraction of black holes to the massive stars responsible for alpha element enrichment is

$$f_{\rm BH} = \frac{150^{1-\alpha} - 25^{1-\alpha}}{150^{1-\alpha} - 13^{1-\alpha}}, \tag{8.3}$$

where $150M_\odot$ has been an accepted upper mass limit for stars. This limit is currently under debate as stars more massive are being discovered and there is no theoretical limit, but using the Kroupa distribution, the estimate of the above fraction is not much depending on this mass. One finds $f_{\rm BH} = 0.4$. In Chapter 6 is found that the number of UCXBs per black hole is 0.15 in the densest clusters we know (47 Tuc, for example). The fraction of BH–WD UCXBs to massive stars is therefore $f_{\rm BH-WD} = 0.4 \times 0.15 = 0.06$. So BH accretion disks produce about $10^{-2} \times 0.4 \times 0.15 = 6 \times 10^{-4}$ less alpha elements heavier than oxygen than massive stars, and $10^{1} \times 0.4 \times 0.15 = 0.6$ times less of carbon and oxygen than massive stars.

Ratio UCXBs to low mass stars in globular clusters To know how BH–WD systems compare to low mass stars in terms of carbon emission, the same calculation as above is done:

$$f_{\rm BH} = \frac{150^{1-\alpha} - 25^{1-\alpha}}{6.5^{1-\alpha} - 1.25^{1-\alpha}} = 0.02. \tag{8.4}$$

The close BH–WD systems is $f_{\rm BH-WD} = 0.02 \times 0.15 = 0.003$. So even if less massive stars eject, per single event, less carbon, they will play a significant role when combined: the fraction of carbon release from BH–WD accretion disk to these stars is $100 \times 0.02 \times 0.15 = 0.3$.

Ratio UCXBs to massive stars in the field The number of 90 UCXBs with a short period derived by Belczynski & Taam (2004), and described in Chapter 6 was done by using a star formation rate in the Milky Way of about $3 M_{\odot}/yr$ (Misiriotis et al., 2006). Using the same star formation rate (widely used) to be consistent with these numbers, I estimated roughly the numer of black holes in the field to:

$$N_{\rm BH} = 6.3 \times 10^7, \tag{8.5}$$

so the number of UCXBs per black hole is $\frac{90}{76.2 \times 10^7} = 1.4 \times 10^{-6}$ UCXBs/BH. This shows that the number of UCXBs per black holes is enormously higher in globular clusters, recall a value of 0.15. The contributions of UCXBs in the fields is therefore expected to be very small. The ratio of UCXBs to massive stars is therefore $f_{\rm BH-WD} = 1.4 \times 10^{-6} \times \times 0.4 = 5.6 \times 10^{-7}$. And the relative mass of elements produced is about 6×10^{-9} for elements heavier than oxygen and 6×10^{-6} for carbon. Any contribution from BH–WD accretion disks is completely ruled out by these numbers, in the Galactic field.

Ratio UCXBs to low mass stars in the field Using the number of UCXBs per black hole in the field from above and the same scaling with the initial mass function, I found a BH–WD short period binary fraction of about $f_{\rm BH-WD} = 1.4 \times 10^{-6} \times 0.02 = 2.8 \times 10^{-8}$, with a carbon relative production of 3×10^{-7}. Carbon contribution from BH–WD binaries in the field is also ruled out under these conditions.

BH–WD disruptions do not enrich the ISM in these conditions! Under the following assumptions:
(a) The Shakura & Sunyaev (1973) model represents well BH disks from WD disruptions.
(b) The disruption is such that a constant accretion rate of $\approx 10^6 \dot{M}_{\rm Edd}$ is maintained through the whole event, and the entire white dwarf is shredded into the disk.
(c) The black hole is accreting from its inner edge at its Eddington limit. The rest of the material is ejected.
(d) The wind profile follows a uniform radial distribution.
(e) Such systems form according to Chapter 6 scenarios.
(f) All systems formed in Chapter 6 become these BH–WD systems described in (b).
(g) The IMF and star formation rate follow those used in the present chapter.
it can be concluded that the products of nucleosynthesis are completely negligible, except for the unburned elements from the WD composition.

In addition to the above assumptions, if we assume that massive stars exploding in supernova expel at least as much material as a $13 M_{\odot}$ star, and that low mass star expel at least as much as a $3 M_{\odot}$ star, then a relative contribution can be estimated. I have done this

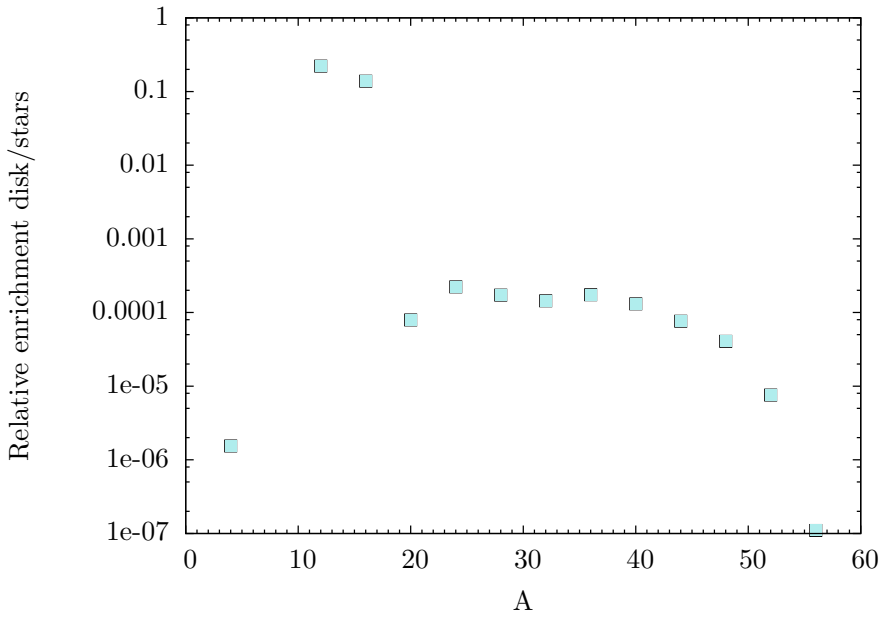

Figure 8.3: Computed relative enrichment of BH–WD systems to dredge up stars and massive stars. It was assumed all BH–WD systems were with a $0.6M_{\odot}$ WD and a $3M_{\odot}$ BH, accreting at $10^6\dot{M}_{\rm Edd}$, where most of the disk is expelled in uniform winds. Low mass stars were represented by a $3M_{\odot}$ star and stars representatives of supernovae were $13M_{\odot}$ stars.

for globular clusters where the yields from the burning are normalized to the distribution of UCXBs and stars, see Figure 8.3.

From Figure 8.3, on can conclude that (1) heavier elements than oxygen are produced in proportions less than 10^{-3} than stars, and in addition, this production seems to be uniform in function of the atomic mass A within $[20, 48]$. This means that the abundance pattern resulting from BH disks is identical to the abundance pattern of other stars. So even if this very small production could be measured, there would be no way to infer whether these elements were made in stars or black hole disks. (2) the production of carbon and oxygen is less than stars, but in higher proportions than heavier elements. Observing them would however not probe for any nucleosynthesis as these are unburned elements. Nucleosynthesis around black holes would not contribute much more than a combination of white dwarf disruptions without burning and usual stellar evolution.

Chapter 9

Conclusion

Studying nucleosynthesis in black hole accretion disks is important. Understanding what are the different sources of new elements is of fundamental importance for studying the history of our Universe. We need it to understand where the elements we are made of come from. We need it to understand how galaxies evolve: we study their current dynamics and chemistry to infer their passed evolution (Galactic archaeology), so we need to know the different events which happened, enriching the gas forming stars of later generations. Because they are hot and dense, leading nucleosynthesis factories are the Big Bang for light elements, and stars, including the subsequent explosions of the most massive ones, for heavy elements. More sources are under current investigation, such as neutron star mergers (Wu et al., 2016), good candidates for enrichment of metal poor stars with r-process elements.
Black holes are extremely compact objects. Inside accretion disks, they are responsible for very high differential rotation leading to viscous heating. In the most extremes conditions, the temperatures and densities become sufficient to trigger nucleosynthesis, producing new elements and ejecting them back to the ISM in the form of winds. The aim of the present work has been to analyse this nucleosynthesis and quantify the production of new elements. In addition, it was possible to constrain the enrichment to the ISM due to black hole accretion disks and compare it to the enrichment from stars.

Accretion disk nucleosynthesis contributes very little to enriching the Milky-Way. To investigate the nucleosynthesis products of accretion disks around black holes, I first identified which black hole masses and which accretion processes (mass transfer from a star, spherical accretion from a gas cloud for example) provide the extreme conditions of temperature and density necessary for nuclear burning. I found that stellar mass black holes tidally disrupting white dwarf would build accretion disks hot and dense enough for nucleosynthesis to happen within a specific location. I modelled the resulting disk using the simple Shakura & Sunyaev (1973) model, and implemented the most representative nuclear burning network at these temperatures. Alpha-elements are synthetised, and the disk has a very defined structure with specific elements dominating the composition at different radii. Most of the nucleosynthesis products are expelled in winds due to a super-Eddington accretion. Assuming a wind profile and determining the rate of these events using literature, I could compute how much these black hole - white dwarf systems could contribute to the chemical content of the Milky-Way. Using literature to know the predicted stellar yields, and comparing them to my results for black hole accretion disks, I found that black hole contributions were negligible.

Current limitations

- Disk Model: The disk model (Shakura & Sunyaev, 1973) I used for the accretion disk is too simple and doest not necessarily account for the dominant physics at such super-Eddington accretion rates. At such high rates, not all photons have time to be emitted in black body radiation, and some should be advected towards the black hole. In other terms, the advection time-scale is not negligible compared to the radiation time-scale.

- Energy conservation: As the disk model implemented in the program is an analytical solution on which I constructed a nuclear burning network, the calculations of energy conservation solved in the disk do not account for the energy generated by nuclear reactions. And this energy is not completely negligible as it represents more than 10% of the viscous energy during carbon burning, oxygen burning, and photodisintegration. The subsequent effects could either be a rise in temperature leading to a different burning products. Or it could have a dynamical effect and perhaps help powering winds, which would then be stronger than predicted at these specific places.

- Mass conservation: As winds are not accounted in the Shakura & Sunyaev (1973) disk model, the mass conservation equation within the disk must be wrong, although it could be argued that the two events *disk formation* and *release in winds* happen at different moments, where first a very dense disk is made by the disruption of the white dwarf on a dynamical time-scale, and subesequently winds arise from the disk. However, this type of argument rule-out the possibility to used a Shakura & Sunyaev (1973) disk model as it assumes a steady state disk.

- Wind: The wind profile used in the present work was an uniform wind in radius. But the wind is generated by physical processes happening within the disk, for example powered by super-Eddington accretion. In this case, the radiation responsible for winds is strongest in the inner disk and so should be the winds. Other wind mechanisms which were not mentioned in the present work are winds powered by magnetic fields, and jets. In the case of a jet, for a given accretion rate, the black hole mass plays a crucial role: the jet will have the composition of the inner disk. A low mass black hole, responsible for a very high inner disk temperature, could release only helium produced in the photodisintegration. A black hole too massive would not allow burning and release only the white dwarf composition. Between the two, heavier elements produced in the disk can be released.

- Neutrino cooling: The disks considered in this work lie in the temperature-density conditons for pair production of electrons and positrons. But the eventual electron capture by other nuclei produces neutrinos. Depending on the interaction of the neutrinos with the disk, the disk could cool by neutrinos. This arguments is on favour of the thin disk model which was used.

- Photodisintegration of helium: In the inner edge of the disk, where heavy nuclei are photodisintegrated back to helium nuclei, higher temperatures would photodisintegrate helium nuclei in their turn, producing neutrons and protons. It would be interesting to see how these particles of different charges behave in the disk, or in presence of a magnetic field.

The presence of neutron in powerful winds could lead to neutron capture nucleosynthesis for example.

Fortunately, there exist several ways to improve these limitations. But efficient improvements require a "big step" in method and techniques, which is why I have been unable to make them on the time-scale of the few weeks left when the most important results were produced. The problems of disk model, energy conservation, mass conservation and wind can be solved at once by replacing analytical solutions for the disk by the use of a magnetohydrodynamical (MHD) code. Implementing a small, simple skeleton of nuclear network within it would take into account for most of the nuclear energy generated in the disk. A more sophisticated network implemented in addition, on the top of the simulation, would allow to compute the nuclear products computationally rapidly. However, the use of such a computationally demanding code would require a different approach of the problem than the one I had. Only a few simulations can be run. The present work then reveals useful for getting an intuition and choosing the runs to do with the improved MHD simulation. Additionally, the mass accretion rate, which was assumed constant thorough the whole event actually varies with time. If more time allowed, I would include this variation in my program. I have done a simple preliminary calculation of the variation of accretion rate during mass transfer in black hole - white dwarf binaries. The binary system of masses M_1 and M_2, mass ratio $q = M_2/M_1$ separated by a looses angular momentum by gravitational radiation (Peters, 1964) as

$$\dot{J}_{\rm GR} = -\frac{32G^{7/2}}{5c^5}\frac{M_1^2 M_2^2\sqrt{M_1+M_2}}{a^{7/2}}, \tag{9.1}$$

and the separation varies as

$$\frac{\dot{a}}{a} = \frac{2\dot{J}}{J} - \frac{2\dot{M}_2}{M_2}(1-q). \tag{9.2}$$

Then, if one knows the mass-radius relation for white dwarf (Equation 5.7), compare it to the size of its Roche lobe (Equation 4.15), then one can infer an instantaneous mass transfer rate according to (e.g Frank et al. (2002)):

$$\dot{M} = \dot{M}_0 \exp\left((R_{\rm WD} - R_{\rm L})/h_{\rm WD}\right), \tag{9.3}$$

where $h_{\rm WD}$ is the scale height of the white dwarf atmosphere, which I took from Bobrick et al. (2017). I did these calculations and the results are plotted in Figure 9.1.

Even if these computations are still pristine as the system should loose more angular momentum due to exchange with a common envelope (Bobrick et al., 2017), they show that the mass transfer rate changes as a function of time. I plotted them as a function of $\Delta M/M_0$, the mass lost by the white dwarf divided by the original white dwarf mass, because it tells us how much of the white dwarf burns at a constant rate in the accretion disk. Here we see clearly that only 10% of the white dwarf is accreted at a constant rate in the stable mass transfer case (left panel in the figure). It means that by neglecting it, I over-estimated the production of new elements. So the estimates of burning products I have found in this thesis need to be rescaled, and more accurate results would show that black hole accretion disks then produce ten times less than my predictions. This is not a worrying result as it emphasises how negligible this outcome is.

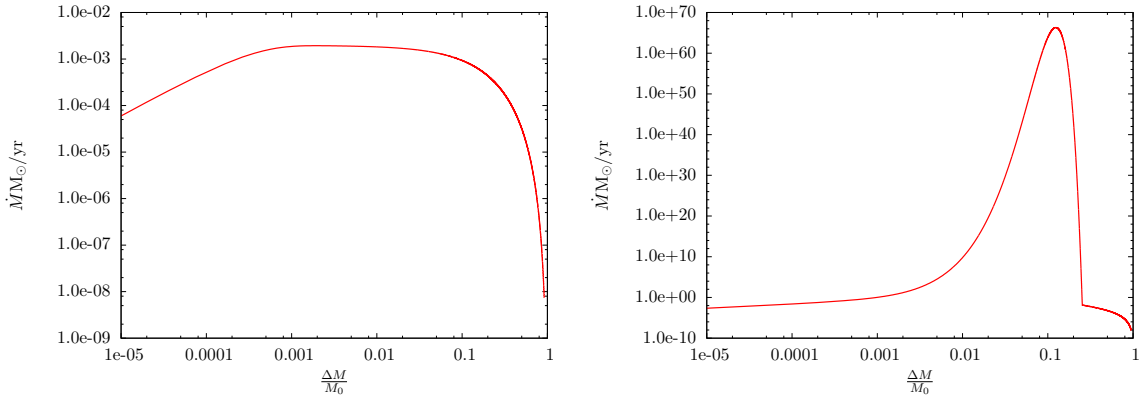

Figure 9.1: Evolution of the accretion rate during the accretion from a $0.6M_\odot$ (left) and a $1.4M_\odot$ white dwarf (right) into a $3M_\odot$ black hole, where conservative mass transfer was assumed.

Nucleosynthesis in black hole accretion disks can be useful. Even such a small outcome may show interesting features in a different context than ISM enrichment. Many of the produced elements, such as Ti, Cr, Fe, Ni are radioactive. When these elements decay, they emit photons. This could produce a decay light curve. So such evens of black hole - white dwarf binaries would leave several electromagnetic counterparts: the thermal emission from the disk, and the light curve in the outflows. Additionally, such mergers could produce detectable gravitational waves (e.g. eLISA, (Antoniadis, 2015, for neutron stars – white darfs). There have been observed events called calcium-rich gap transients, and neutron stars - white dwarf binaries could be a source (Metzger, 2012; Bobrick et al., 2017). Black hole - white dwarf binaries could be a class of these events. In such circumstances, nucleosynthesis in black hole accretion disks can be a very useful tool to recognise and classify events. Similarly, tidal disruptions of white dwarfs have been proposed to be used to probe the presence of intermediate mass black holes. Intermediate mass black holes can disrupt low mass helium white dwarf but not more massive white dwarfs because they are too compact and are swallowed before disruption. A recognisable electromagnetic counter part from helium burning could be very useful to recognise tidal disruption events of white dwarfs in the future, perhaps with the data coming from the future surveys such as LSST. If nuclear burning in accretion disks is inefficient in enriching the ISM, its applications to recognise localised events may still be of use.

Appendix A

Integration of a nuclear network

Nuclear reactions are very temperature dependant, and nuclear networks lead to stiff differential equations. For numerical stability, they need to be integrated with an implicit scheme. Given a function f, its derivative is defined as:

$$f'(x) = \lim_{h->0} \frac{f(x+h) - f(x)}{h} \tag{A.1}$$

In a differential equation this is a function y of f itself:

$$f'(x) = y(f) \tag{A.2}$$

In numerical work, the quantity h cannot tend to zero indefinitely. The programmer needs to find a compromise between the accuracy of an approximation to this equation and a value which makes the numerical computation possible and fast. Hence the derivative is computed with:

$$f' \approx y = \frac{f(x+h) - f(x)}{h} \tag{A.3}$$

where the condition

$$h << f/f' \tag{A.4}$$

must be satisfied. In these last two equations we dropped the argument x of the functions on purpose. Now that h is a number and not a limit to zero, we need to set a convention and choose if this formula is an evaluation of the derivative at the point x or a the point $x + h$. Said differently, the two following equations can be equally correct:

$$f'(x) \approx y(x) = \frac{f(x+h) - f(x)}{h} \tag{A.5}$$

$$f'(x+h) \approx y(x+h) = \frac{f(x+h) - f(x)}{h} \tag{A.6}$$

To solve numerically a differential equation, using equation A.5 is straightforward since usually, $f'(x) = y(f(x), x)$ is known, $f(x)$ is known, and we want to find $f(x + h)$. This can be integrated using any forward solver: Euler in the following example or, Runge kutta, predictor-corrector and so on. This is called explicit differentiation.

$$f(x+h) = f(x) + hf'(x) \tag{A.7}$$

If n is the iteration index, we get:

$$f_{n+1} = f_n + hy_n \tag{A.8}$$

Using equation A.6 (implicit differentiation) is more difficult and requires a more elaborated method: this time, $f'(x+h) = y(f(x+h), x+h)$ is not known since it is a function of $f(x+h)$ which is what we want to find. The quantity to compute is

$$f_{n+1} = f_n + hy_{n+1} \tag{A.9}$$

It was found that for stiff differential equations, the implicit Euler method is numerically much more stable than the explicit Euler method. Without proving it, we can give some arguments with the typical differential equation (e.g. in Arnett & Truran (1969)):

$$y' = -ay \tag{A.10}$$

with a a positive real constant. An analytic solution is $y(x) = y_0 e^{-ax}$. This is a decreasing exponential. With the Euler explicit scheme, we can integrate:

$$y_{n+1} = y_n - ahy_n \tag{A.11}$$

so for any n we get $y_n = (1-ah)^n y_0$ if the time-step h remains constant. This solution is completely divergent if $|1-ah| > 1$ as it is to the power of n. When n is large, this should tend towards zero for the solution to look like the decreasing exponential. This requires the time-step h to be small: stability is satisfied if $|1-ah| < 1$, which requires $h < 2/a$. This is a condition of the time-step: it cannot be arbitrarily large for the solution to be stable. On the other hand, with the Euler implicit scheme, we can integrate:

$$y_{n+1} = y_n - ahy_{n+1} \tag{A.12}$$

$$t_{n+1} = \frac{y_n}{1+ah} \tag{A.13}$$

So for any n we get $y_n = y_0 \left(\frac{1}{1+ah}\right)^n$, stable if $|\frac{1}{1+ah}| < 1$, which requires only $h > 0$. There is no condition on the time-step this time, and the only dependency on the time-step is that the solution will be, for Euler, accurate to the first order $\mathcal{O}(h)$. In the physical context of nuclear network, the form of the differential equations describing nuclear reactions is as in Equation 2.27. To evaluate $y'_{n+1} = f'(x) = \dot{Y}(t+h)$, we re-write Equation 2.27

$$\dot{Y}_A(t+h) = -\sum_i \rho Y_A(t+h) Y_i(t+h) < \sigma v >_{Ai} + \sum_{i,j \geq i} \rho Y_i(t+h) Y_j(t+h) < \sigma v >_{ij} \tag{A.14}$$

Writing $\Delta_i = Y_i(t+h) - Y_i(t)$:

$$\dot{Y}_A(t+h) = -\sum_i \rho (Y_A(t)+\Delta_A)(Y_i(t)+\Delta_i) < \sigma v >_{Ai} + \sum_{i,j \geq i} \rho (Y_i(t)+\Delta_i)(Y_j(t)+\Delta_j) < \sigma v >_{ij} \tag{A.15}$$

We then linearise this equation. Each element $(Y_i(t)+\Delta_i)(Y_j(t)+\Delta_j)$ is developed and the second order terms Δ^2 are neglected.

$$\begin{aligned} \dot{Y}_A(t+h) = &-\sum_i (\rho (Y_A(t) Y_i(t) < \sigma v >_{Ai} + Y_A \Delta_i < \sigma v >_{Ai} + Y_i \Delta_A < \sigma v >_{Ai}) \\ &+ \sum_{i,j \geq i} (\rho (Y_i(t) Y_j(t) < \sigma v >_{ij} + Y_i \Delta_j < \sigma v >_{ij} + Y_j \Delta_i < \sigma v >_{ij}) \end{aligned} \tag{A.16}$$

$$\dot{Y}_A(t+h) = \dot{Y}_A(t) - \sum_i \rho(Y_A\Delta_i < \sigma v >_{Ai} + Y_i\Delta_A < \sigma v >_{Ai}) + \sum_{i,j\geq i} \rho(Y_i\Delta_j < \sigma v >_{ij} + Y_j\Delta_i < \sigma v >_{ij}) \tag{A.17}$$

Replacing $\dot{Y}_A(t+h)$ by Δ_A/h, this equation can be factorised and put in a final form:

$$\Delta_A(1+h\sum_i \rho Y_i < \sigma v >_{Ai}) + \sum_i \rho Y_A\Delta_i < \sigma v >_{Ai} - \sum_{i,j\geq i} \rho(Y_i\Delta_j < \sigma v >_{ij} + Y_j\Delta_i < \sigma v >_{ij}) = \dot{Y}_A(t)h \tag{A.18}$$

Doing this to the other isotopes involved in the network, the given set of linear equations like Equation A.18 can be writen as a matrix product:

$$M\Delta = B \tag{A.19}$$

Where Δ is the unknown for which we want to solve the equation:

$$\Delta = \begin{pmatrix} \Delta_A \\ \Delta_B \\ \Delta_C \\ ... \end{pmatrix} \tag{A.20}$$

B is the known vector containing the rate of change in composition of each element at time t:

$$B = h \begin{pmatrix} \dot{Y}_A(t) \\ \dot{Y}_B(t) \\ \dot{Y}_C(t) \\ ... \end{pmatrix} \tag{A.21}$$

And M is the matrix containing the information from the linearisation:

$$M = \begin{pmatrix} 1+h\sum_i \rho Y_i < \sigma v >_{Ai} & \rho Y_A(t) < \sigma v >_{AB} & \rho Y_A(t) < \sigma v >_{AC} & ... \\ \rho Y_B(t) < \sigma v >_{BA} & 1+h\sum_i \rho Y_i < \sigma v >_{Bi} & \rho Y_B(t) < \sigma v >_{BC} & ... \\ & & & \\ & & & \\ ... & & & \end{pmatrix} \tag{A.22}$$

This can be written in clearer way: $M = Id_n - J_n$ where J_n is the $(n \times n)$ identity matrix and J_n is the Jacobian:

$$J_n = \begin{pmatrix} \frac{\partial \dot{A}}{\partial A} & \frac{\partial \dot{A}}{\partial B} & \frac{\partial \dot{A}}{\partial C} & ... \\ \frac{\partial \dot{B}}{\partial A} & \frac{\partial \dot{B}}{\partial B} & \frac{\partial \dot{B}}{\partial C} & ... \\ \frac{\partial \dot{C}}{\partial A} & \frac{\partial \dot{C}}{\partial B} & \frac{\partial \dot{C}}{\partial C} & ... \\ ... & & & \end{pmatrix} \tag{A.23}$$

Now, we only need to invert M and the nuclear network can finally be integrated: $\Delta = M^{-1}B$ and if all the abundances of elements are also written in an array Y, we get with an Euler step: $Y_{n+1} = Y_n + \Delta$

Looking back at the matrix M in Equation A.22, we see that this matrix is very very close to the identity matrix: the diagonal terms contain a term in $1 + (...)$ where the second term is close to zero as it represents mainly the cross section of the reaction. The non diagonal terms are also expected to be small. If this matrix M was rigorously the identity matrix, then the differential equation system would not be stiff. The difference from the Identity matrix

qualifies the stiffness of the equations, and then we would have $\Delta = B$ An example of this matrix is showed below in Equation A.24, where only (9×9) terms are shown (physical size of the page), instead of 13, for the 13 isotopes network. This matrix is computed at every time-step and the non diagonal terms become large in different temperature conditions (the more different reactions with rates of different orders of magnitudes are involve, the stiffer).

$$\begin{pmatrix} 1 & 10^{-17} & 10^{-53} & 10^{-32} & 10^{-66} & 10^{-72} & 10^{-52} & 10^{-52} & 10^{-56} \\ 10^{-09} & 1 & 10^{-53} & 0 & 0 & 0 & 0 & 0 & 0 \\ 10^{-07} & 0 & 1 & 10^{-32} & 0 & 0 & 0 & 0 & 0 \\ 10^{-07} & 10^{-17} & -0 & 1 & 10^{-66} & 0 & 0 & 0 & 0 \\ 0 & -0 & -0 & -0 & 1 & 10^{-72} & 0 & 0 & 0 \\ 0 & 0 & -0 & 0 & -0 & 1 & 10^{-52} & 0 & 0 \\ 0 & 0 & 0 & 0 & 0 & -0 & 1 & 10^{-52} & 0 \\ 0 & 0 & 0 & 0 & 0 & 0 & -0 & 1 & 10^{-56} \\ 0 & 0 & 0 & 0 & 0 & 0 & 0 & -0 & 1 \end{pmatrix} \tag{A.24}$$

Appendix B

Matrix inversion and LAPACK++ package

The integration of a nuclear burning network requires so solve a system of linear equations. This is not a problem, but the numerical challenge is to do it fast. To solve the equation

$$\Delta = M^{-1}B \tag{B.1}$$

We use the linear algebra package recommended by Press et al. (2007).

Package and installation The `LAPACK++` package is a free of use linear algebra package allowing simple manipulation of vectors and matrices to `C++` users. The author of the first versions are J. J. Dongarra, E. Greaser, R. Pozo, D. Walker. The version I used, `lapackpp-2.5.4` is an update from 2010 mainly by Christian Stimming. To install it, open the terminal and type the command
`sudo apt-get install build-essential liblapack-dev libblas-dev checkinstall` [1]
Download the version `lapackpp-2.5.4.tar.gz` from `http://sourceforge.net/projects/lapackpp/files/` and unpack it. Then, in the terminal, run the commands

```
./configure
make
sudo checkinstall
sudo cp/usr/local/lib/liblapackpp.so* /usr/lib
```

where the two first commands install the package, the third one is a check of the installed package, and the last one consists in placing the package in the correct file to be found by the compiler. (`README.txt` file).

Linear algebra data types The main data types I have used in the code are vectors and matrices. The declaration of a vector which can be used with the linear algebra package is done as follows:

```
LaVectorDouble compo(n);
```

where a vector `compo` of size n and containing double precision elements has been created. A matrix is declared as

```
LaGenMatDouble deriv_linear(n,n);
```

where a matrix `deriv_linear` of size $(n \times n)$ was created, containing double precision elements.

[1] website `askubuntu.com`

Inversion command To invert a matrix, the routine to call is defined as:

```
void LaLinearSolve  (  const LaGenMatDouble &   A,
LaGenMatDouble &   X,
const LaGenMatDouble &   B
)
```

and uses factorisation algorithm and partial pivots to solve linear equations. I then tested it, inverted the identity matrix without mistakes, and went on using it for the purpose of this work. The next paragraph shows how I used it in the code I wrote.

A piece of code An incomplete piece of code showing how the integration was performed is pasted below, where a use of this package was done.

```
   // declaration of the composition vector (molar fraction)
   LaVectorDouble compo(n);

   // declaration of the mass fraction vector
   LaVectorDouble mass_fraction_initial(n);

   for(i=0;i<n;++i){ input_file >> compo(i);}
   mass_fraction_initial = compo;
(...)

// Mass of elements in the disk
    LaVectorDouble mass(n);
    LaVectorDouble mass_fraction(n);

// Integration initialisation
(...)

// initialise parameters of the system
    parameters param;
    param.alpha = alpha;   param.dm = dm; param.m1 = m1;
    param.spin = spin*(G*m1*Ms/(c*c)); param.wind = 0;
    states state;
    rates_alpha rate_a;
    LaGenMatDouble deriv_linear(n,n);    // matrix used for the linar equation solver
    LaVectorDouble deriv_compo_expl(n); // time derivative of the molar fraction
    LaVectorDouble deriv_compo_impl(n); // time derivative for implicit integration

(...)


// INTEGRATE R(t) (AND STATE(t))
(...)
```

```
// STEP 1.
// Initialise state object
r = R_max; state.R = r; cout<< "r = "<< r << endl;
init_state(&state,&param);
(...)

// Calculate nuclear reaction rates
compute_alpha_rates(&state, &rate_a);

// compute variation elements
rate_of_change_alpha(&state, &rate_a, compo, deriv_compo_expl);

// Linearize (compute matrix to invert)
linearize_alpha(&state, compo, &rate_a, dt, deriv_linear);

// Solve Linear system
LaLinearSolve(deriv_linear, deriv_compo_impl, deriv_compo_expl*dt);

// New composition
compo = compo + deriv_compo_impl;
compute_mass_fraction(compo, mass_fraction);

while (state.R > R_min){
// Calculate nuclear reaction rates
compute_alpha_rates(&state, &rate_a);

// compute variation elements
rate_of_change_alpha(&state, &rate_a, compo, deriv_compo_expl);

// Linearize (compute matrix to invert)
linearize_alpha(&state, compo, &rate_a, dt, deriv_linear);

// Solve Linear system
LaLinearSolve(deriv_linear, deriv_compo_impl, deriv_compo_expl*dt);

// New abundances
compo = compo + deriv_compo_impl;

// Update disk state
r = state.R;  f = compute_f(r,RSCH(&param));
RK4(&state,&param,f,dt);
init_state(&state,&param); vr = -compute_vr(r,&param,f);

// Increment stuff & save results
(...)
}
```

Appendix C

Program

The program I wrote and used consists in a `C++` code with three main parts: integration of the nuclear network, disk model and main program. it will be available online on `https://github.com/NeigeF/MSc_Project` from Monday 15 May 2017. A detailed description is given in the following `readme.txt` file and a flowchart is in Figure C.1.

```
This folder contains the main programs and routines of the project
valid on 15/12/2016
updated until 04/2017

Updated nuclear reaction rates are available in the folder
[Accretion_disk/nuclear_rates_updated]
which contains a program to plot the burning rates
in function of temperature

-------------------------------------------------------------------------------
The user only needs to change parameters (initial composition of the disk,
  accretion rate, black hole mass...) in the input file (see "use")

-------------------------------------------------------------------------------
List of "include" files

- includeall.h is the only one the user needs to care about.
It declares the functions of "functions.cpp" and includes "include_rates.h"
as well as mathematical functions and C++ print functions.

- include_rates.h contains the declaration of the nuclear burning rates.

-------------------------------------------------------------------------------
List of subroutines:

- functions_v3.cpp contains all the functions used in the main programs,
mainly regarding the accretion disk structure under Shakura-Sunavey regime
and a model of ADAF to compare to Shakura-Sunyaev
-> contains matrix A to be inverted for complete alpha network
```

```
works on 14/11/2016 - updated until 04/2017

- functions_v4.cpp update of functions_v3.cpp for adding pp chain network.
did not finish.
do not know if it works.

- nuclear_rates.cpp contains the nuclear burning rates to use.
They are numbered "rateX()" X = 0, 1, ... with X increasing with the nuclei
sizes or X = C12C12, O16O15, C12O16 etc. contains the two nuclei interacting

-------------------------------------------------------------------------------
List of the programs:

- abundances_v3.cpp latest version, works on 15/12/2016, updated 04/2017
integrates the radial composition of the disk and the total yields
of NS during accretion onto the black hole.
to be fed with input file (e.g. input.txt)

- rhoTplane.cpp, works on 15/12/2016
computes:
path of a gas blob through the disk in the rho-T plane
path of the center of a star in the rho-T plane through its evolution
path of a blob of gas in the rho-T plane during the Big Bang
conditions necessary for nuclear burning in the rho-T plane
data exported in 4 separate output files.

- rhoTplane_v3.cpp, works on 15/12/2016
same as rhoTplane.cpp, updated with possiblity of BH spin
with parameter 0 < a < 1.

- mmdotplane.cpp, works on 15/12/2016
computes for various ranges of BH mass and accretion rates
the greatest disk temperatures and density (inner most)
the accretion time scale (viscous)
the burning time scale for triple alpha and C12+alpha

- mmdotplane_v3.cpp, works on 02/2017
same as mmdotplane.cpp, updated with possiblity of BH spin
with parameter 0 < a < 1.


-------------------------------------------------------------------------------
Download LAPACK++ PACKAGE
sudo apt-get install build-essential liblapack-dev libblas-dev checkinstall
Download the version lapackpp-2.5.4.tar.gz from
http://sourceforge.net/projects/lapackpp/files/
and unpack it
```

```
./configure
make
make install
sudo checkinstall

--------------------------------------------------------------------------------
Compilation
1. compile the files and link to objects:
g++ -c abundancesx.cpp functionsx.cpp nuclear_rates.cpp -I /usr/local/include/lapackpp
2. compile objects to make program
g++ abundancesx.o  functionsx.o nuclear_rates.o -o program_name.exe -llapackpp
3. give path to shared library
export LD_LIBRARY_PATH=/usr/local/lib

--------------------------------------------------------------------------------
Run:
./abundances_v3.exe input.txt

--------------------------------------------------------------------------------
description of input file: input.txt
--------------------------
M_BH M_WD
Mdot alpha spin
n_iso h

He
C
O
Ne
(...)
Ni
Output_name
-------------------------
where:
M_BH = black hole mass in solar mass
M_WD = white dwarf mass in solar mass
Mdot = accretion rate in Eddington units
alpha = viscosity parameter
spin = normalised BH spin (between 0 and 1)
n_iso = number of isotopes in the network (can only be 13 in current version!!!)
h = maximum time-step
He = mass fraction of helium
Output_name = name of output file (don't write the extension)

================================================================================
LIMITATIONS (explained in thesis text)
================================================================================
```

```
- WD mass must be < 1.4 Msun
- BH mass must be < 300 Msun
- Sum of mass fractions for initial disk composition must be 1
```

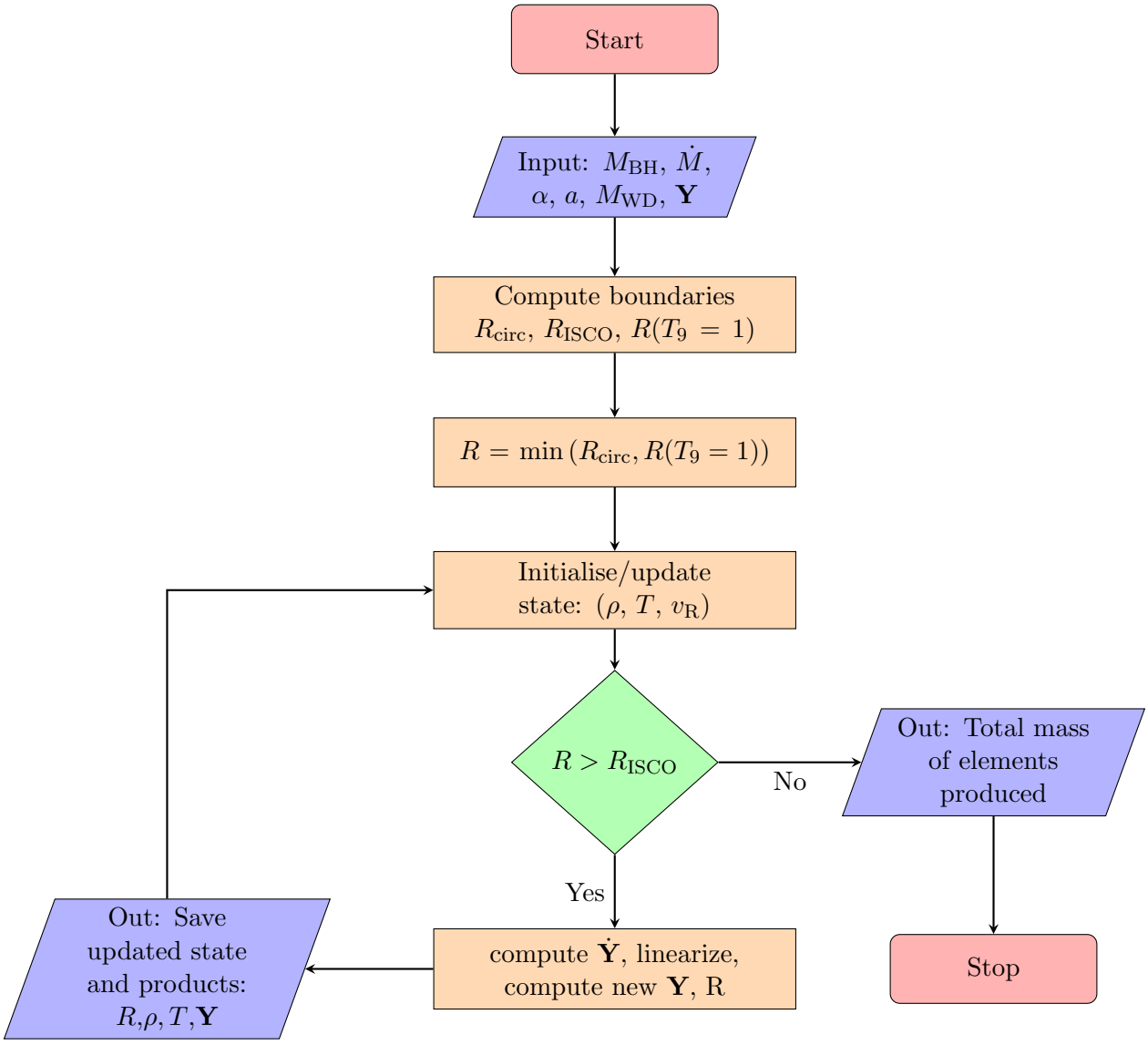

Figure C.1: Global flowchart of the program integrating the nuclear burning network of a blob of gas through an accretion disk.

Appendix D

Tables of reaction rates

Nuclear reaction	Reference
$\alpha + \alpha + \alpha \longrightarrow \gamma + {}^{12}\mathrm{C}$	Angulo et al. (1999)
${}^{12}\mathrm{C} + \alpha \longrightarrow \gamma + {}^{16}\mathrm{O}$	Angulo et al. (1999)
${}^{16}\mathrm{O} + \alpha \longrightarrow \gamma + {}^{20}\mathrm{Ne}$	Angulo et al. (1999)
${}^{20}\mathrm{Ne} + \alpha \longrightarrow \gamma + {}^{24}\mathrm{Mg}$	Angulo et al. (1999)
${}^{24}\mathrm{Mg} + \alpha \longrightarrow \gamma + {}^{28}\mathrm{Si}$	Harris et al. (1983)
${}^{28}\mathrm{Si} + \alpha \longrightarrow \gamma + {}^{32}\mathrm{S}$	Woosley et al. (1978)
${}^{32}\mathrm{S} + \alpha \longrightarrow \gamma + {}^{36}\mathrm{Ar}$	Woosley et al. (1978)
${}^{36}\mathrm{Ar} + \alpha \longrightarrow \gamma + {}^{40}\mathrm{Ca}$	Woosley et al. (1978)
${}^{40}\mathrm{Ca} + \alpha \longrightarrow \gamma + {}^{44}\mathrm{Ti}$	Woosley et al. (1978)
${}^{44}\mathrm{Ti} + \alpha \longrightarrow \gamma + {}^{48}\mathrm{Cr}$	Woosley et al. (1978)
${}^{48}\mathrm{Cr} + \alpha \longrightarrow \gamma + {}^{52}\mathrm{Fe}$	Woosley et al. (1978)
${}^{52}\mathrm{Fe} + \alpha \longrightarrow \gamma + {}^{56}\mathrm{Ni}$	Woosley et al. (1978)
${}^{12}\mathrm{C} + {}^{12}\mathrm{C} \longrightarrow \gamma + {}^{24}\mathrm{Mg}$	Caughlan & Fowler (1988)
${}^{12}\mathrm{C} + {}^{16}\mathrm{O} \longrightarrow \gamma + {}^{28}\mathrm{Si}$	Caughlan & Fowler (1988)
${}^{16}\mathrm{O} + {}^{16}\mathrm{O} \longrightarrow \gamma + {}^{32}\mathrm{S}$	Caughlan & Fowler (1988)

Table D.1: Alpha-chain reactions and the references used for their reaction rates

References

Abbott B. P., et al., 2016, Physical Review Letters, 116, 061102

Abramowicz M. A., Czerny B., Lasota J. P., Szuszkiewicz E., 1988, ApJ, 332, 646

Angulo C., et al., 1999, Nuclear Physics A, 656, 3

Antoniadis J., 2015, in Sopuerta C. F., ed., Astrophysics and Space Science Proceedings Vol. 40, Gravitational Wave Astrophysics. p. 1

Arai K., Hashimoto M., 1992, A& A, 254, 191

Arnett 1996, Princeton Series in Astrophysics

Arnett W. D., Truran J. W., 1969, ApJ, 157, 339

Bahramian A., et al., 2017, preprint

Balbus S. A., Hawley J. F., 1998, Reviews of Modern Physics, 70, 1

Belczynski K., Taam R. E., 2004, ApJ, 603, 690

Blandford R. D., Payne D. G., 1982, MNRAS, 199, 883

Bobrick A., Davies M. B., Church R. P., 2017, MNRAS, 467, 3556

Brandenburg A., Nordlund A., Stein R. F., Torkelsson U., 1995, ApJ, 446, 741

Carr B., Kühnel F., Sandstad M., 2016, Phys. Rev. D, 94, 083504

Cartwright T. F., Engel M. C., Heinke C. O., Sivakoff G. R., Berger J. J., Gladstone J. C., Ivanova N., 2013, ApJ, 768, 183

Caughlan G. R., Fowler W. A., 1988, Atomic Data and Nuclear Data Tables, 40, 283

Chakrabarti S. K., Liping J., Arnett D., 1987, AJ, 313, 674

Chen W.-C., Podsiadlowski P., 2016, ApJ, 830, 131

Clayton D., 1968, Mc Graw-Hill

Davies M. B., Benz W., Hills J. G., 1992, ApJ, 401, 246

Eggleton P. P., 1983, ApJ, 268, 368

Fabrika S., 2004, Astrophysics and Space Physics Reviews, 12, 1

Fernández R., Metzger B. D., 2016, Annual Review of Nuclear and Particle Science, 66, 23

Frank King Raine 2002, Cambridge University Press

Gamow G., 1928, Phys., pp 204–212

Gillessen S., Eisenhauer F., Trippe S., Alexander T., Genzel R., Martins F., Ott T., 2009, ApJ, 692, 1075

Harris M. J., Fowler W. A., Caughlan G. R., Zimmerman B. A., 1983, ARA&A, 21, 165

Hu T., Peng Q., 2008, ApJ, 681, 96

Hubble E., 1929, Proceedings of the National Academy of Science, 15, 168

Hurley J. R., Tout C. A., Pols O. R., 2002, MNRAS, 329, 897

Ivanova N., Rasio F. A., Lombardi Jr. J. C., Dooley K. L., Proulx Z. F., 2005, ApJ, 621, L109

Ivanova N., Heinke C. O., Rasio F. A., Belczynski K., Fregeau J. M., 2008, MNRAS, 386, 553

Ivanova N., Chaichenets S., Fregeau J., Heinke C. O., Lombardi Jr. J. C., Woods T. E., 2010, ApJ, 717, 948

Janka H.-T., 2012, Annual Review of Nuclear and Particle Science, 62, 407

King A., Muldrew S. I., 2016, MNRAS, 455, 1211

Kroupa P., 2001, MNRAS, 322, 231

Kuranov A. G., Postnov K. A., Prokhorov M. E., 2001, Astronomy Reports, 45, 620

Law-Smith J., MacLeod M., Guillochon J., Macias P., Ramirez-Ruiz E., 2017, preprint

Levan A., Crowther P., de Grijs R., Langer N., Xu D., Yoon S.-C., 2016, Space Science Review, 202, 33

Lombardi Jr. J. C., Proulx Z. F., Dooley K. L., Theriault E. M., Ivanova N., Rasio F. A., 2006, ApJ, 640, 441

Lundmark K., 1925, MNRAS, 85, 865

MacDonald J., Mullan D. J., 2009, Phys. Rev. D, 80, 043507

Margalit B., Metzger B. D., 2016, MNRAS, 461, 1154

Metzger B. D., 2012, MNRAS, 419, 827

Misiriotis A., Xilouris E. M., Papamastorakis J., Boumis P., Goudis C. D., 2006, A& A, 459, 113

Mukhopadhyay B., Chakrabarti S. K., 2000, A& A, 353, 1029

Narayan R., Yi I., 1994, ApJ, 428, L13

Nelemans G., Jonker P. G., 2010, New Astronomy Review, 54, 87

Nomoto K., Kobayashi C., Tominaga N., 2013, ARA&A, 51, 457

Özel F., Psaltis D., Narayan R., McClintock J. E., 2010, ApJ, 725, 1918

Panei J. A., Althaus L. G., Benvenuto O. G., 2000, A& A, 353, 970

Peters P. C., 1964, Physical review, 136

Postnov K. A., Yungelson L. R., 2014, Living Reviews in Relativity, 17, 3

Press W., Teukolsky S., Vetterling W., Flannery B., 2007, Numerical recipes

Prialnik 2010, Cambridge University Press

Pringle J. E., 1981, ARA&A, 19, 137

Sana H., et al., 2012, Science, 337, 444

Schneider P., 2015, Extragalactic astronomy and cosmology, an introduction

Schödel R., Merritt D., Eckart A., 2009, A& A, 502, 91

Schutz B., 2009, A first course in general relativity; 2nd ed.. Cambridge Univ. Press, Cambridge

Shakura N. I., Sunyaev R. A., 1973, A& A, 24, 337

Sneden C., Cowan J. J., Gallino R., 2008, ARA&A, 46, 241

Stephenson C. B., Sanduleak N., 1977, Astrophysical Journal, Suppl., 33, 459

Strader J., Chomiuk L., Maccarone T. J., Miller-Jones J. C. A., Seth A. C., 2012, Nature, 490, 71

Toonen S., 2017, preprint

Vangioni-Flam E., Coc A., Cassé M., 2000, A& A, 360, 15

Verbunt F., Hut P., 1987, in Helfand D. J., Huang J.-H., eds, IAU Symposium Vol. 125, The Origin and Evolution of Neutron Stars. p. 187

Verbunt F., Rappaport S., 1988, ApJ, 332, 193

Watarai K.-y., Fukue J., 1999, Publ. Astron. Soc. Japan, 51, 725

Woosley S., Fowler W., Holmes J., Zimmerman B., 1978, Atomic data and nuclear data tables, 22, 371

Wu M.-R., Fernández R., Martínez-Pinedo G., Metzger B. D., 2016, MNRAS, 463, 2323

Zorotovic M., Schreiber M. R., Gänsicke B. T., Nebot Gómez-Morán A., 2010, A& A, 520, A86